Improving Dexterity and Reliability of Restored Hand Movements Using a Brain-Machine Interface and Functional Electrical Stimulation

by

Matthew J. Mender

A dissertation submitted in partial fulfillment
of the requirements for the degree of
Doctor of Philosophy
(Biomedical Engineering)
in the University of Michigan
2024

Doctoral Committee:

Associate Professor Cynthia A. Chestek, Chair
Associate Professor Tim M. Bruns
Assistant Professor Daniel K. Leventhal
Professor James D. Weiland

Matthew J. Mender

mmender@umich.edu

ORCID iD: 0000-0003-1562-3289

Dedication

I dedicate this dissertation to my family. This wouldn't have been possible without your support and motivation. To my parents for "checking in" regularly and making sure Kaleigh and I are happy and safe while living 500 miles away. To my brothers and sister whose competitiveness may have played a non-zero role in my decision to get a higher degree than theirs. To my family in-law, the Koegels, for your support and fun outlook on life. And especially to my wife Kaleigh, my son Callan, and our dogs Konah and Wally. Your unending support (from one of you at least) has meant the world to me, and you help me to remember that what is most important in life is to be happy.

Acknowledgements

This work has been a collaboration at every step and I would like to thank everyone who has helped me along the way.

My advisor Cindy, deserves special recognition for her support of my work and my career. While I can't undersell your constant mentorship, your endless enthusiasm in particular has made this research so much better to work on. Being able to leave our weekly meetings excited about new paths forward or even the future of the field in general has helped to keep this work feeling fresh and exciting. Your career mentorship has also been vital; to say the least, I wouldn't be defending now without your constant help navigating my career path. I would also like to extend a thanks to my committee, Dan Leventhal, Tim Bruns, and Jim Weiland. Your input has been influential on my research and helped add a wider perspective to my work. I especially appreciate your assistance with the tight timelines with which I decided to submit this dissertation. I also owe a major thanks to Parag Patil, who at times has been an unofficial second advisor and who's philosophical view of research and life in general has helped me to grow my life.

I would also like to thank my lab mates for their mentorship, assistance, and friendship throughout my time in lab. Sam Nason-Tomaszewski, I was lucky to have you as a mentor in my first years here. You taught me so much about the technical and experimental sides of our research that I don't think I could list it. Paras Patel, you somehow added both a sense of fun and responsibility to the lab environment that I envy. Eric Kennedy, you really helped me to get better with and enjoy working with animals. And together, you, Sam, and Eric also demonstrated a fun

lab environment in my first years here that I hope to be able to provide wherever I end up. Julianna Richie, while you claim to be intimidating, I know that you really care about other people and you have always been willing to help with animals, last minute experiments, writing accountability, providing fudge, and more. Luis Cubillos, you have been a great unofficial social chair for the lab, and you have been around and willing to help with experiment setup too often to count. I would also like to thank my other labmates old and new, Elissa Welle, Joseph Letner, Alex Vaskov, Philip Vu, Hisham Temmar, Dylan Wallace, Joey Costello, Madison Kelberman, Olivia Lee, Miranda Copenhaver, Jake Joseph, Matt Willsey, Ayo Ward, Jordan Lam, and the many undergraduates that I have had the pleasure of mentoring. Hisham, Dylan, and Joey, we in particular have run so many experiments together over the last few years. I appreciate the chance to mentor you all and now at this point you are teaching me new things regularly.

I would like to acknowledge that this wouldn't have been possible without my family. Kaleigh, you've been with me for every step of this and while you haven't participated in the research I'd bet you helped with every presentation I gave. I'm so excited to start the next phase of our lives with Callan. My parents, Gayle, Mike, and my step-mom Sheila. I appreciate the support while I decided to move a few states away first for a job and then second for a long term degree program. Also my family in law, the Koegels, you've supported Kaleigh and I throughout this journey and you've been very generous including me in your family.

Lastly, I would like to thank the research animals Monkeys N, W, R, F, and B that I have had the privilege to work with. These animals have had a significant contribution to science and will help improve the lives of many people.

Table of Contents

List of Tables

List of Figures

Abstract

Up to 60 percent of spinal cord injuries occur at the cervical level which often results in a reduction or even complete loss of hand function, severely impacting a person's ability to interact with the world around them. In the past few decades, significant research has gone into using brain-machine interfaces (BMIs) to help restore independence in more severe cases where rehabilitative therapies are not effective. These interfaces can read out a user's intentions, allowing them to control devices by thinking about movements rather than relying on residual movements. BMIs have especially gained traction in the last 20 years; clinical studies have used them to control cursors, robotic arms, synthesize speech, type text, and even to restore native limb function by controlling stimulation to paralyzed muscles. Stimulating muscles to restore functional movements is a therapy called functional electrical stimulation (FES), and brain-controlled FES presents a promising but challenging method to restore the full chain of hand control, bypassing damage to the spinal cord. However, this method has seen limited translation to clinical use, chiefly due to a lack of dexterity that it can restore in the hand and reliability with which it can be restored. The aim of this work is to inform how robust BMI are for the type of control required for brain-controlled FES, to assess to what extent FES can restore two-degree-of-freedom movements in the hand and what factors impact reliability, and then to extend FES methods to restoring movements to multiple joints in the hand.

In my first study, I investigated the impact that wrist postures and resistance at the fingers, two task perturbations occurring commonly in acts of daily living, have on a BMI for controlling virtual finger movements in non-human primates (NHP). I found that these changes impact cortical neural activity during the task, resulting in increased prediction error for intended movements and the NHP needing to adjust their control of the BMI. In my second study, I showed that current intramuscular FES methods can achieve graded control of simultaneous finger and wrist flexion as well as how well a BMI can control virtual finger and wrist movements. Additionally, I found that stimulation restored a large range of movements in both the wrist and the fingers, but the range

of movements is significantly impacted by muscle fatigue and interactions between stimulation-evoked movements for each degree-of-freedom. In my third study, I present a proof-of-concept intramuscular FES implant method targeting multiple nerve entry points in each muscle. Using this method, stimulation evoked more discrete finger movements with individual electrodes, theoretically increasing the available hand postures that can be restored.

The results of this work demonstrate that BMI can be used to infer intended finger and wrist movements in real-time and FES can be used to control graded movements of the wrist and fingers. We found reduced efficacy in both BMI decoding accuracy and stimulated range of movements due to interactions controlling both the wrist and fingers. As future work continues to increase the degrees-of-freedom that are simultaneously controlled, there is a need to design stimulation protocols that account for interactions with stimulation on more electrodes and design BMI algorithms that are intentionally trained to generalize well, for example with variable postures and force requirements.

Chapter 1 Introduction

Sections 1.1 and 1.3 in this chapter were adapted from sections that I authored in the review article "Neurotechnologies to restore hand functions" published in the journal Nature Reviews Bioengineering (Losanno, Mender, et al., 2023).

The hand is a person's most fundamental tool for interacting with the world around them, even the most mundane activities require a variety of hand postures. Spinal cord injury often leads to motor disabilities in the hands, severely impacting people's ability to interact with the world. There are an estimated 18,000 new spinal cord injuries in the Unites States every year (Jain et al., 2015; National Spinal Cord Injury Statistical Center, 2023) and 59.6% of spinal cord injuries can be classified as complete or incomplete tetraplegia (National Spinal Cord Injury Statistical Center, 2023) which involves injury to the cervical spine. Hand function is present as low as the thoracic spine (level T1), so any injury to the cervical spine can result in hand impairment. As the degree of spinal cord injury becomes more complete and the injury is more chronic, interventions transition from restorative to compensatory (Rupp, 2020). At the same time, the highest priority for people with tetraplegia is the improvement of hand function (Anderson, 2004; Collinger et al., 2013).

Electrical stimulation of the muscles or motor nerve fibers produces muscle contractions and can be used to rehabilitate or restore movements. As the peripheral nerve fibers are much more responsive to electrical stimulation than muscles (Mortimer, 2011), the peripheral nerve fibers are the target of stimulation to elicit movements. As a result, this type of therapy has primarily been

studied in motor disabilities where lower motor neurons are still intact such as stroke and cervical spinal cord injury. In stroke and many spinal cord injuries, typically both upper motor neurons and lower motor neurons are still intact or partially intact and voluntary movement can be rehabilitated by exercise. With more severe injuries, rehabilitation can instead be done with electrical stimulation, matching intended movements with artificially generated movements to generate the same regenerative processes (Nagai et al., 2016). Significant research has gone into clinical applications aimed at rehabilitating voluntary movement with stimulation (Marquez-Chin & Popovic, 2020) and there is evidence for rehabilitation working in different severity of spinal cord injury (Kapadia et al., 2013; Mangold et al., 2005; Popović et al., 1999; Popovic et al., 2011). However, electrical stimulation therapy is often not able to completely restore voluntary movements. Instead, devices can be engineered to use electrical stimulation to restore functional movements such as arm movements and grasping. This is referred to as functional electrical stimulation (FES) and represents an opportunity to restore a person's own movements rather than just compensating for motor disability. To date, multiple clinical trials have reported using FES to restore specific grasps (Ajiboye et al., 2017; Coste et al., 2022; Tigra et al., 2020), however restoring full dexterity to the hand is a challenge.

FES devices are often controlled with residual body movements (section 1.3.1). However, patients with higher tetraplegia have little residual movement left with which to control the devices. Brain-machine interfaces (BMIs) are promising methods for controlling stimulation in an intuitive way. In BMIs, intended movements are decoded from neural activity to control devices. These have been used to control computer cursors or robotic arms for over a decade (Collinger, Wodlinger, et al., 2013; Hochberg et al., 2006; Kim et al., 2008). With advances in the understanding of neurophysiology and significant improvements in machine learning (Glaser et

al., 2020), BMIs are reaching new milestones in performance (Metzger et al., 2023; Willett et al., 2023; Willsey et al., 2024). BMIs have also been used for controlling FES, although with relatively simple algorithms (Ajiboye et al., 2017; Ethier et al., 2012). With the high dimensionality of hand control, advances in BMI algorithms are needed to expand the dimensionality of BMI control to restore movements (Nason et al., 2021). In this chapter I review the different methods for restoring upper extremity movements with FES and for decoding upper extremity movements in BMI applications. Then I end with a discussion of the current state of brain-controlled FES applications, ultimately motivating the need for more robust BMI algorithms and more characterization of FES for controlling multi-degree-of-freedom movements in the hand.

1.1 Normal Control of Hand Movements

The human hand is a complex biomechanical system with 27 degrees-of-freedom (DoFs) (ElKoura & Singh, 2003), 6 in the wrist (1 for flexion–extension, 1 for radio-ulnar deviation, 1 for supination–pronation and 3 for translation in space), 5 in the thumb (3 for flexion–extension and 2 for abduction–adduction) and 4 in each of the other fingers (3 for flexion–extension and 1 for abduction– adduction) with some finger interdependence (Martin et al., 2011), which allow for a variety of shapes and functions. Although hand movements are very similar between humans and non-human primates (NHPs), human hand dexterity is unique, partly owing to its morphology: a higher thumb-to-finger-length ratio and a more complex muscular structure in the thumb than in NHPs allow higher flexibility in finger opposition and the ability to create forceful precision grips (Nanayakkara et al., 2017). The collection of human hand movements can be divided into two main groups, namely prehensile and non-prehensile movements, used for grasping and pushing or lifting objects, respectively (Napier, 1956) (Figure 1-1a). Prehensile movements are more prevalent (Gracia-Ibáñez et al., 2018; Kilbreath & Heard, 2005) and have been studied more

extensively. Prehensile movements have been systematically arranged into 33 grasp types based on hand configuration and object geometry, which can be reduced to 17 prototypical types when not considering object geometry (Feix et al., 2016). Moreover, each grasp movement can be classified as power, precision or intermediate, based on whether large force, precision or a mixture of both is required. The occurrence of different grasp types in daily life has been extensively studied to determine their importance for neuroprosthetics and neurorehabilitation (Bullock et al., 2013; Vergara et al., 2014). However, despite providing some general guidance — for example, the prevalence of lateral and medium wrap grasps — there is high variability in the frequency of grasp types across environments and subjects investigated (Feix et al., 2016). Thus, neuroprostheses that restore a large set of hand movements are needed to benefit more patients in more contexts.

1.1.1 Anatomical Pathway

Human hand movements are controlled by coordinated contractions of extrinsic and intrinsic hand muscles, located in the forearm and within the hand itself, respectively (Figure 1-1b). Extrinsic muscles provide strength, whereas intrinsic muscles allow fine movements. These muscles contract owing to electrical signaling originating from motoneurons in the ventral horn of the spinal cord. The motoneurons travel out of the spinal cord in the spinal nerves at different levels to reach their target muscle, where they enter at a location called the motor point. The muscles of the hand are targeted by the spinal roots at the C5–T1 levels, according to a rostro-caudal somatotopy (Schirmer et al., 2011): the more proximal the muscle, the more rostral the peak of the spinal motoneuron pool that innervates it, but with a high degree of overlap of the motoneuron pools across muscles. In the upper extremity, the C5–T1 spinal nerves first form the brachial plexus, where they reorganize into different nerve trunks to efficiently travel to different

regions of the arm (Bollini & Wikinski, 2006). The nerve trunks that form in the brachial plexus and are responsible for hand function are the median nerve, which innervates most flexor and pronator muscles in the ventral forearm and some intrinsic hand muscles, the ulnar nerve, which innervates the flexor carpi ulnaris and the medial half of the flexor digitorum profundus as well as the majority of intrinsic hand muscles, and the radial nerve, which innervates extensor and supinator muscles in the forearm and hand (Boles et al., 2000; Bollini & Wikinski, 2006; Jabaley et al., 1980). Motoneuron axons travel within fascicles in these nerves. The density, diameter and functional topography of nerve fascicles depend on the distance from the spinal cord (Delgado-Martínez et al., 2016): more, smaller and better functionally partitioned fascicles emerge distally, as fibers innervating the same muscle organize in separate patches and eventually form a distinct fascicle to branch out of the nerve trunk towards the muscle.

Spinal motoneurons receive input from multiple neural pathways, that is, sensory afferents and supraspinal regions, either directly or through spinal interneurons (Lemon, 2008; Porter & Lemon, 1995). Multiple cortical regions are involved in voluntary movements, where the primary motor cortex (Broadmann's area 4) mainly contributes to the execution of movements. Here, pyramidal cells in layer 5 of the primary motor cortex project to spinal interneurons and motoneurons and constitute about 30% of the corticospinal tract. Anatomical and evolutionary differences have led to the classification of two areas in the primary motor cortex that are thought to affect dexterous movements like those of the hand, namely the caudal and rostral regions (Rathelot & Strick, 2006; Strick et al., 2021; Witham et al., 2016). Compared with caudal primary motor cortex, the rostral primary motor cortex is evolutionarily older, has primarily disynaptic connections with motoneurons through interneurons and is thought to use spinal cord mechanisms to control a wide range of motor behaviours. Caudal primary motor cortex is more developed in

humans and apes, is characterized by monosynaptic connections to motoneurons and is thought to control highly skilled movements. A large area of human primary motor cortex, about 9 cm^2 (Roux et al., 2020), is associated with hand movements; although cortical representations for different fingers largely overlap (Sanes et al., 1995), multiple studies support the hypothesis that finger somatotopy is present in this area (Beisteiner et al., 2001; Dechent & Frahm, 2003).

Since the 1960s, investigators have asked how the motor system, with more than 30 muscles and 20 joints in the human hand contributing to motion production, reduces the burden of regulating the large number of variables available (Bernshteĭn, 1967). Despite the great number of muscles involved, most voluntary movements in vertebral species can be generated from the activation of relatively few muscle synergies (Bizzi & Cheung, 2013). In the human hand, postures and movements have been represented by the activation of a few joint, force or muscle synergies (Bicchi et al., 2011; Mason et al., 2001; Santello & Soechting, 2000; Thakur et al., 2008; Weiss & Flanders, 2004). Whether these synergies are a fundamental property of neural motor control or whether they are an artefact of task structure is still debated (Tresch & Jarc, 2009). Motor responses to cutaneous (Tresch et al., 1999) and intraspinal stimulation (Lemay & Grill, 2004; Tresch & Bizzi, 1999) revealed that the spinal cord in vertebrates is organized into modules that generate specific patterns of muscle activation. Additionally, cortical stimulation in NHPs evokes complex movements (Overduin et al., 2015). Together, these findings have led to the idea that movement is generated by the activation of modular muscle synergies with the motor cortex determining the patterns of activation (Bizzi & Cheung, 2013). Nonetheless, evidence suggests that the motor cortex might be more involved and also encodes muscle synergies (Rathelot & Strick, 2006) and contributes to the flexible activation of motor units (Marshall et al., 2022).

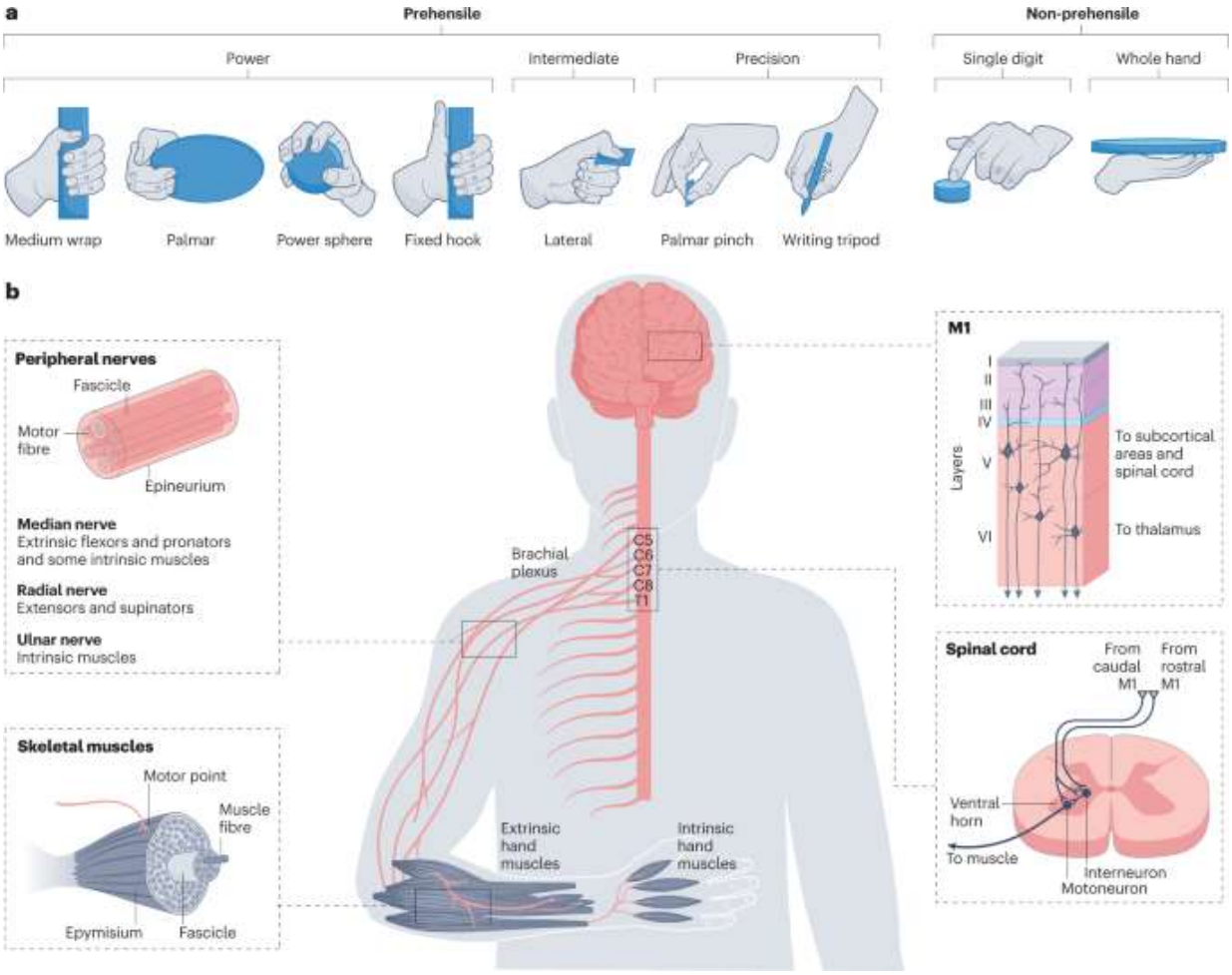

Figure 1-1 Normal hand movements and their anatomical pathway.
a, Examples of prehensile and non-prehensile hand movements, used for grasping and pushing or lifting objects, respectively (Napier, 1956). Prehensile movements are classified into power, precision and intermediate grasps (Feix et al., 2016). Non-prehensile movements can involve single digits or the whole hand. **b**, Hand movements are generated by contracting extrinsic and intrinsic hand muscles, located in the forearm and in the hand, respectively. The skeletal muscle is composed of muscle fibres organized in fascicles, surrounded by a connective tissue called epymisium. The nerve motor branch enters the muscle belly at the motor point. Hand muscles are innervated by the median, radial and ulnar nerves, which form in the brachial plexus. A peripheral nerve is composed of motor fibres organized into fascicles, surrounded by a connective tissue called epineurium. Hand muscles are targeted by the C5–T1 spinal nerves. Spinal motoneurons, originating in the ventral horn of the spinal cord, receive input directly from cells originating in the caudal primary motor cortex (M1, which is composed of six layers) or from spinal interneurons, which in turn receive input from cells originating in the caudal and rostral M1. Large pyramidal cells in layer 5 send their axons to the spinal cord.

1.1.2 Motor Control

Although anatomical pathways for human hand motion production are well described, how the motor cortex controls movement is still debated. The historical view of motor control in higher vertebrates has been that the cortex must take a neural representation of high-level parameters,

such as movement direction or velocity, and convert that into commands for muscles through a series of transformations (Bizzi et al., 1991). The classical approach has relied on trying to find the movement parameter that the motor cortex is representing by correlating extracellular intracortical recordings in primary motor cortex of animal models with a variety of movement parameters during movement tasks (Kalaska, 2009). Ultimately, a multitude of variables represented in primary motor cortex have been found, ranging from movement direction (Georgopoulos et al., 1982) and instantaneous hand kinematics (Moran & Schwartz, 1999) to muscle activations (Townsend et al., 2006). However, no consensus has been reached on what the role of the motor cortex is in motor control. Alternatively, neurophysiology recordings in NHPs have pointed out heterogeneity in the parameters represented by individual neurons in primary motor cortex (Churchland & Shenoy, 2007; Graziano, 2006; Kalaska, 2009; Scott, 2008; Stephen H. Scott et al., 2001), suggesting that a paradigm shift away from representational modelling is needed to understand the encoding of movements. With the rise of microelectrode arrays and the ability to record from up to hundreds of neurons at the same time (Nicolelis et al., 2003), research focus has shifted towards looking at the covariance of neurons activating in the motor cortex of NHPs to understand how they work together to compose movement-generating outputs. In this view, the role of neurons is not to represent any specific movement covariate; instead the primary motor cortex activity reflects a mixture of signals, some of which output to drive muscles, but many of which are internal processes composing those outputs (Churchland et al., 2012). Dimensionality-reduction methods have become widely used to visualize the covariance of neural activity (Cunningham & Yu, 2014; Kalaska, 2019), revealing various aspects of motor control, including preparatory activity (Kaufman et al., 2014), motor learning and plasticity (Golub et al., 2018b; Oby et al., 2019; Sadtler et al., 2014), and the formation of descending motor commands

(Churchland et al., 2012; Russo et al., 2018; Shenoy et al., 2013). One view is that a large amount of variance of neural activity resides in a low-dimensional space, which ensures robustness in movement execution (Russo et al., 2018). This subspace might be preserved between different movements, with only a small amount of neural variance accounted for by movement specific subspaces. These dynamics have been studied largely in upper arm movements in NHPs and, although they could also be applied to hand movements, the increased sensory feedback during hand movements points to different dynamics (Suresh et al., 2020). Therefore, a systematic evaluation of motor cortex dynamics during hand movements and the impact of sensory feedback is needed to understand whether these findings can be extended to hand movements.

1.2 Restoring Hand Movement with Electrical Stimulation

Based on the anatomy and physiology of natural hand movements, there are multiple available targets for stimulation to restore hand movements. Primarily this includes targeting either the peripheral nerves, the muscles, or the spinal cord. Functionally, these approaches vary by the dexterity of restored movements and the reliability of evoked movements. Notably, the methods also have key differences in the potential for deployment (i.e. cost and surgical complexity) and comfort (Losanno et al., 2023). Figure 1-2a illustrates how different stimulation methods fare with respect to restored dexterity, potential for deployment, and comfort. In order to restore dexterous movements, stimulation needs to be able to selectively target specific muscles in the wrist and hand. Typically, this is done by stimulating at more invasive locations closer to the muscles or closer to the peripheral nerves. A key factor in the reliability of evoked movements is the resistance to fatigue, a phenomenon in which muscles produce less force after repeated activation. Due to key differences between muscle fiber recruitment from electrical stimulation and from physiologically natural recruitment, fatigue occurs rapidly in electrical stimulation (Giat et al.,

1993; Singh et al., 2000; Veltink et al., 1989). First, in natural muscle fiber recruitment, fibers are recruited asynchronously and tetanic contraction is achieved through a temporal summation of many muscle fibers activated at 6-8Hz (Lynch & Popovic, 2008). In contrast, electrical stimulation, both at muscles and peripheral nerves, recruits all motor fibers in an area synchronously, timed with each stimulation pulse. Therefore, to achieve tetanic contractions stimulation is at a higher frequency (e.g. 20-40Hz) than what is physiologically natural. Second, natural fiber recruitment activates small, fatigue resistant, slow twitch fibers before larger fast twitch fibers (Henneman, 1957). Electrical stimulation preferentially activates nearby motor axons and large axons which deviates from the natural order of recruitment or even goes in a reverse order of recruitment (Bickel et al., 2011). Due to this, methods that are more fatigue resistant either are closer to axons to be more specific in the ones that they activate or are able to activate the natural recruitment pathways in the spinal cord.

1.2.1 Surface Stimulation

The most widely used and least invasive method for FES is using surface electrodes. With this method, electrodes are placed on the surface of the skin, preferably near the targeted muscle's motor point and then stimulation activates muscles transcutaneously (Figure 1-2b). There are multiple assistive devices commercially available specifically aimed at restoring grasping through surface stimulation, for example, the bionic glove (Prochazka et al., 1997), now known as the ReGrasp, and the NESS Handmaster (Snoek et al., 2000). These devices rely on external electrodes which must be placed correctly in order to restore functional movements. They typically use gloves or orthoses to align electrodes and can either strengthen or restore one to two grasps. The bionic glove consisted of a neoprene, fingerless glove, with electrodes on the inside over the thenar

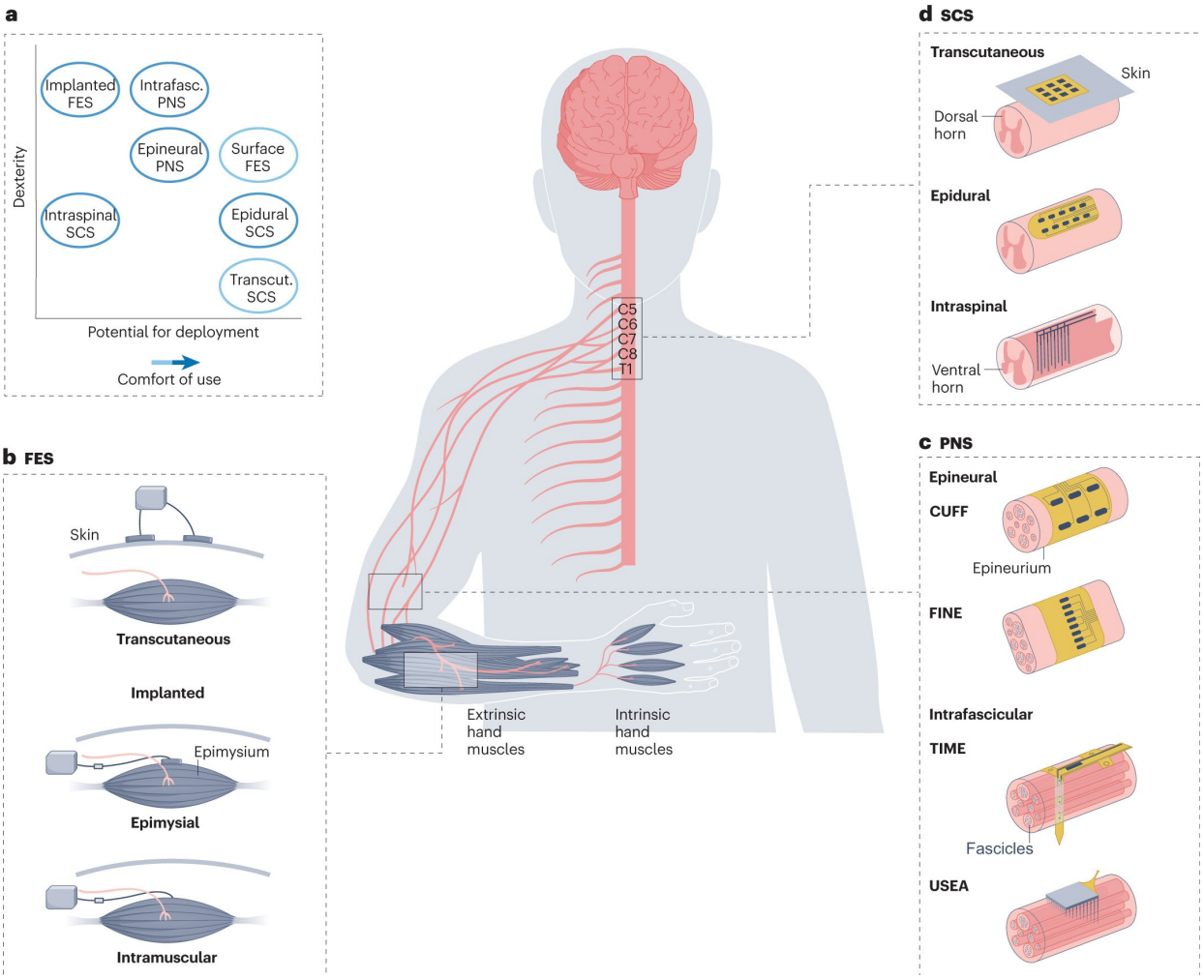

Figure 1-2 Neurotechnologies to restore hand functions.
Hand functions can be restored by electrically stimulating different regions of the neuromuscular system using different interfaces. a, Dexterity versus potential for deployment and comfort of use for different strategies to restore hand functions. b, Functional electrical stimulation (FES) is performed using transcutaneous or implanted (epymisial or intramuscular) electrodes targeting the extrinsic and intrinsic hand muscles. c, Peripheral nerve stimulation (PNS) is applied through epineural electrodes, such as the cuff electrode and the flat interface nerve electrode (FINE), or intrafascicular electrodes, such as the transverse intrafascicular multichannel electrode (TIME) and the Utah slanted electrode array (USEA) (Yoshida et al., 2017), targeting the median, radial and ulnar nerves above their bifurcations. d, Spinal cord stimulation (SCS) is implemented using transcutaneous, epidural or intraspinal leads targeting the C5–T1 spinal nerves. Figure 4 from (Losanno et al., 2023)

eminence and forearms. It functioned by detecting wrist movement and then stimulating muscles in the forearm to flex or extend the fingers. This setup improved the strength and dexterity of participants' tenodesis grasping, a grasp made by flexing or extending the wrist which would in turn move fingers by shortening or lengthening the muscles of the fingers. The NESS Handmaster consisted of a fitted wrist splint with five surface electrodes on the inside. The device could provide

either key or palmar grasp, controlled by a sequence of stimulation after pressing the trigger button on the control unit, as well as stimulate muscles to exercise muscles.

Surface stimulation suffers from multiple factors impacting the effectiveness of stimulation. In surface stimulation, the electrodes are relatively far from the motor points. As a result, stimulation current often spreads to multiple muscles and it is difficult to selectively activate deep muscles (Koutsou et al., 2016; Kuhn et al., 2010). With stimulation far away from the nerves, surface stimulation activates overlapping groups of muscle fibers repeatedly with a preference for large fast fatiguing fibers, resulting in fast fatigue occurring within minutes (Vromans & Faghri, 2018). Additionally, surface stimulation requires a high stimulation amplitude for current to reach the target muscles. This activates superficial sensory fibers and pain receptors and potentially leads to discomfort (Kuhn et al., 2010). Lastly, there is also a lack of reliability with movement such as pronation and supination changing the relative position of the skin electrode and muscles (Bao et al., 2018; Popović-Bijelić et al., 2005). Due to the lack of dexterous movements and quick fatigue, surface FES has instead had a lot of success as an easily accessible neurorehabilitation therapy (Mangold et al., 2005; Marquez-Chin & Popovic, 2020; Popovic et al., 2011).

Advances to surface stimulation have used electrode arrays to improve the selectivity of evoked movements. With more electrodes, stimulation parameters can be modified to shape the generated electric field to activate desired muscles (Koutsou et al., 2016; Popović-Maneski et al., 2013). This has even been used to evoke single finger movements (Bao et al., 2018; Bouton et al., 2016). One clinical trial for example used up to 130 surface electrodes embedded in a wearable sleeve to restore grasp and wrist movements (Bouton et al., 2016; Friedenberg et al., 2017). New technologies also aim to improve comfort and conformity for individual patients (Moineau et al., 2021; RaviChandran et al., 2023).

1.2.2 Muscular Stimulation

A step more invasive than surface stimulation are intramuscular and epimysial stimulation. Electrodes can be implanted percutaneously without an incision by using a needle to poke through the skin into the muscle belly, however percutaneous sites increase the infection risk with the implants. For chronic implants, an incision is made and electrodes are sutured onto (epimysial) or into (intramuscular) the muscle belly where they scar into place over time (Figure 1-2b). Electrodes can then be tunneled to one percutaneous site, or to an implanted stimulator (Smith et al., 2005). Like surface stimulation, the electrodes are generally implanted near the motor point in order to more easily activate the nerve without current spreading to other muscles and nerves. In practice, electrode locations are determined with intraoperative stimulation.

This approach resulted in the clinically available Freehand system for restoring hand movements, which was implanted in more than 250 users (Peckham et al., 2001). The Freehand system used 8 epimyseal electrodes implanted in muscles of the hand and wrist to restore palmar and lateral grasps. A second version of the Freehand system attempted to improve on some limitations of the Freehand system (Kilgore et al., 2018; Peckham et al., 2002), including a lack of finger extension, arm reaching, and forearm pronation. In the second version, 3 participants were implanted with four additional stimulating channels, two of which went into intrinsic hand muscles to provide two additional grasps unique to the participant.

Muscular stimulation is perhaps the best suited approach for restoring hand dexterity. Electrodes can be implanted in all muscles including deep muscles and small intrinsic hand muscles, so stimulation can selectively activate individual muscles (Grandjean & Mortimer, 1986) as long as they can be identified intraoperatively. Electrodes can even be implanted into neuromuscular compartments within muscles, that is the portion of a muscle innervated by one

primary muscle nerve branch (English et al., 1993). In hand muscles like flexor digitorum profundus, neuromuscular compartments have functional differences (Schieber et al., 2001), further increasing the selectivity of muscle fibers that can be activated. Additionally, because electrodes are implanted, stimulation can be consistent over years (Kilgore et al., 2003, 2009).

Muscular electrodes preferentially recruit muscle fibers with axons near the stimulating electrode, in a pattern that spreads out radially from the current source (Singh et al., 2000). Because of this, force recruitment from activating muscle fibers with intramuscular electrodes is smooth within individual muscles (Grandjean & Mortimer, 1986) or individual neuromuscular compartments (Gruner & Mason, 1989; Singh et al., 2000), but may become nonlinear when current spreads to new neuromuscular compartments (Gruner & Mason, 1989). This type of stimulation suffers from quick fatigue due to the high stimulation frequencies (20-30Hz) and the recruitment pattern being equally effective at activating large fast fatiguing fibers as small fatigue-resistant fibers. The fatigue effect may be less pronounced in intramuscular stimulation than nerve stimulation due to large motoneurons branching to reach more muscle fibers compared to small motoneurons. Example estimates using intermittent stimulation (330ms of 40Hz stimulation every 1s) in cat medial gastrocnemius show peak force declining to 19.7% or 4% of the initial peak force after 15 minutes for intramuscular stimulation and nerve stimulation (bipolar hook electrodes) respectively (Singh et al., 2000). Fatigue is still rapid in intramuscular stimulation, reaching 20% of initial peak force within an average of 101s (Singh et al., 2000), although fatigability varies with muscle fiber composition (Vromans & Faghri, 2018).

Intramuscular electrodes also have practical issues for clinical translation. Implanting many electrodes becomes surgically difficult quickly. In the forearm for example, one estimate includes 19 muscle targets with an average of 58.8 motor points that could be targeted (Safwat &

Abdel-Meguid, 2007). While difficult, in clinical trials 36 electrodes have been implanted throughout the arm (Ajiboye et al., 2017), and systems with more electrodes (up to 58) are being tested in preclinical studies (Hasse et al., 2022; Holly et al., 2022).

1.2.3 Peripheral Nerve Stimulation

Stimulating the peripheral nerves themselves is a promising route for evoking selective movements with minimal electrodes. Nerves are composed of fascicles that are selectively carrying both afferent and efferent fibers for single muscles or synergistic sets of muscles the more distal they go from the spinal cord (see section 1.1). If nerves are targeted before they bifurcate, then one implant could activate many different motoneuron populations. Electrodes can be placed on the nerve (epineural), typically with a cuff electrode, or electrodes can penetrate the nerve (intrafascicular) in order to target specific fascicles (Figure 1-2c). Theoretically, by steering current with multiple electrode contacts, epineural stimulation can achieve selective activation of muscles (Dali et al., 2018; Polasek et al., 2009). In practice, clinical trials have shown that using nerve cuffs can evoke synergistic movements with single contact (Herring et al., 2023), or multipolar stimulation (Coste et al., 2022; Tigra et al., 2020) in order to produce functional grasps. Intrafascicular electrodes stimulate very close to the axons as they travel to the muscles, so they can selectively activate muscles as long as an electrode contact is near the motoneuron population. In preclinical studies, intrafascicular electrodes have been shown to be able to selectively activate individual muscles in the arm (Badi et al., 2021; Ledbetter et al., 2013). By coordinating stimulation on multiple contacts of a slanted Utah array (Ledbetter et al., 2013) or a linear array (Badi et al., 2021), three different grasps were restored in non-human primates.

When comparing epineural and intrafascicular stimulation, intrafascicular is typically more fatigue resistant and more selective. While nerve cuff stimulation can evoke some selective

movements (Coste et al., 2022; Tigra et al., 2020), these clinical trials typically combined synergistic movements to make grasps. Epineural stimulation results in a relatively large spread of current over the fascicles which activates multiple groups of motor fibers. As a result, stimulation from multiple contacts tends to activate overlapping groups of motor fibers. Additionally, this type of stimulation is susceptible to reverse recruitment because of the different sized fibers present in the fascicles (Veltink et al., 1989). Preclinical studies have shown that pulse waveforms can be designed to enact a more natural recruitment order and improve fatigue resistance (Fang & Mortimer, 1991), however they have not been implemented in clinical trials for restoring hand movements due to the complexity of generating the waveforms.

Intrafascicular stimulation is able to activate distinct groups of motor fibers, or groups of afferent fibers for sensory restoration, and is less susceptible to reverse recruitment due to the close proximity to the target fibers (Veltink et al., 1989). Simulations show that intrafascicular electrodes are able to activate more individual muscles, and are better than nerve cuffs at activating motoneuron axons deep in the fascicle (Badi et al., 2021). As different contacts can activate different motor fiber groups, intrafascicular stimulation can be used to produce more fatigue resistant-movements by interleaving stimulation on multiple contacts at a lower frequency. Interleaving stimulation creates a tetanic contraction by sequentially activating a different group of motor fibers on each contact (McDonnall et al., 2004; Normann et al., 2012; Yoshida & Horch, 1993). This approach however results in a decrease in maximal achievable force (Yoshida & Horch, 1993).

1.2.4 Spinal Cord Stimulation

A different approach to FES has been to activate the lower motor neurons where they originate in the spinal cord. The spinal cord is commonly accessed transcutaneously, with

intraspinal stimulation, or with epidural stimulation. Spinal cord stimulation activates motoneurons transynaptically, preferentially activating afferent sensory fibers which subsequently activate motoneurons through reflex circuits in the spinal cord. For example, intraspinal stimulation with microwires in the ventral horn activates sensory afferent axons at lower stimulus levels than motoneurons (Gaunt et al., 2006), and both transcutaneous and epidural stimulation activate afferent sensory fibers in the dorsal root (Capogrosso et al., 2013; De Freitas et al., 2022; Hofstoetter et al., 2018). Cervical intraspinal microstimulation can activate upper limb muscles, typically coactivating synergist or antagonist muscles as well (Moritz et al., 2007). Additionally, it has been used in nonhuman primates to restore palmar grasp (Zimmermann et al., 2011) but has not been used clinically for restoring hand movements. Epidural stimulation has been translated to clinical trials much more successfully. Due to success in restoring gait (Angeli et al., 2018; Gill et al., 2018; Harkema et al., 2011; Wagner et al., 2018), epidural spinal cord stimulation has been extended to cervical levels for restoring upper limb and hand movements, in non-human primates (Barra et al., 2022), then in patients after stroke (Powell et al., 2023), as well as a pilot with patients with tetraplegia (D. C. Lu et al., 2016).

Selectivity and fatigue of epidural spinal cord stimulation have not been characterized as in depth as other stimulation methods. This partly owes to the different mechanism of movement restoration. With regard to generating movements, epidural stimulation is not very selective. Studies have shown that laterally placed epidural electrodes will preferentially activate the dorsal roots segmentally which will result in muscle activations primarily in the muscles innervated by that spinal segment (Greiner et al., 2021; McIntosh et al., 2023). There is however an interaction between descending cortical commands and epidural stimulation. Cortical input is necessary for restoring movement through epidural stimulation, and the stimulation may be facilitating

movements rather than directly generating movements (Barra et al., 2022; Greiner et al., 2021). Additionally, due to the natural recruitment of spinal motoneurons (Moraud et al., 2016), epidural stimulation is expected to be fatigue-resistant.

1.3 Decoding Intended Hand Movements

In order to control stimulation and restore a range of hand movements, it is necessary to estimate an intended hand movement from the user. Various approaches can be taken to infer intended hand movements. For example, discrete commands can be extracted, such as to perform grasping, to select a certain type of grasp, or to flex or extend a certain finger or group of fingers. Discrete commands can be substituted or combined with continuous control of single DoFs, such as the level of grasp or finger closure or force. Discrete decoding has been implemented using noninvasive interfaces with the body (decoding through residual body movements) or the brain (using electroencephalography, EEG). Higher decoding accuracy on several finger movements has been obtained with implantable electrodes placed on the surface of the brain (using electrocorticography, ECoG). However, restoring hand dexterity for a larger spectrum of daily activities is more complex. In this case, the decoder should allow continuous and independent control of multiple DoFs. Although decoding all 27 DoFs of the hand is probably not necessary for functional performance in daily life, decoding at least 7 DoFs (flexion–extension of the wrist, flexion–extension and abduction–adduction of the thumb, and flexion–extension of the other four fingers) would allow graded control of a variety of prehensile and non-prehensile movements and recovery of many tasks. For more flexibility, abduction–adduction of the index finger, but also of the other fingers, adding 1 to 4 DoFs, could be considered. So far, continuous multi-DoF hand control has been obtained only with intracortical electrodes that penetrate the brain. In this section

we describe existing neurotechnologies that use various sources to decode hand movements. We present solutions based on residual body movements, EEG, ECoG and intracortical electrodes

1.3.1 Residual Body Movement Decoding

Most of the current clinical applications of neuroprostheses for hand movement restoration rely on the user's residual body movements to provide motor commands. Body control sources can be distinguished into homologous and non-homologous solutions depending on whether they are part of the natural 'command chain' (that is, neuromuscular control pathway) of the hand, or not. Examples of nonhomologous approaches include movements of the contralateral shoulder and button presses, used in the first-generation Freehand system (Peckham et al., 2001) and the NESS H200 (Bioventus LLC, Durham, NC, USA; Snoek et al., 2000), respectively, to select the desired type of grasping and its onset and offset. Despite non-homologous approaches being robust and easy to implement, they scale poorly in controlling multiple DoFs for more complex movements and increase the cognitive load.

A more intuitive, but not truly homologous, solution was implemented in the Bionic Glove (Prochazka et al., 1997), now commercialized as ReGrasp (Rehabtronics, Edmonton, Canada), whereby people with C6 tetraplegia controlled the onset and offset of grasping using the residual extension and gravity-induced flexion of the wrist, respectively. This technique resulted in a natural amplification of their already mastered tenodesis grasp, a passive grasp mechanism in which extension of the wrist leads to shortening of the finger flexors and thus to flexion of the fingers. This approach was later extended to the second-generation Freehand system (Kilgore et al., 2008), employing implanted electromyography (EMG) or kinematic wrist sensors (Hart et al., 1998). The use of multi-muscle EMG signals recorded from the forearm and hand has been proposed as a truly homologous solution providing an increased control of dimensionality, that is,

more DoFs can be controlled. Classification of hand postures has been performed using myoelectric pattern recognition in subjects with incomplete tetraplegia (Liu & Zhou, 2013; Z. Lu et al., 2019). In addition, subthreshold muscle activity — detectable with EMG but without producing open movements — has been reported in most patients diagnosed with motor complete SCIs (Heald et al., 2017; Sherwood et al., 1992). These low-level EMG signals were recorded with surface electrode arrays positioned on the forearm in a patient with complete SCI and used to discriminate between attempted single finger movements (Ting et al., 2021). One limitation of homologous residual body control is that there is currently no robust solution to disentangle in real time the voluntary activity from that evoked by the neuroprosthesis without loss of data (Osuagwu et al., 2020). Moreover, it must be tailored to each patient and is not applicable when the residual kinematic and muscle activities are completely absent.

1.3.2 Brain-Decoding

A more generalizable solution would be to use neurotechnologies that decode hand movements from brain activity. Brain activity can be recorded using interfaces with different levels of invasiveness (transcutaneous, intracranial or intracortical; Figure 1-3a), leading to different recording and decoding resolutions (Figure 1-3b).

1.3.2.1 Non-Invasive Signals: EEG

The non-invasive (transcutaneous) solution using EEG has generated the largest number of human studies in the field. EEG signals have high temporal but low spatial resolution because they are based on the cumulative activity of many neurons. Therefore, to decode specific movements it is necessary to extract relevant features across time and electrodes. Frequency-related features are generally extracted using Fourier transform, wavelets or bandpass filtering, and it is common to see spatial features extracted through Laplacian filters, spatial patterns,

principal component analysis and independent component analysis (McFarland et al., 2006). Sensorimotor-related rhythms commonly extracted are the mu band (8–12 Hz) and beta band (18–30 Hz), as these change in amplitude with overt movement, imagined movement and movement preparation. EEG recordings have been used in healthy subjects and patients with tetraplegia for discrete decoding of hand movements. Linear discriminant analysis classifiers can decode the onset of grasping (Randazzo et al., 2015) and discriminate between two or three grasp types (Iturrate et al., 2018; Jochumsen et al., 2016; Muller-Putz et al., 2019; Ofner et al., 2019; Sburlea et al., 2021; Schwarz et al., 2018) and object affordances (Sburlea et al., 2021) using EEG signals over the motor cortex and fronto-parietal areas. Unfortunately, classification accuracy has never reached high values; that is, not exceeding 70% in binary classification. EEG signals have low amplitude and lack the specificity to decode motor intentions for the hand well above chance levels. Therefore, the accuracy of predicted movements might not be high enough to control a hand in daily life. In addition, EEG caps are cumbersome and require skill and time to be placed and calibrated, further limiting their acceptance for daily assistance. However, EEG signals can also be used to trigger muscle stimulation (Gant et al., 2018) or to control an orthosis or exoskeleton (Al-Quraishi et al., 2018) in a neurorehabilitation setting. A double-blind study with 32 patients with chronic stroke showed substantially higher motor improvement in the BMI group (the BMI was used to trigger an orthosis attached to the plegic limb) compared with a sham-BMI group after 4 weeks of training (Ramos-Murguialday et al., 2013), as measured by the modified Fugl–Meyer assessment motor score (Fugl Meyer et al., 1975), which assesses voluntary movement of the upper limb. In this case, the contingent link between brain activity and repetitive activation of the afferents is thought to promote a Hebbian-like plasticity mechanism (a form of synaptic plasticity caused by the causal relationship between pre and post-synaptic activity), which might increase

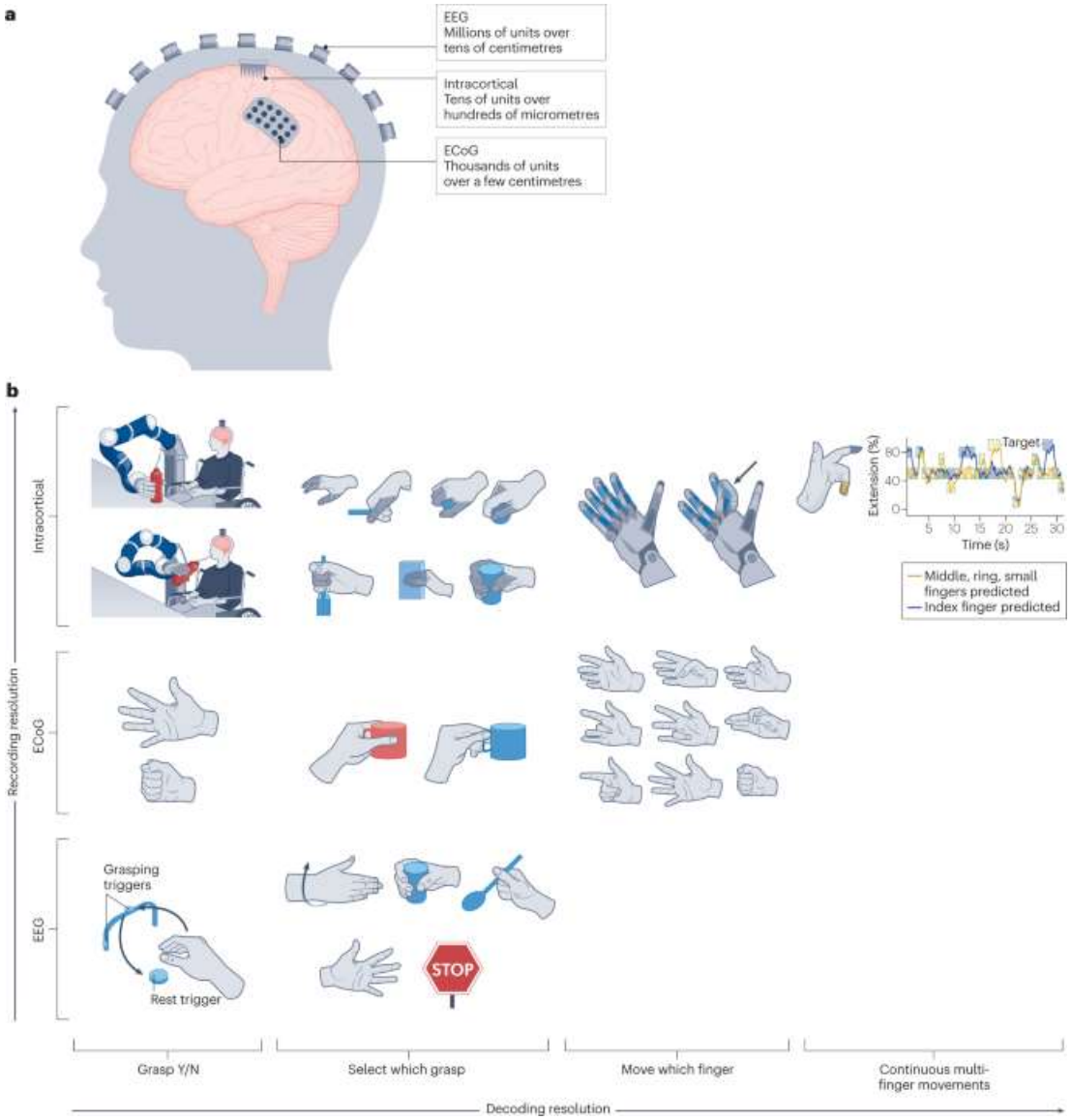

Figure 1-3 Interfaces and strategies to decode hand movements from brain activity.
a, Brain signals can be recorded with transcutaneous (electroencephalography, EEG), intracranial (electrocorticography, ECoG) or intracortical electrodes, from the least to the most invasive interface, resulting in different levels of spatial resolution (number of recorded neurons, or units, and the covered area of cortical tissue). b, Classification of selected studies in terms of type of brain interface used and decoded information, such as the intention to grasp (Pistohl et al., 2012; Randazzo et al., 2015) (with 3D control of a robotic arm; Hochberg et al., 2012), discrete grasps (Colachis et al., 2018; Muller-Putz et al., 2019; Pistohl et al., 2012) discrete single finger movements (Chestek et al., 2013; Jorge et al., 2020) and continuous multi-finger kinematics (Nason et al., 2021). Part b is adapted from (Hochberg et al., 2012), Springer Nature Limited. Part b is adapted from (Colachis et al., 2018), CC BY 4.0 (https://creativecommons.org/licenses/by/4.0/). Part b is adapted with permission from (Jorge et al., 2020), Wolters Kluwer Health, Inc. Part b is adapted with permission from (Nason et al., 2021), Elsevier. Part b is adapted from (Pistohl et al., 2013). CC BY 4.0 (https://creativecommons.org/ licenses/by/4.0/). Part b is adapted with permission from (Pistohl et al., 2012), Elsevier. Part b is adapted with permission from (Chestek et al., 2013), IOP. © [2015] IEEE. Reprinted, with permission, from (Randazzo et al., 2015), adaptation permission from author. © [2019] IEEE. Reprinted, with permission, from (Muller-Putz et al., 2019), adaptation permission from author.

the excitability of motor circuits to a level that allows voluntary activation of preserved, functional corticospinal fibers (Ethier et al., 2015). The key element here is high temporal resolution such that the cortical motor command is synchronized with the afferent signal (Ethier et al., 2015; McFarland & Wolpaw, 2017; Mrachacz-Kersting et al., 2012), rather than achieving 100% decoding accuracy.

1.3.2.2 Invasive Signals: ECoG

In comparison with EEG, a higher spatiotemporal resolution and the elimination of external components can be obtained by recording signals from the surface of the brain using ECoG. Because ECoG electrodes are large and far from the neurons in the cortical layer V projecting to the spinal cord, they still record the combined activity of many neurons. However, ECoG motor signals are more specific and have a larger frequency range of interest than EEG, with mu and beta rhythms still present and a higher-frequency gamma range that is thought to be related to the activity of single neurons (Buzśaki & Wang, 2012). ECoG recordings have been used to accurately classify up to five hand postures and single finger movements (Chestek et al., 2013; Miller et al., 2009; Pistohl et al., 2012, 2013). Moreover, ECoG activity has also been used to control prosthetic hands through online detection and classification of hand or finger movements (Hotson et al., 2016; Yanagisawa et al., 2011). These studies employ linear classifiers, such as linear discriminant analysis or support vector machines. Moreover, offline studies demonstrate accurate 1-DoF continuous hand control with ECoG. For example, linear decoders with nonlinear transforms at the output applied to ECoG recordings can predict single finger kinematics (Flint et al., 2017, 2020) and force (Flint et al., 2020). Moving to completely non-linear methods, a convolutional neural network combined with a long short-term memory has been used for decoding single finger trajectories (Xie et al., 2018), with the convolutional layer replacing the feature extraction pipeline.

ECoG electrodes remain on the surface of the brain and cause little damage or foreign body response, which is thought to allow longer electrode lifetimes and more consistent signals over time compared with more invasive approaches (Schalk & Leuthardt, 2011). However, despite having great potential for clinical applications, it might be difficult to substantially increase the number of hand DoFs controlled by ECoG-based systems. The limited spatial separation of human cortical areas devoted to different fingers limits the specificity that can be reached using ECoG electrodes, which record the summation of the activity of many units.

1.3.2.3 Invasive Signals: Intracortical

The solution that has shown the highest levels of accuracy, control rate and dimensionality involves the recording of spikes through intracortical electrodes. Intracortical electrodes penetrate the cortex, recording from neurons micrometres away and allowing the spiking rate of single units or multi-units to be calculated, thus estimating the neural activation in highly localized areas. Since the early 2000s, intracortical multi-electrode arrays have been used for movement decoding because they allow large ensembles of neurons (100–400 units) to be recorded, which is necessary for dexterous control. Discrete hand movements can be accurately decoded online and offline using intracortical signals. Linear discriminant analysis classifiers applied to intracortical activity can predict the grasping intention during 3D control of a robotic arm (Hochberg et al., 2012) or discriminate between single finger movements (Jorge et al., 2020) in humans with tetraplegia. Similarly, support vector machines applied to intracortical signals could accurately classify four to six grip types offline (Carpaneto et al., 2012) and allow switching between seven hand postures in a human BMI controlled FES study (Colachis et al., 2018). Classification from intracortical recordings has also been performed using non-linear methods, specifically neural networks. Applied on a dataset from the 1990s, in which intracortical activity was recorded one electrode at

a time from NHPs moving all five fingers individually (Schieber & Hibbard, 1993), neural networks were reported to be particularly accurate at classifying which finger was moving (Aggarwal et al., 2008; Hamed et al., 2007), with nearly 100% success offline. Moreover, compared with a support vector machine, a deep neural network showed lower decline in accuracy and lower increase in response time when increasing the number of hand postures to classify (Skomrock et al., 2018). Intracortical signals are also effective for continuous hand control. For example, an intracortical BMI reported continuous decoding of a hand grasp aperture using simple linear regression (Carmena et al., 2003). Similarly, linear control enabled modulation of the grasp aperture of a robotic hand to enable self-feeding in a patient with paralysis (Collinger, Wodlinger, et al., 2013). In this case, accuracy was improved using ridge regression to prevent overfitting (Wodlinger et al., 2015), and in many of these linear-only approaches, part of the time history (typically 100–200 ms) of the signal is included to achieve a better fit. Extending to more DoFs, a linear decoder with one nonlinear transform at the output was used to predict EMGs of up to five hand muscles in a brain-controlled FES system for grasping in NHPs (Ethier et al., 2012). Intracortical signals can be used to decode not only the kinematics of the hand as a whole (Irwin et al., 2017), but also of separate finger groups simultaneously (Nason et al., 2021; Vaskov et al., 2018), showing great potential for recovery of complete hand dexterity. The decoder applied in these studies is the Kalman filter, which was introduced in intracortical BMI studies of the 2000s and is still widely used, and which enables smoother and more controllable movements than traditional linear regression (Kim et al., 2008; Wu et al., 2004).

From an algorithmic perspective, improved performance in continuous BMIs has emerged from refining rather than replacing linear models. For example, retraining parameters based on online data have been developed for 2D cursor movements (Gilja et al., 2012; Orsborn et al., 2014),

but can also improve accuracy when applied to decoding finger kinematics (Vaskov et al., 2018). Neural networks were being explored for continuous control in the early 2000s (Sanchez et al., 2004), but their performance was not yet competitive with linear algorithms. After more than a decade of offline analysis of intracortical data using neural network methods, it is now clear that they can achieve a much better fit to kinematic data than their linear counterparts (Glaser et al., 2020; Haghi et al., 2019; Pandarinath et al., 2018; Willsey et al., 2022). Moreover, the neural network field is constantly advancing, not only for increasing decoding accuracy but also for preventing overfitting, reducing training data and improving computation speed (Gu et al., 2018). Neural networks are being tested for regression in online settings (Willsey et al., 2022) using faster parallel computing and training paradigms (Mehrotra et al., 2018; Santurkar et al., 2018) and regularization methods to prevent overfitting (Ioffe & Szegedy, 2015; Li et al., 2019; Srivastava et al., 2014).

Currently, intracortical electrodes outperform ECoG in hand control in terms of accuracy, control rate and dimensionality, but at the cost of more invasive surgery and potentially less signal stability over time (Schalk & Leuthardt, 2011), which could affect decoder performance. There is ongoing effort to improve intracortical electrode electronics (Even-Chen et al., 2020) and flexibility to increase the stability of the implants and to implement automatic, unsupervised recalibration methods to avoid the frequent collection of calibration data (Bishop et al., 2014; Jarosiewicz et al., 2015).

1.3.3 Intracortical Electrode Technologies

Most intracortical brain–machine interface (BMI) studies in humans and non-human primates (NHPs) have been performed using one or more Utah arrays, arrays of 100 microelectrodes on a 4 mm by 4 mm silicon substrate (Nordhausen et al., 1996; Normann &

Fernandez, 2016). This device has remained the gold standard for decades, establishing a strong track record of long-term safety in dozens of patients (Bullard et al., 2020). However, this device causes substantial scarring in the immediate vicinity of the electrodes (Szymanski et al., 2021; Welle et al., 2020), resulting in a low neuronal yield per electrode, with 70% of arrays having only a 40% or greater yield in the first 3 months and decreasing to 50% of arrays with such a yield at 1 year after implant (Sponheim et al., 2021), thereby limiting performance.

One strategy to solve this problem is to record from more channels and optimize power consumption by recording spiking activity features with lower power than the traditional spike threshold crossing rate (Even-Chen et al., 2020; Nason et al., 2020). There is also an emerging class of subcellular electrodes (<20um cross-sectional area) that cause minimal scarring and which can enable higher long-term neuronal yields than silicon arrays (Guitchounts et al., 2013; Luan et al., 2017; McNaughton et al., 1983; Musk, 2019) using soft materials to match the mechanical properties of the brain (Chung et al., 2019; Hanson et al., 2019; Hong & Lieber, 2019; Liu et al., 2015; Luan et al., 2017; McCallum et al., 2017). However, approaches using soft materials usually require a stiff insertion shuttle to implant the electrode, which can cause damage during insertion. Subcellular electrodes can also be made out of stiff materials that do not require a shuttle such as metals (Ali et al., 2021; Obaid et al., 2020), silicon carbide (Frewin et al., 2016) or carbon fiber (Patel et al., 2015; E. J. Welle et al., 2021; Yoshida Kozai et al., 2012). Even for traditional silicon probes, emerging devices have dramatically higher channel density than the Utah array; for example, the Neuropixel probe has 384 recording sites on a 10-mm-long 70 μm × 20 μm cross-sectional shank, allowing for recording from hundreds of well-isolated neurons per probe (Jun et al., 2017). Another approach is to minimize the foreign body response by coating the implanted electrodes with a neuroadhesive protein coating (Golabchi et al., 2020). With hermetic

feedthroughs (which allow electrical signal transmission without transfer of particles or fluids) getting smaller, miniaturized titanium ceramic packages (Shah et al., 2012) could soon be used in BMIs. Another approach to increase channel count could be achieved using 'neural dust', that is, submillimeter-sized electronic implants spread over large areas of cortex that wirelessly transmit neural data using ultrasound backscatter (Seo et al., 2016), transcutaneous radiofrequency links (J. Lee et al., 2021) and optical interfaces (S. Lee et al., 2018; Lim et al., 2020). Unlike existing high channel-count devices that record hundreds of intracortical signals but only from a few cortical locations, like the Neuropixel probe (Jun et al., 2017), neural dust would allow for single unit-level signals to be obtained across several centimeters of cortex. Moreover, these small electronic implants would eliminate the need for chronic dura openings or a percutaneous connector, allowing for more electrodes to be implanted with lower risk of adverse events to the patient.

1.4 Brain-Controlled Functional Electrical Stimulation

Thus far we have detailed methods to infer intended movements and methods to restore movements. An ultimate goal in this field is to combine these two parts, bypassing the damaged spinal cord to restore dexterous hand movements. Much research has been dedicated to combining these, primarily using intracortical BMI to control stimulation. Studies in non-human primates for example have used intracortical spiking activity to control muscle force with intramuscular electrodes (Ethier et al., 2012; Moritz et al., 2008), to control stimulation to the radial nerve to open the hand for a ball grasp task (Badi et al., 2021), to control continuous hand opening and closing with intramuscular electrodes (Nason-Tomaszewski et al., 2023) or with intrafascicular electrodes (Losanno et al., 2022), and to control epidural spinal cord stimulation to restore voluntary upper limb movements (Barra et al., 2022). A few of these methods have been used in clinical trials as well. Intracortical signals have been decoded into joint angles for controlling arm,

hand, and wrist movements through 36 intramuscular electrodes, ultimately allowing the participant to perform a functional task drinking from a mug of coffee (Ajiboye et al., 2017). Similarly, intracortical signals have been decoded into elbow flexion and hand opening and used to control nerve cuff stimulation in real time to enable a participant to do a self-feeding task (Herring et al., 2023). Another study used intracortical signals to classify hand movements and then was able to classify intended movements in real time and stimulate forearm muscles with an array of surface electrodes to enable a participant to do a pour and stir task (Bouton et al., 2016). Lastly, while a BMI hasn't been used to control epidural spinal cord stimulation at the cervical level, similar stimulation at the lumbar level was controlled with ECoG electrodes, classifying which joint was moving (ankle, hip, or knee), and enabling an individual with tetraplegia to walk (Lorach et al., 2023). A similar control strategy was used with intracortical recordings and cervical spinal cord stimulation to allow NHP with SCI to do a reach-grasp-pull task (Barra et al., 2022) indicating that this could be a viable method in clinical trials.

Notably, in all of these clinical trials the functional tasks were limited to reaching and one or a few grasps. More work is needed both on the BMI side and the FES side to truly restore dexterous hand movements in patients with SCI. On the BMI side, while the dimensionality of control has been improving with better recording technologies and algorithms, it will also be important to understand how well decoding methods will generalize to changes in a task. For example, in FES the hand will be opening and closing in different wrist postures and will be manipulating objects with different forces. In these scenarios, the fingers are expected to move with the same kinematics, however the muscle activations required to move the fingers will change. In addition, similar movements can be made with the hands but with different intentions (i.e. prehensile versus nonprehensile). Ultimately, it is not fully understood how cortical activity

drives movements (see section 1.1.2), so it is unknown how cortical activity will change in these situations. BMI decoders on the other hand have been trained on very structured movements. As a result, error is introduced to the decoders when the task changes for example when moving the wrist at different forces (Naufel et al., 2019), or while trying to maintain a grasp while moving the arm (Bouton et al., 2016). Studies have been successful in designing BMI decoders to be robust for specific applications by augmenting training data (Naufel et al., 2019) or by engineering features for the specific application (Dekleva et al., 2021; Schroeder et al., 2022). More work is needed to determine how accurate BMI decoders will remain in situations common to upper limb FES control and then how to decode intended movements in a robust manner when controlling FES.

Similarly, more work is needed in characterizing how well FES performs when controlling hand movements in different postures or when simultaneously controlling multiple joints. Studies controlling hand and upper limb movements have controlled each joint independently (Ajiboye et al., 2017; Herring et al., 2023). Muscles can have multiple tendons or cross multiple joints, therefore exerting a force on multiple joints when activated. This happens especially in the hand where extrinsic finger muscles cross the wrist and have tendons to each finger. Individuated finger movements for example are generated by the activation of several muscles, all acting on multiple fingers (Schieber, 1995). As a result, stimulation to control the fingers is not independent from stimulation to control other fingers or the wrist like typical FES control strategies would treat them. Unfortunately, there has yet to be a characterization of how well FES can individuate the joints in the hand. Future work should focus on stimulation strategies to individuate joints in the hand as well as how to successfully control the stimulation with a BMI.

1.5 Summary of Thesis

In this thesis, I investigate generalizable BMI decoding for FES applications and using intramuscular FES to restore graded multi-DOF movements in the wrist and fingers, ultimately to improve the reliability and dexterity of restored hand movements with brain-controlled FES.

In Chapter 2, I investigate the impact of task changes, similar to those that may be experienced in FES and acts of daily living, on BMI performance. We have previously established an intracortical BMI to control two finger groups in a virtual hand (Nason et al., 2021). I found that when I changed the context of the task by either adding springs to each finger group or altering the wrist posture, that trained decoders did not generalize well to these new contexts, leading to significant increases in prediction error, especially for muscle activation predictions. Interestingly, context changes only had a small impact on BMI performance when using the decoders in the closed-loop virtual BMI task. I explain this dichotomy by showing that the structure of neural population activity remained similar in new contexts, which could allow for fast adjustment online. Additionally, I found that neural activity shifted neural trajectories proportional to the required muscle activation in new contexts, suggesting a feature that could help predict different magnitude muscle activations while producing similar kinematics. These results suggest that BMIs making predictions of intended kinematics can successfully produce command signals for an FES application and using additional neural features could provide a method to modulate FES commands by the required muscle activation of the task.

In Chapter 3, I investigate how well current FES control strategies can provide graded control of two-DOFs, wrist flexion and hand opening and closing, simultaneously. Two rhesus macaques were implanted with intramuscular electrodes in muscles of the forearm controlling the wrist and fingers. I found that controlling each DOF independently allowed us to move the desired

DOF through a large range of movements, however the stimulation evoked movements in both DOFs. That is, moving the fingers also evoked large movements in the wrist, and moving the wrist also evoked smaller but still significant movements in the fingers. As a result, when controlling both DOF simultaneously, the resulting range of motion changes due to interactions in stimulation for each DOF. Additionally, muscle fatigue has a large and quick (within minutes) impact on the range of motions of evoked movements. Despite this, graded stimulation can be used to acquire targets throughout the range of motion. I also demonstrate a BMI to control continuous finger and wrist flexion that could be used in a nerve block model of hand and wrist paralysis. These results are the first characterization of the effectiveness of intramuscular FES for continuously controlling more than one-DOF in the hand and emphasize that evoked movements in one DOF should not be treated as independent despite that being the common approach for BMI commands.

In Chapter 4, I investigate the efficacy of a new intramuscular electrode implantation method for evoking selective finger movements with NHP. I show that by targeting the various nerve entry points to the extrinsic finger muscles, we can evoke twitches in single fingers and larger movements in combinations of two fingers. This approach gives us control of more distinct finger movements, suggesting a method that can control individual fingers with stimulation on combinations of these electrodes.

Finally, in Chapter 5, I will discuss the results of each study with respect to the full set of research chapters and the current state of the field, present my projections for immediate next steps of this work, and discuss my visions for brain-controlled FES.

Chapter 2 Cortical Activity Changes and Error in Brain-Machine Interface Predictions of Intended Finger Movements Due to Task Context

A version of this chapter "The impact of task context on predicting finger movements in a brain-machine interface" was published in eLife in June 2023 (Mender et al., 2023)

2.1 Introduction

Spinal cord injury affects an estimated 302,000 people in the United States (National Spinal Cord Injury Statistical Center, 2023). People with quadriplegia have ranked the restoration of hand and arm function as very important for quality of life (Anderson, 2004; Collinger, Boninger, et al., 2013). Functional electrical stimulation (FES) is a therapy that can restore hand and arm function by electrically stimulating muscles in order to cause contractions. Studies have demonstrated the use of FES to restore at least some hand function since the 1980s (Kilgore et al., 1989; Peckham et al., 1980), which has resulted in commercially available systems such as the Freehand System (Peckham et al., 2001) that was available until the late 2000s. These systems, however, typically relied on external motion or myoelectric commands from residual muscles. These control schemes for FES require residual function and can be unintuitive to use, especially when controlling more than one degree-of-freedom.

Brain-machine interfaces (BMIs) have the potential to provide more intuitive control signals that enable people with paralysis to interact with computers, prostheses, or control therapies like FES. These BMI capabilities have been made possible by a history of neuroscience studies

finding that motor cortex activity is correlated with a multitude of movement variables, from intrinsic variables like joint angle and muscle activation (Evarts, 1968), to extrinsic movement direction (Georgopoulos et al., 1986). Taking advantage of these correlations allows linear models to predict these movement variables from neural activity. This approach has been used in BMIs to allow non-human primates to control computer cursors (Gilja, Nuyujukian, Chestek, Cunningham, Yu, Fan, Churchland, et al., 2012; Serruya et al., 2002; Taylor et al., 2002), prosthetic arms (Carmena et al., 2003; Velliste et al., 2008), and FES (Badi et al., 2021; Ethier et al., 2012; Moritz et al., 2008). Additionally, success in animal BMIs led to the use of similar models in clinical trials as well (Ajiboye et al., 2017; Bouton et al., 2016; Collinger, Wodlinger, et al., 2013; Gilja et al., 2015; Wodlinger et al., 2015). These studies, however, are generally performed in a controlled lab environment, and use relatively simple linear models to make predictions. One key factor in the translation of lab BMI FES systems to tasks of daily living will be how robust they are to the varying environment found in patient's homes. Groups have included object interaction in their tasks, for example grabbing single objects (Ajiboye et al., 2017; Downey et al., 2017), or different size objects (Wodlinger et al., 2015), however there has not yet been a systematic effort to understand how task context affects BMI performance.

Offline studies of how motor cortex controls movement have helped to inform how well we can expect BMI models to generalize. This work has shown that the linear encoding of movements in motor cortex can change with many factors such as posture or task duration (Churchland & Shenoy, 2007; Kakei et al., 1999; Naufel et al., 2019; Sergio et al., 2005; Stephen H. Scott et al., 2001). Recent studies have emphasized instead that the role of motor cortex is to generate movements rather than represent movements (Churchland et al., 2012; Russo et al., 2018; Shenoy et al., 2013). In this view, the activations of single neurons are coordinated. The underlying

network connectivity constrains population activity to a low-dimensional manifold and activations on this low-dimensional manifold then form the basis for neural dynamics which generate movements (Gallego et al., 2017; Shenoy et al., 2013). A key feature of these dynamics that is different from a representation model is that they may have a more computational function, for example ensuring that outgoing commands can be generated reliably (Russo et al., 2018). The resulting activity may then change when the same movements are done in different ways because a different computation is needed to generate the movements. As a result, an individual neuron's activity, which is related to the latent activity in this low-dimensional manifold, could correlate with movements differently when the task is changed to one that requires different neural dynamics. With respect to BMI applications, the decoding models assuming a linear relationship, and non-linear models that do not account for these changes, would then be unable to make accurate predictions in the new tasks.

It is still unclear how large of a task change will require different neural dynamics and thus a different decoding strategy. It has been shown that different dynamics are required for large changes in a task, such as forward versus backward arm pedaling (Russo et al., 2018), reaching or walking (Miri et al., 2017), or using one arm or the other (Ames & Churchland, 2019). At the same time, there is evidence that tasks with the same movements performed differently may have similar neural dynamics. A recent study found that cycling at different speeds led to similar elliptical trajectories in high variance neural dimensions, with a lower variance dimension encoding task speed (Saxena et al., 2022). Additionally, a study of isometric, resisted, and free-moving wrist movements found a neural manifold that explained a large amount of neural variance in all tasks (Gallego et al., 2018) and a similar study comparing the same wrist movements found that they could still predict muscle activations between the contexts although it required a gain-factor related

to required muscle activation (Naufel et al., 2019). These observations suggest that the neural dynamics may be similar across tasks with small changes, such as a change in speed or muscle exertion, with differences occurring in lower variance dimensions of population activity.

Which tasks require a change in neural dynamics is a particularly important question to study for hand movements, as the hand is the major end effector interacting with the environment in varying postures and with different loads. However, this work has not yet been extended to continuous finger movements. Finger movements are less studied than arm reaches but initial studies show that grasping movements may show different dynamics due to the increased proprioceptive and tactile feedback present (Goodman et al., 2019; Suresh et al., 2020). In a promising start to studying decoder generalization for individuated finger movements, it has been shown previously that multiple finger movements can be predicted simultaneously, in real-time, and that a linear model trained with data from individual finger movements could also predict combined finger movements (Nason et al., 2021), suggesting that individual finger movements and combined finger movements may have similar neural dynamics.

In this study, we investigate how well the decoding of finger movements from intracortical neural activity in nonhuman primates can generalize to realistic alterations of the context in which a task is performed, similar to those that may be found in a BMI user's home. These context shifts represent a small range of the possible shifts but relate back to common musculoskeletal changes in the task, i.e. muscle length and activation. We ask how the relationship between intracortical neural activity, non-prehensile finger movements, and the related muscle activations are impacted by context changes, such as spring-like resistances and postural changes. We show that these context changes reduce our ability to predict finger kinematics and finger-related muscle activations offline. However, in an online kinematic-based finger BMI task, the monkey can

accommodate for the changed task context and achieve near equivalent performance with or without the context change. We explain this by showing that the underlying neural manifolds stay well aligned between contexts, the neural dynamics are shifted due to context, and the shift in neural dynamics can be related to the muscle activation required in the new context.

2.2 Results

2.2.1 Context Changes Alter Muscle Activations and Neural Activity

We are ultimately interested in understanding the impact of context changes, such as wrist flexion or spring resistance, on BMI decoding performance. In the virtual finger movement task (Figure 2-1A), the monkey moves their fingers within a manipulandum in order to move virtual fingers on a screen in front of them. Cortical spiking activity is recorded during these movements. The monkeys perform center-out and back movements in which they individuate index and middle-ring-small (MRS) finger groups to make one of eight movements (Figure 2-1B) starting from rest, hold the target, then return to rest. In some versions of the task the monkeys performed these movements with all fingers held together for 1-degree-of-freedom (1-DOF, Figure 2-1B bottom). Monkey N additionally had eight chronic electromyography (EMG) leads implanted in muscles of the hand and wrist (see Methods, Table 2-2) which were recorded from during manipulandum control trials. During the BMI task, a Kalman filter (KF) model is trained to relate cortical activity to finger movements, and the monkey controls the virtual hand with their brain activity through this model. We first asked whether introducing context changes during the manipulandum controlled virtual finger movement task causes any change in behavior, muscle activation, or neural channel activation. Our first manipulations were the addition of torsional springs or the static flexion of the wrist by 23 degrees (Figure 2-1C), referred to as the spring and

wrist contexts, respectively, during the 1-DOF center-out task. The torsional springs resist flexion such that more force is required to flex the fingers but less force is required to extend the fingers.

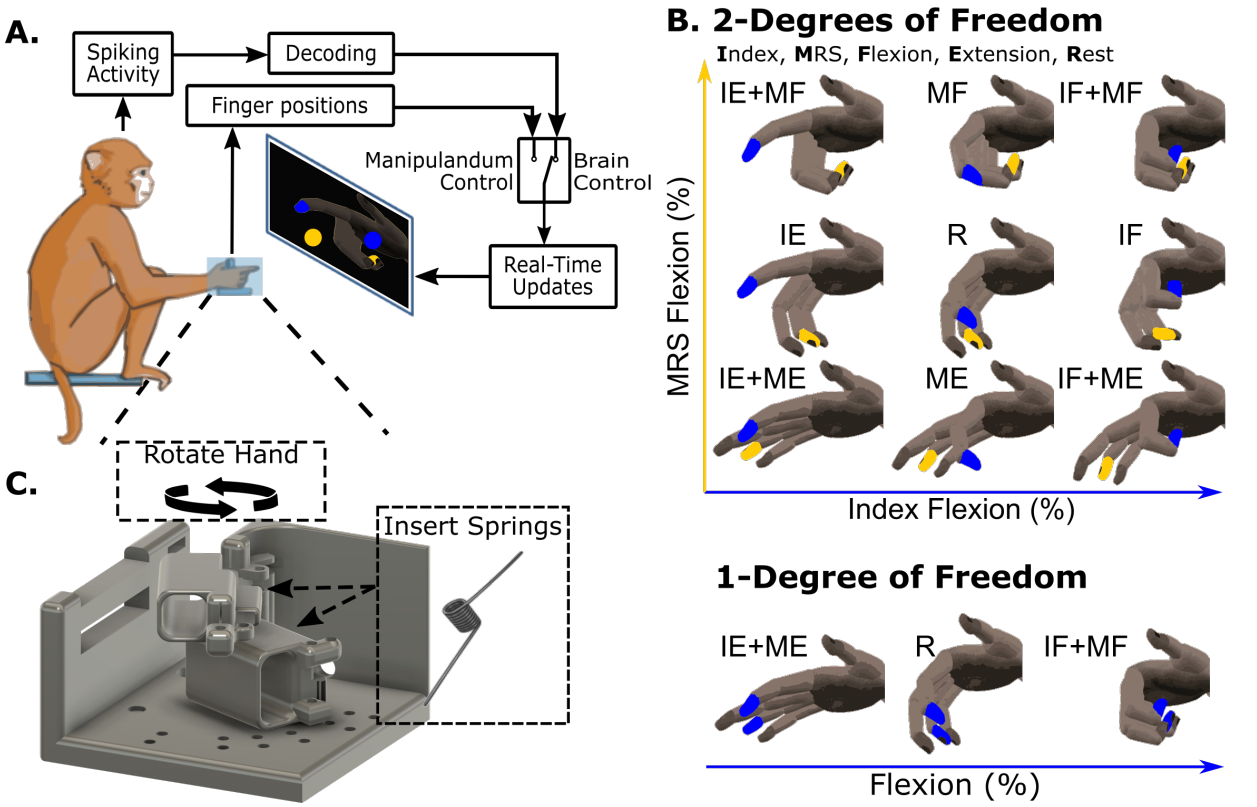

Figure 2-1 Illustration of the behavioral task and context changes.
(A) Experimental setup during manipulandum control and brain-machine interface (BMI) control experiments. The monkey individuates their index and middle-ring-small finger group, moving each in the manipulandum in order to acquire targets on the screen in front of them. During this task, neural activity and finger positions are both recorded. A model relating neural activity to intended finger movements can be trained and then used in real time to control the virtual hand in front of them. (B) Illustration of the possible finger movements. For 2-degree-of-freedom (2-DOF) movements, the index flexion is represented on the x-axis and MRS flexion is represented on the y-axis. In some tasks the monkeys also did a 1-DOF movement, which required flexing or extending all fingers together. (C) To alter the context of the task, the manipulandum could be rotated so that the wrist was flexed and torsion springs could be added to the underside of the finger doors. The torsion springs were at rest when the finger doors were at full extension and thus resisted flexion and assisted with extension.

We expected the springs to cause minimal change in finger velocity during movements but a large increase in muscle activation for flexor muscles during flexion and a decrease in activation for extensor muscles during extension. The springs were chosen to be as strong as possible without decreasing the monkey's motivation during the 2-DOF task. As a result, the task could still be completed close to as fast as their reactions allow. Figure 2-2A shows finger position and velocity

traces averaged over all flexion trials (solid lines) and all extension trials (dashed lines) on one representative day with the 1-DOF task for Monkey N where the spring manipulation was tested. We see small changes between the velocities in normal trials (black traces) and spring trials (blue traces). To quantify this change, we compared the peak velocities between normal trials and other context trials for one representative session with each context (Figure 2-2C). Each monkey had slight behavioral differences in how quickly they performed the task with context changes leading to small changes in peak velocities. We found that the largest changes in peak velocity were Monkey N extending fingers 12.5% faster during wrist trials ($p=5e-24$, two-sample t-test), and Monkey W flexing fingers 22.3% faster during wrist trials ($p=2.6e-11$, two-sample t-test), with both monkeys showing small changes in peak movement velocity for at least one movement in each context ($p<0.05$, two-sample t-test).

In contrast, during the same 1-DOF task, muscle activations change substantially for trials toward both targets (Figure 2-2B), showing trends such as increased flexor digitorum profundus (FDP) muscle activation for flexion and less extensor digitorum communis (EDC) activation for extension. All muscles implanted for Monkey N are included in Table 2-2 (Methods) while Monkey W did not have EMG electrodes. Using the same representative sessions for Monkey N, we compared the average muscle activations from Monkey N in a 420ms window around peak movement between normal trials and off-context trials (Figures 2-2D and 2-2E). During spring trials, we found that every muscle except FCR required significantly higher than normal muscle activation for flexion (Figure 2-2D blue, $p<0.004$ two-sample t-test), an average increase of 91.9% for the finger flexor muscles (FDPid, FDPip, FDP), and every muscle except FDP and FCU required less muscle activation for extension (Figure 2-2E blue, $p<1e-5$ two-sample t-test), an average decrease of 8.2% in finger extensor muscles (EIP, EDC). Interestingly, even extensor

muscles were more activated during spring flexion trials, indicating that Monkey N was co-contracting muscles more and moving with more stiffness. During wrist trials, finger flexor muscles showed an average 53.3% increase in activation for flexion trials (Figure 2-2D yellow) and finger extensor muscles had an average 32% decrease in activation for extension trials (Figure 2-2E yellow).

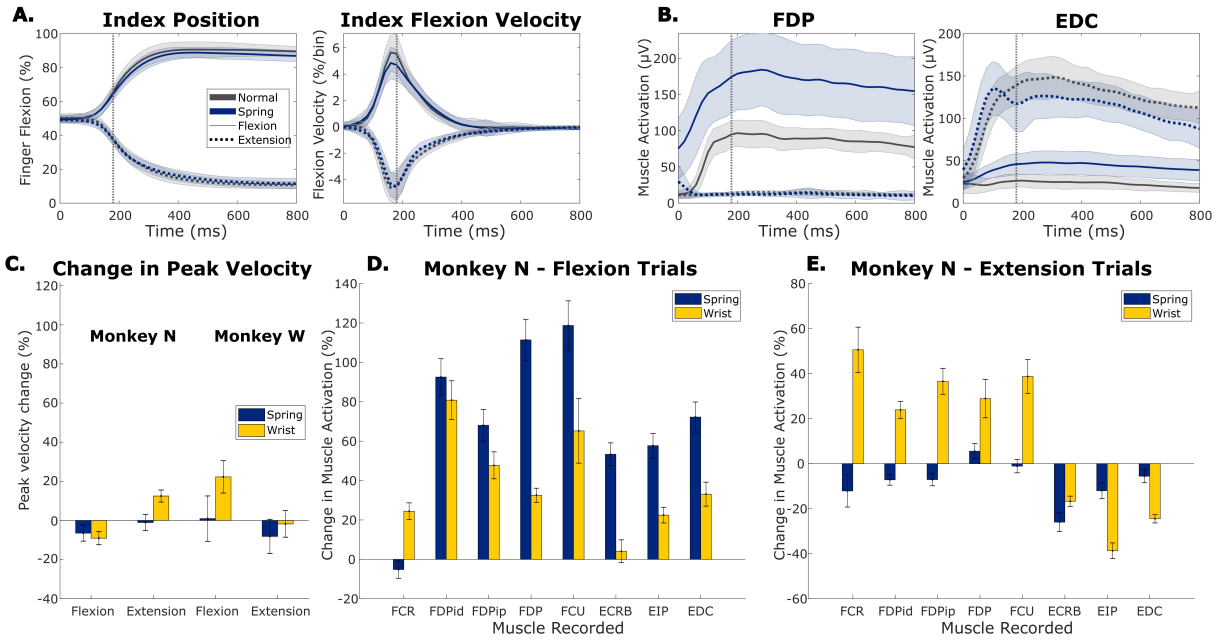

Figure 2-2 The impact of context changes on kinematics and muscle activation.
(A) Trial-averaged traces of index finger position and index finger flexion velocity for an example 1-degree-of-freedom (1-DOF) spring session with Monkey N. Trials are aligned to peak movement (vertical gray line). Black traces are normal trials, blue are trials with springs in the manipulandum, solid traces are for flexion trials, and dotted traces are for extension trials. Shaded area shows one standard deviation. (B) Trial-averaged traces of flexor digitorum profundus (FDP) muscle activation and extensor digitorum communis (EDC) muscle activation for an example spring session with Monkey N. Formatted the same as (A). (C) Change in peak velocity between normal trials and trials with either springs present or the wrist flexed for both Monkey N (left) and Monkey W (right). Trials are split by movement direction, either flexion or extension. Error bars indicate 99% confidence interval based on a two-sample t-test. (D, E) Change in average muscle activation in a window around peak movement between normal trials and trials in the spring (blue) or wrist context (yellow) for all eight muscles recorded in Monkey N. Trials are split between flexion (D) and extension (E) movements. Error bars indicate 99% confidence interval based on a two-sample t-test.

After establishing that context had a large effect on muscle activity with a relatively small effect on finger kinematics, we next evaluated whether neural activity changed due to the addition of springs or altered wrist posture. For each neural channel we recorded two features, the threshold crossing firing rate (TCFR) and spiking band power (SBP). SBP is a low-power feature that has

been previously shown to be well correlated with the firing rate of the largest amplitude unit (Nason et al., 2020), often enabling us to identify more tuned channels. For both Monkey N and Monkey W, we evaluated how many channels were tuned to movement and how many of these tuned channels modulated activity with context change. Tuning and context modulation were determined by regressing finger kinematics with channel activity and channel activity multiplied by a dummy variable for context, as described in the Methods, one channel at a time. Regression coefficients were tested for significance with a t-test, a significant channel activity coefficient indicated that channel was tuned, and a significant dummy variable coefficient indicated that context modulated the channel's tuning. The results are included in Table 2-1. The SBP feature resulted in an average of 86.9 and 28 tuned channels of 96 for Monkey N and Monkey W, respectively, while TCFR resulted in an average of 36.7 and 11.8 tuned channels of 96 for Monkey N and Monkey W, respectively. An average of 24.4% of the tuned TCFR channels and 37.7% of the tuned SBP channels significantly changed activity with the wrist context and an average of 56.8% of the tuned TCFR channels and 52.3% of the tuned SBP channels significantly changed activity with the spring context. As both features had a similar proportion of tuned channels that

Table 2-1 Channels tuned to movement and modulated by context
The number of channels tuned to any movement using two features (threshold crossing firing rate [TCFR] and spiking band power [SBP]) and the percentage of tuned channels that showed a significant change in neural feature between normal trials and trials in the tested context for four types of experimental sessions (Monkey N or Monkey W with the spring or wrist context).

	TCFR		**SBP**	
	Tuned Channels	% Context Modulated Channels	Tuned Channels	% Context Modulated Channels
Monkey N Spring Days (n=3)	**38.3** (SD=4.0)	**47.0%** (SD=2.8)	**89.3** (SD=2.1)	**61.7%** (SD=12.0)
Monkey N Wrist Days (n=2)	**35.0** (SD=1.4)	**43.1%** (SD=9.8)	**84.5** (SD=7.8)	**54.4%** (SD=0.8)
Monkey W Spring Days (n=3)	**12.0** (SD=1.0)	**66.5%** (SD=2.8)	**35.0** (SD=6.9)	**42.8%** (SD=7.1)
Monkey W Wrist Days (n=2)	**11.5** (SD=3.5)	**5.6%** (SD=7.9)	**21.0** (SD=5.7)	**20.9%** (SD=4.5)

Standard deviation (SD) is calculated across sessions of the same type and n is the number of sessions of that type which is indicated in the first column.

were modulated by context changes, we opted to use SBP as the primary feature for the subsequent analyses in order to increase the number of tuned channels available for analysis.

2.2.2 Decoding Neural Activity Across Task Context

After confirming that these context changes had large impacts on muscle activation (Figure 2-2) and affected many channels of neural activity (Table 2-1), we next asked how this will impact the ability to decode intended movements for BMI applications. Typically, BMIs use linear models to relate neural firing rates to the desired control variable (Ajiboye et al., 2017; Nason et al., 2021; Wodlinger et al., 2015). Given the work showing that task changes similar to those tested here can alter how motor cortex linearly encodes muscle activations during different wrist movements across tasks (Naufel et al., 2019), we next ask if the same is true for individuated finger movements. To test this, we recorded kinematics for both monkeys and muscle activations for Monkey N during the 2-DOF task and then trained linear models with data from normal trials to predict muscle activations or kinematics in unseen normal trials or other context trials.

We first present the results for decoding Monkey N's muscle activations across context. Figure 2-3A shows average predictions of FDP and EDC muscle activations for normal trials and spring context trials from one example experimental day, both using a linear model trained on normal trials. We found that within-context linear models, that is models trained and tested on trials of the same context, could predict muscle activations well during individuated finger movements, with accuracy comparable to predictions of kinematics (Appendix Tables A-1 – A-4). However, models trained on normal trials are consistently unable to predict muscle activations well in the off-context trials (Figure 2-3B). For example, when springs are present the predictions do not account for the large changes in FDP activation magnitude or EDC activation during flexion trials (Figure 2-3A, Figure 2-4). Across three sessions in each context including the wrist, spring,

or both wrist and spring contexts, prediction mean-squared error (MSE) increased significantly from the normal trial baseline. This held true for both flexor muscles (FDP, FDPip) and extensor muscles (EDC, EIP) (evaluated by paired t-test, p<2e-9), in each tested context, with an average increase of 188.7% across all context changes and muscles. The increases in error varied widely, ranging from a 21% increase (flexor muscles with wrist-flexed) to a 356% increase (flexor muscles with both wrist-flexed and springs).

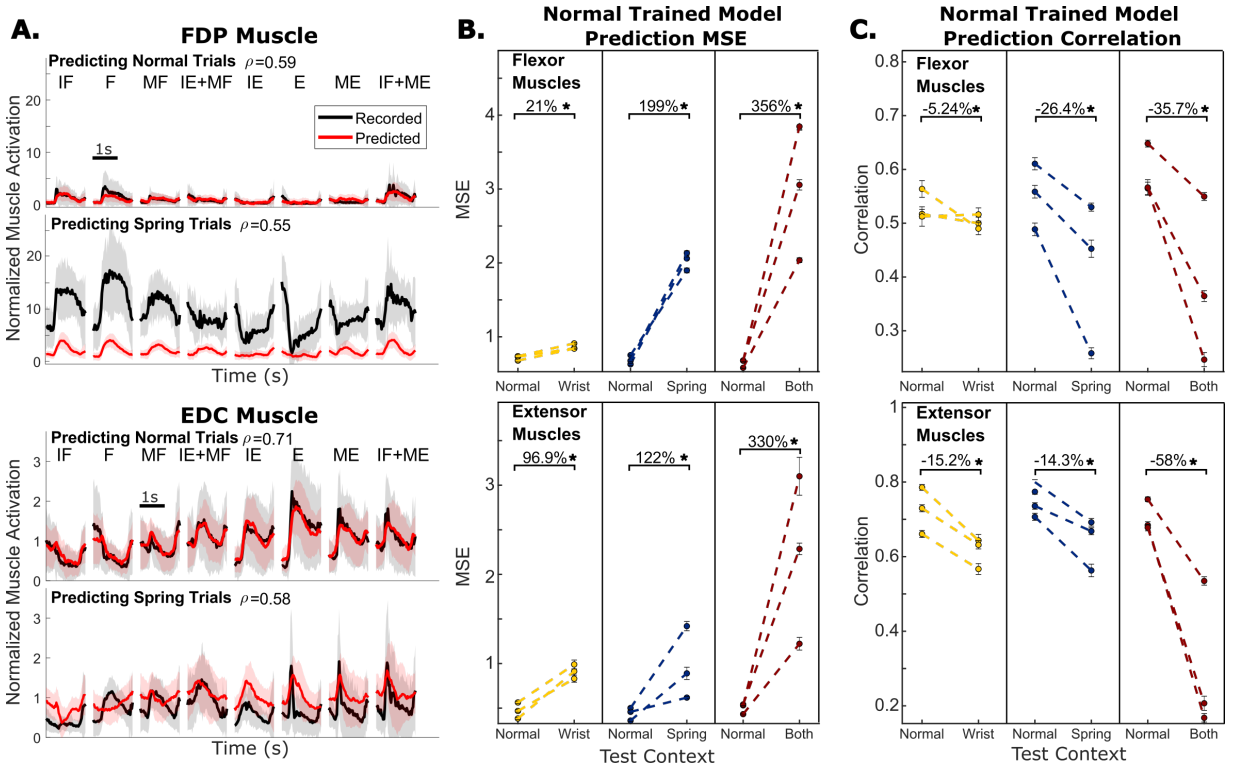

Figure 2-3 Offline predictions of muscle activations.
(A) Recorded and predicted muscle activation traces for flexor digitorum profundus (FDP) muscle (top half) and extensor digitorum communis (EDC) muscle (bottom half) from one example session with Monkey N. Traces are aligned to peak movement and averaged over trials to the same target, shading represents one standard deviation. Predictions are from a model trained only on normal trials and the model is evaluated either on normal trials (top) or trials with springs present (bottom). r indicates the linear correlation coefficient between recorded and predicted muscle activations using all trials in the specified context for that session, excluding the normal context trials used for training the model where applicable. IF – index flexion, MF – MRS flexion, F – both fingers flexion, IE – index extension, ME – MRS extension, (E) – both fingers extension. (B) Change in prediction mean-squared error (MSE) when a model trained on normal trials is evaluated on trials in a different context. Color indicates which context is being tested, yellow is wrist, blue is spring, and both is red. Each dashed line and pair of dots represent one session during which the same model was used for both measurements. Error bars on the dots indicate one standard deviation for model performance calculated with 10-fold cross-validation. (C) Same as (B) but model performance is measured with prediction correlation.

We next asked whether this dramatic increase in prediction error is driven by a simple offset or magnitude change, or a reduced linear relationship with recorded muscle activations. For example, while the off-context predictions of FDP activation during flexion in Figure 2-3A both do not account for the offset in muscle activation at the beginning of trials and do not predict a large enough change in the magnitude of muscle activation throughout the trial, the same linear correlation is maintained. As a result, these predictions might only need a bias and scaling adjustment to recover performance. Alternatively, during flexion, the off-context predictions of EDC activation are less correlated with measured EDC activation because the model predicts EDC inactivation, which occurs during normal trials. However, in spring trials, measured EDC activation actually increases for flexion due to Monkey N co-contracting to move more stiffly. Since MSE is influenced by both changes to linear correlation and changes to offsets and scaling, we also measured prediction correlation (Figure 2-3C) which is less affected by the changes to offsets and scaling. Using the same sessions and models trained on normal trials as when we measured MSE, we found that prediction correlation decreased from normal baseline by an average of 25.8% across tested contexts and muscles. This change was significant for all tested contexts (paired t-test), ranging from a 2.4% decrease for FDPip in the wrist context ($p=0.03$) to a 69.4% decrease for EDC in the both context ($p=1.3e-17$). While significant, the change in correlation was a smaller effect than the change in MSE.

Kinematics are used as a control signal in BMI applications more frequently than muscle activation so we next examined the error in predicting finger position and velocity across contexts. Figure 2-4A shows trial-averaged predictions for each target from training a linear model on normal trials and predicting normal trials or spring trials for an example session with Monkey N. In both index and MRS flexion predictions, we observed the off-context predictions to be worse

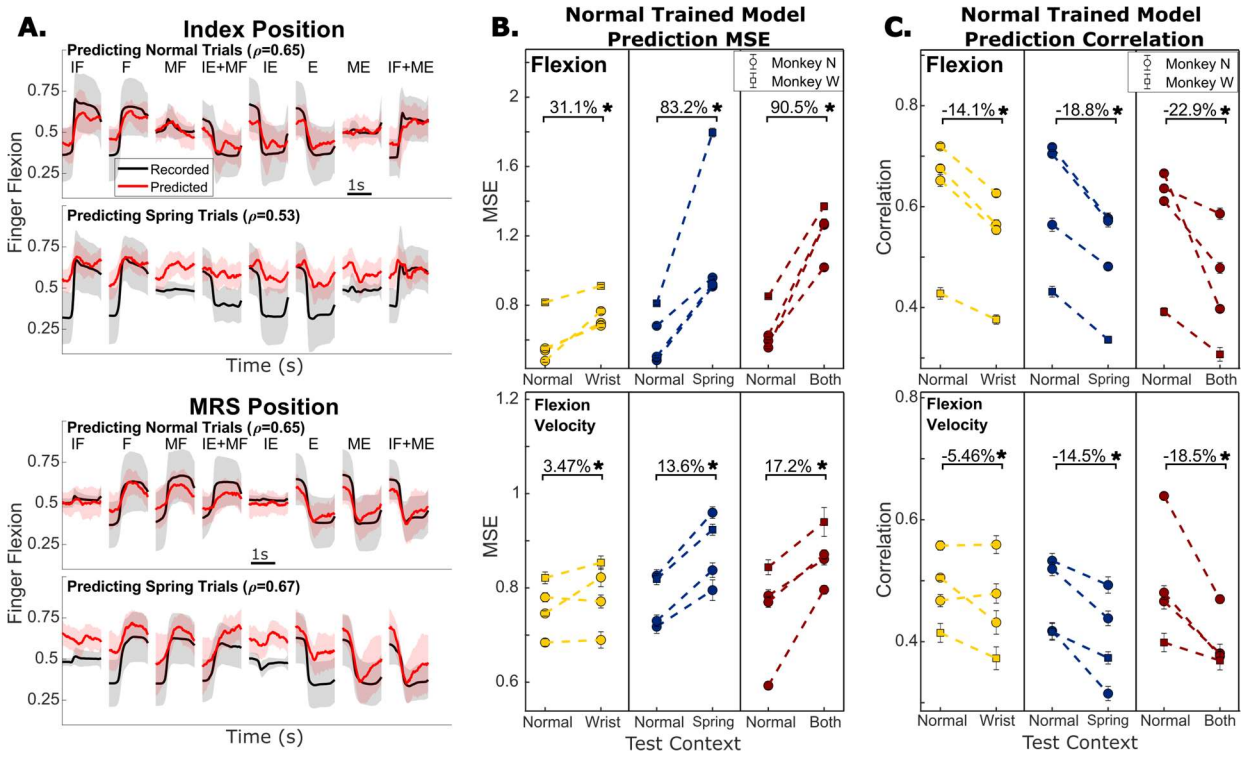

Figure 2-4 Offline predictions of kinematics.
(A) Recorded and predicted position traces for index finger position (top) and middle-ring-small (MRS) finger group position (bottom), averaged across all trials toward each target. Shading represents one standard deviation. Predictions are from a model trained only on normal trials and the model is evaluated either on normal trials or trials with springs present. r indicates the linear correlation coefficient between recorded and predicted finger positions using all trials in the specified context for that session, excluding the normal context trials used for training the model where applicable. (B) Change in prediction mean-squared error (MSE) when a model trained on normal trials is evaluated on trials in a different context. Color indicates which context is being tested, yellow is wrist, blue is spring, and both is red. Each dashed line and pair of dots represent one session during which the same model was used for both measurements. Error bars on the dots indicate one standard deviation for model performance calculated with 10-fold cross-validation. (C) Same as (B) but model performance is measured with prediction correlation.

than the normal trial predictions. Predictions during the spring trials often showed a bias towards flexion. We measured changes in prediction accuracies on three days for each context – spring, wrist, and both – for Monkey N, and one additional day with each context for Monkey W (Figure 2-4B, Figure 2-4C). All context changes resulted in significantly higher prediction MSE (paired t-test, p<1e-4), averaging 68.2% for finger position and 11.4% for finger velocity. All context changes also resulted in small but significant decreases in prediction correlation (paired t-test, p<1e-4), averaging -18.6% for finger position and -12.8% for finger velocity. The smaller change

in the correlation of position predictions indicates that much of the prediction error is coming from offsets or magnitude differences in the predictions.

2.2.3 Changing Task Context Has Small Effects on Online BMI Performance

Based on these offline prediction results, we might expect that in a real-time BMI when cortical activity is controlling the virtual hand, a model trained on normal trials will be more difficult to use when controlling a virtual hand in a new context. We investigated this by training either a KF or a ReFIT Kalman filter (RFKF), as done previously by Nason et al. (2021), and having the monkey control the virtual hand with the model while we applied context changes to this virtual task. Briefly, the KFs are standard position/velocity KFs that update virtual finger position by integrating the predicted finger velocity in the current time step. We introduced context changes in two separate ways. First, we added springs, a static wrist flexion, or both to the manipulandum and had the monkey control the virtual hand with an RFKF trained on normal trials. Second, we trained different KFs using training data collected in different contexts and had the monkeys use the KFs in the online task without any context changes applied to the manipulandum. Due to the quality of recorded neural signals, Monkey W controlled only 1-DOF online while Monkey N controlled 2-DOF online

We first tested whether online BMI performance changed when using a standard RFKF with context changes added to the manipulandum, referred to as the manipulandum context change BMI experiments. One RFKF model could be tested on multiple context changes in a single session. For example, Figure 2-5A shows the acquisition times during an experimental session where two contexts, spring and wrist, were tested in sets of separate trials. Figure 2-5B summarizes the changes in online performance over six experimental sessions for Monkey N and four sessions for Monkey W. During these 10 sessions the context changes were tested 15 times: four times for

the wrist context, seven times for the spring context, and four times for the combined wrist and spring context. Each bar compares the performance during one of the 15 tests between normal trials and one off-context condition in a session when using the same model for both. In two of these tests with Monkey N (one spring and one combined wrist and spring), random target presentation was used instead of center-out to increase task difficulty. Ultimately, both monkeys reached the same levels of performance despite added context changes to the manipulandum. Of the 15 tests, only one test resulted in a significant change in at least one of the performance metrics ($p<0.01$, two-sample t-test). In this case, Monkey N using the RFKF while his wrist was flexed resulted in a 13.0% increase in time to target ($p=6.7e-3$), the equivalent of 86 ms. This overall lack of change was somewhat surprising since the offline decoding results had greater prediction error. The expectation was that when the monkey moved their hand along with the BMI task, the performance would be impacted due to the context change. However, the data show that the monkeys made adjustments to how their hand moved with the online task (Appendix Figure A-1).

To measure the amount that the monkeys had to adjust during online trials to get to average performance, we calculated the average acquisition time, defined as the time to reach the target plus the time to finish orbiting the target, for the first five trials after the start of online trials and compared that between normal and off-context runs of BMI trials. Acquisition times were z-scored within a series of trials performed in the same context before calculating the average in the first five trials. Figure 2-5C shows the distribution of these average acquisition times for every instance the online trials were started, split between normal trials and off-context trials. Monkey N had slightly worse initial performance during normal online BMI use as the average acquisition time during the first five trials was significantly greater than zero ($p=0.002$, one-sample Kolmogorov-Smirnov test). Monkey W, on the other hand, did not have significant adaptation from the first five

BMI trials (p=0.22, one-sample Kolmogorov-Smirnov test). Interestingly, the performance in the first five off-context trials is not different from normal trials for both monkeys (two-sample Kolmogorov-Smirnov test, p=0.88 for Monkey N, p=0.79 for Monkey W). This suggests that adaptation to a BMI with the context changes tested here is as difficult as adaptation from hand control to BMI control.

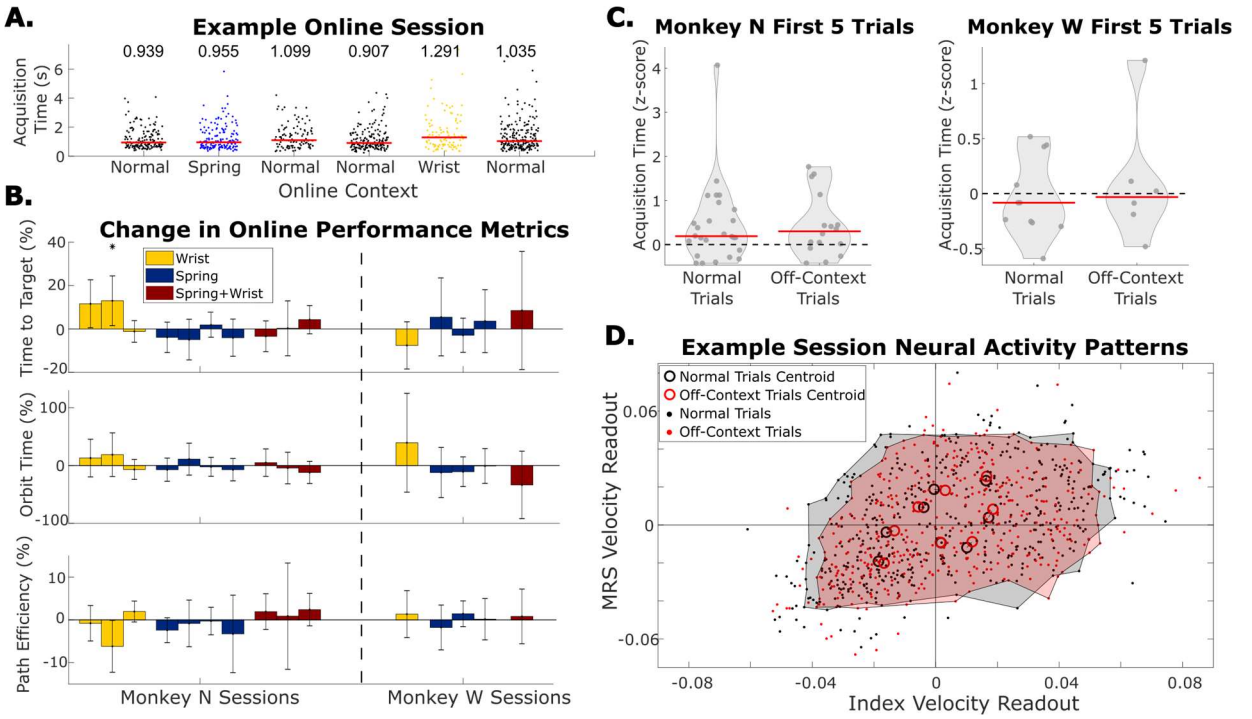

Figure 2-5 Online performance when context changes are tested by adding changes to the manipulandum during online trials.
(A) Example online session in which both the spring and the wrist context are tested. Each dot indicates acquisition time of one trial, each grouping of dots is a series of trials before the context was changed. Red bars and numbers above each grouping illustrate the median acquisition time (in seconds) for that series of trials. (B) Change in performance metrics between normal online trials and online trials with the context change indicated by the bar color in the manipulandum. Each bar indicates one session where off-context online trials are compared to the normal online trials immediately before and after them. Error bars indicate 99% confidence interval in performance metric change. Dashed line separates Monkey N sessions from Monkey W sessions. (C) Average acquisition time during the first five trials each time online trials were started, split between normal trials and trials with context changes applied to the hand (off-context). Acquisition times were z-scored within a series of trials in the same context. Red lines indicate the median. (D) Neural activity patterns for one example session. Neural activity patterns are velocity predictions at the time point of peak brain-machine interface (BMI) movement using a single linear regression model trained on normal offline trials. Each dot indicates the readout velocity for one trial using the same linear model but for either a normal trial (black) or an off-context trial (red). Larger open circles indicate the centroid of velocity readouts for trials to one of eight target directions split by normal and off-context trials. Shaded areas bound patterns for all trials excluding trials outside the 95th percentile of index or middle-ring-small (MRS) velocities.

To help explain this minimal change in online performance, we examined the monkeys' neural activity during online trials. Similar to other BMI adaptation work (Golub et al., 2018a), we used predicted velocities as a low-dimensional behaviorally relevant readout of neural activity during online trials. The velocity predictions are made using a linear regression model trained on SBP from the normal offline training trials in that session with an additional 250 ms history (five 50 ms bins) of SBP from each channel appended as additional features. We call the predicted index and MRS velocity at the time of peak online velocity the 'neural activity pattern' for that trial. An example session for Monkey N is shown in Figure 2-5D with trials split between normal BMI trials (black dots) and off-context BMI trials (red dots). This session was one of two sessions near the median change in online acquisition time between contexts across the 10 sessions for Monkey N. Open circles show the centroid of velocity readouts for all trials in that context toward the same target. The close proximity of the centroids and the overlap of the cluster of normal and off-context points in general indicate that similar neural activity patterns were being produced. This suggests that the monkey was using the same strategy in both types of trials even though the precise patterns may have differed. Across 13 online tests, the target neural activity pattern centroids did not change their magnitude along the target direction when compared between context for flexion targets, extension targets, and split targets (Appendix Figure A-2, two-sample t-test with 5% false discovery rate correction). Note that we excluded the two sessions with random target presentation from this analysis because trials did not have consistent target directions for calculating centroids.

In a second online experiment, referred to as the two decoder BMI experiments, the monkeys alternated between using two KFs: one trained on normal trials and another trained on off-context trials. In this paradigm the context change is added to the model used in a closed loop BMI so that it directly impacts BMI control. Monkeys N and W performed these tests on 9 and 6

separate days, respectively. On each day, two decoders were trained in order to compare one context change. Figure 2-6A shows an example session alternating between a decoder trained on normal trials and a decoder trained on wrist trials. Figure 2-6B shows the performance changes for 15 sessions with five, six, and four sessions testing the wrist, spring, and combined wrist and spring contexts, respectively. In 15 sessions, this experiment revealed small but significant changes in at least one performance metric for 11 sessions (Figure 2-6B, $p<0.01$, two-sample t-test) although only two sessions had worse online performance for all three metrics. The significant decreases in performance averaged 32.6% for time to target, 46.5% for orbit time, and 8.5% for path efficiency, with the combined context having the largest effect.

We compared the acquisition time in the first five trials while using the normal decoder or an off-context decoder (Figure 2-6C). Normal and off-context trials on average did not show different relative performance in the first five trials. Similar to Figure 2-5C, Monkey N had higher acquisition times in the first five trials ($p=0.008$, one-sample Kolmogorov-Smirnov test) that is the same between using the normal model and off-context models ($p=0.99$, two-sample Kolmogorov-Smirnov test). Monkey W once again did not show a significant initial adaptation ($p=0.17$, one-sample Kolmogorov-Smirnov test) which was the same between using the normal model and off-context models ($p=0.5$, two-sample Kolmogorov-Smirnov test). This indicates that for both monkeys, adapting to the off-context decoder was as difficult as adapting to the normal decoder.

As the off-context online performance was worse in many of the two decoder BMI sessions, we next asked if this BMI task required more adaptation than when context changes were added to the manipulandum. As done previously, we calculated neural activity patterns, that is velocity readouts from neural activity for each online trial. These patterns were calculated using

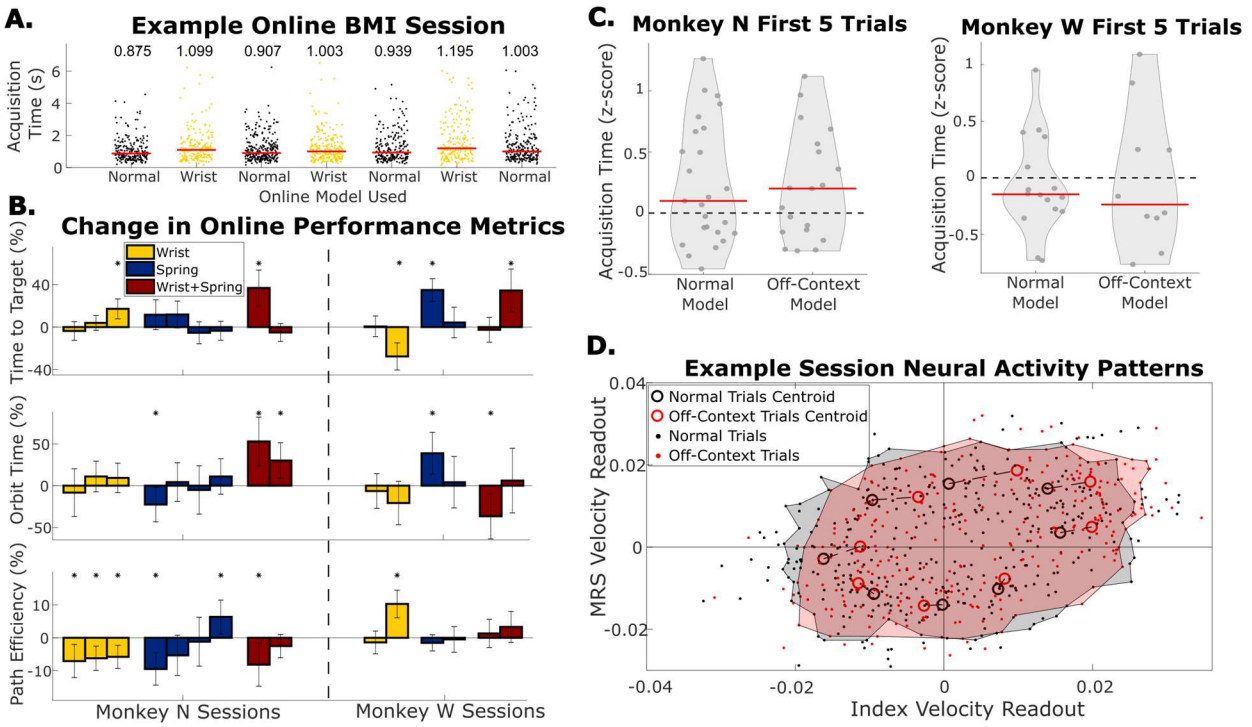

Figure 2-6 Online performance when context changes were tested by using decoders trained with normal training data or off-context training data.
(A) Example online session in which the wrist context was tested. Each dot indicates acquisition time of one trial, and each grouping of dots is a series of trials before the context was changed. Red bars and numbers above each grouping illustrate the median acquisition time (in seconds) for that series of trials. (B) Change in performance metrics between normal online trials and online trials with the context change indicated by the bar color. Each bar represents one session where off-context online trials are compared to the normal online trials immediately before and after them. Error bars indicate 99% confidence interval in performance metric change. The dashed line separates Monkey N sessions from Monkey W sessions. (C) Average acquisition time during the first five trials each time online trials were started, split between trials performed with the model trained on normal trials and the model trained on off-context trials. Acquisition times were z-scored within a series of trials with the same model. Red lines indicate the median. (D) Neural activity patterns for one example session. Neural activity patterns are velocity predictions at the time point of peak brain-machine interface (BMI) movement using a single linear regression model trained on normal offline trials. Each dot indicates the readout velocity for one trial using the same linear model but for either a normal trial (black) or an off-context trial (red). Larger open circles indicate the centroid of velocity readouts for trials to one of eight target directions split by normal vs off-context trials. Shaded areas bound patterns for all trials excluding trials outside the 95th percentile of index or middle-ring-small (MRS) velocities.

one linear regression model trained on the normal context offline training trials from the same session. Ultimately, observed adaptation was a small effect, likely due to very high correlations between the velocity decodes with both KFs (Appendix Figure A-3). Neural activity patterns for an example session for Monkey N with the median change in acquisition time are shown in Figure 2-6D. Neural activity patterns for trials using the normal model are represented in black and patterns for trials using the off-context model are represented in red. While the overall repertoire

of neural activation patterns largely overlaps, we saw small shifts in the centroids of patterns for individual targets. These shifts in this session included higher velocity for flexion and smaller velocities for extension in the off-context trials. A shift toward higher velocities suggests that the monkey was 'pushing' harder during those trials. When comparing these centroids in all sessions the shifts along the target direction were generally larger for these two decoder sessions than the manipulandum context changing sessions (Appendix Figure A-2, Appendix Figure A-4). Additionally, across the 15 sessions there was a trend that if the monkey had to push harder, that would happen during flexion trials (Appendix Figure A-4), all three significant increases (two-sample t-test with 5% false discovery rate correction) were for flexion targets. Altogether, this indicates a small trend that the monkeys would re-aim during off-context flexion trials in the two decoder sessions by aiming for a target further from center (i.e. pushing harder).

2.2.4 Context Shifts Population Neural Activity

To help explain how the monkeys were able to adjust to different contexts during the online task, we further examined changes in neural activity during the offline task in different contexts. First, we ask if there are any obvious trends in how the channel activity changes during simple 1-DOF movements, for example increasing neural activation when flexion requires more muscle activation. In one experimental session, Monkey N performed the 1-DOF task normally as well as in the wrist, spring, and rubber band contexts. The rubber bands altered the required muscle activations for the task in the same way as the springs, however to a larger extent, and as such were only used in this 1-DOF task. In two additional sessions, Monkey W performed the 1-DOF task normally as well as in the wrist context in one session and spring context in the other session. Figure 2-7A shows trial-averaged neural activation traces from two example modulated channels, one from each monkey, both comparing the activation during spring trials and normal trials. We

found that neural channels showed a mix of changes with context. For example, Monkey W's channel 12 was activated more compared to normal for spring flexion targets (blue solid), similar to the muscle activations of the finger flexors. However, other example channels like Monkey N's channel 90 show less neural activation during movement in the spring contexts for both flexion and extension targets.

To quantify changes in activation for the population of tuned channels, we compared the average channel activation in a window spanning 420 ms around peak movement for each type of trial. Figure 2-7B and 2-C shows the change in SBP for all tuned channels between off-context trials and normal trials, split by flexion and extension trials, for Monkey W and Monkey N, respectively. Black dots indicate channels with significantly different trial SBP between off-context and normal trials toward that target according to a two-sample t-test ($p<0.01$). During spring trials, context modulated channels were activated significantly less on average for extension and were activated significantly more for flexion with both monkeys ($p<0.01$, paired t-test). During wrist trials, context modulated channels were activated significantly less for extension for Monkey N only ($p<0.01$, paired t-test) and there were no trends for channels increasing or decreasing activation on average for flexion or extension for Monkey W. Notably, the majority of changes in neural activation are on the order of 10% or less for individual channels, fairly small relative to the large changes in muscle activation observed in Figure 2-2, which is consistent with the results from Naufel et al., 2019, with wrist movements.

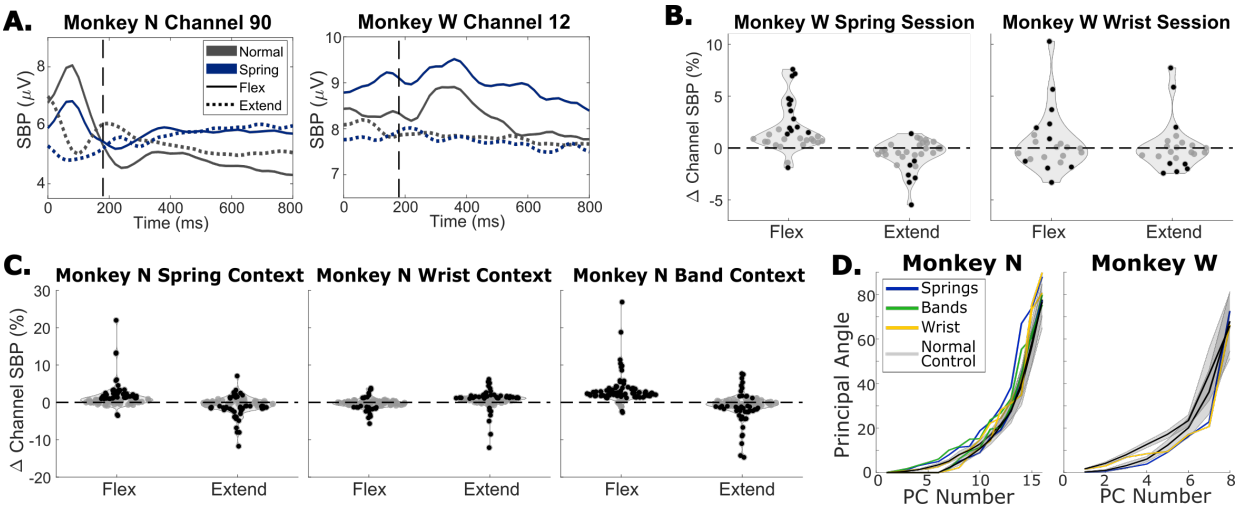

Figure 2-7 The impact of context changes on neural activity.
(A) Trial-averaged spiking band power (SBP) for two channels during a spring session for each monkey. Trials were aligned to peak movement before averaging, vertical dashed lines indicate peak movement. Black traces show normal trials, blue traces show trials with springs present, solid traces are flexion trials, and dotted traces are extension trials. (B) Change in average SBP in a window around peak movement for each tuned channel for a spring session (left) and wrist session (right), both for Monkey W. Black dots indicate significant differences according to a two-sample t-test ($p<0.01$). (C) Same as (B) but for Monkey N and using one session where the task was performed normally and in the spring, wrist, and rubber band contexts. (D) Principal angles between the PCA space calculated for normal trials and the PCA spaces calculated for spring trials (blue), band trials (green), or wrist trials (yellow). Black lines are average angles between PCA spaces for two random sets of normal trials, with gray shading indicating one standard deviation.

We next investigated how consistent the covariance structure of the neural activity is across different task contexts. We calculated the principal components (PCs) underlying the neural activity in each context in order to obtain one manifold for each context. We then found the minimum angles, also known as the principal angles, required to align the PCs from each type of off-context trial with the PCs calculated from normal trials (Figure 2-7D), similar to what has been previously presented (Gallego et al., 2018). Principal angles were also calculated between manifolds calculated from random sets of normal trials to create a set of control angles. Two sessions with normal, spring, wrist flexed, and rubber band trials in the same session are included for Monkey N (Figure 2-7D Left), and two sessions, one with normal and wrist flexed and one with normal and spring trials, are included for Monkey W (Figure 2-7D Right). We found that the principal angles between off-context trial neural activity and normal trial neural activity match the

normal control angles well. This indicates that the activity in each context falls within well-aligned manifolds.

Next we looked at how much variance in neural activity is due to the context changes. We calculated 16-dimensional demixed PCA (dPCA, Kobak et al., 2016) components for a neural manifold spanning neural activity during trials from all contexts in a single session. Figure 2-8A shows the dPCA components for one session with Monkey N. The components are organized in rows according to which behavioral parameter they explain the most variance for: time (condition-independent), context, target, or context-target interaction. Using the four sessions included in Figure 2-7D and one additional session for Monkey N that included normal, spring, and rubber band trials, the amount of variance explained by each behavioral parameter is summarized in Figure 2-8B for both monkeys. The condition-independent and target components together explain the majority of the neural variance. On average, the target components explain 36.4% of neural variance, the condition-independent components explain 47.2% of neural variance, and the context and context-target interaction components together explain 24.1% of neural variance for Monkey N and 8.6% of neural variance for Monkey W.

In inspecting the activation of components in Figure 2-8A, the context-related components add a shift to neural activity before and after movement (component #3) and separate normal and wrist trials from spring and rubber band trials during movement (component #6). This creates the picture of trajectories that are largely the same between context but slightly shifted, perhaps in response to a change in proprioceptive input or to generate more muscle activation. We compared the average activation around peak movement of the context-dependent dPCA component that explained the most neural variance with the average muscle activation of flexor or extensor muscles during flexion or extension trials in each context. Figure 2-8C shows this comparison for

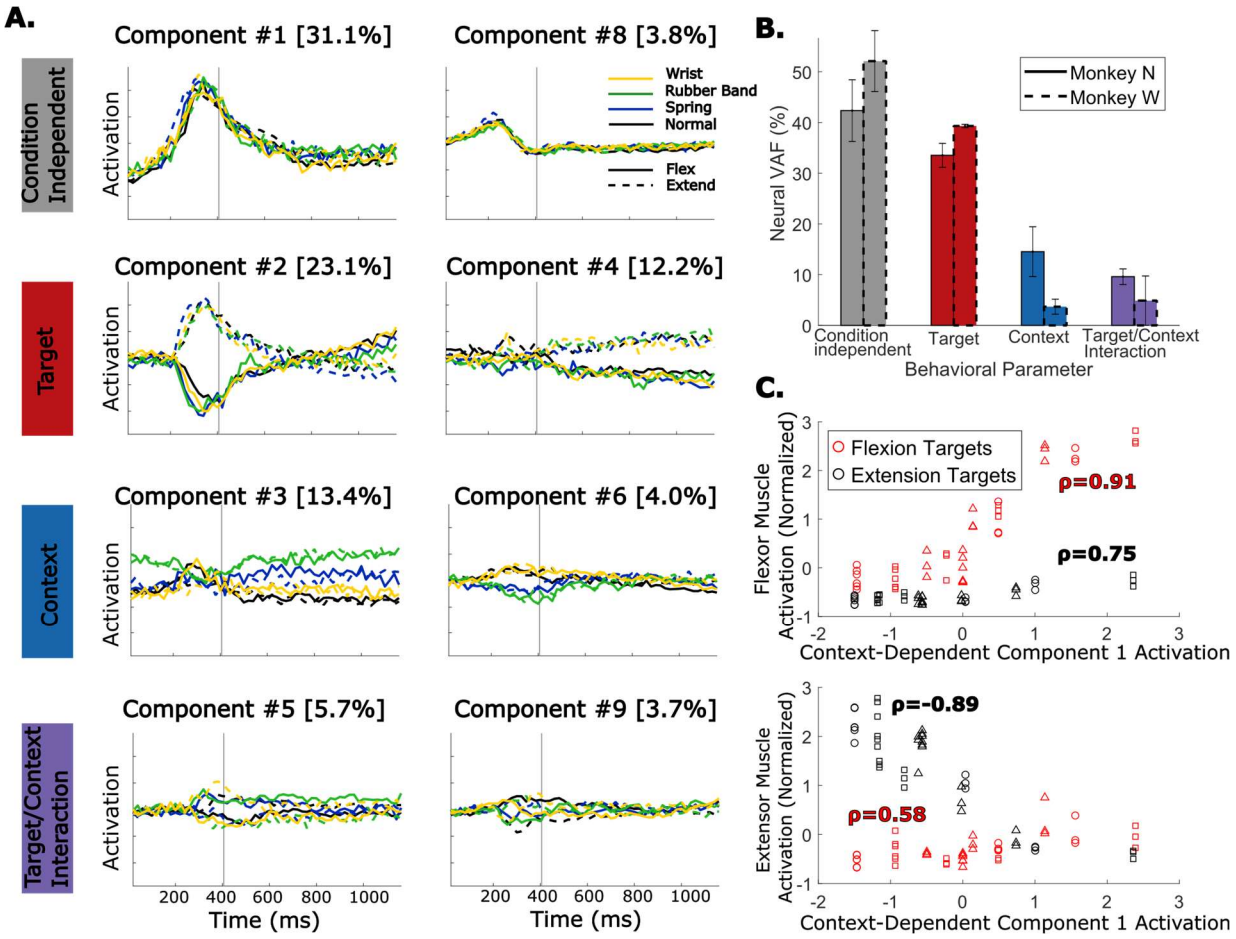

Figure 2-8 Dimensionally reduced representation of neural activity across contexts.
(A) Demixed PCA (dPCA) components for an example session with Monkey N performing normal trials (black), wrist trials (yellow), spring trials (blue), and rubber band trials (green). Solid traces are flexion trials, and dashed traces are extension trials. Components are organized by which behavioral parameter they explain the most neural variance for. Component numbers are ordered by how much neural variance they account for and the percent in brackets is the neural variance accounted for. (B) Percent of neural variance accounted for by each behavioral parameter. Bars with solid edges are for Monkey N, and bars with dashed edges are for Monkey W. Error bars indicate standard deviation across sessions. Three sessions are included for Monkey N, and two sessions are included for Monkey W. (C) Average muscle activation around peak movement for flexor muscles (top) or extensor muscles (bottom) during trials for each context and target plotted against the average activation of the first context-dependent dPCA component during the same trials. Each point represents the average activations in a series of trials in one context toward one target. Markers indicate which session the sample is from. Correlations are calculated within samples for one target, either flexion (red) or extension (black).

the three sessions with Monkey N included in Figure 2-8B. Note that one session only included normal, spring, and rubber band trials (no wrist). Interestingly, we found that the first context-dependent component correlated very strongly with the activation of the active muscle (i.e. flexor muscles during flexion or extensor muscles during extension) across contexts, with correlations of

0.91 for flexor muscles and –0.89 for extensor muscles. This result suggests a feature from neural activity that could be used to account for changes in required muscle activation between contexts.

2.3 Discussion

In this study we examined the impact of altering the context of a motor task, either adding an elastic resistance or postural change, while using a BMI for continuous finger control. These context changes represent a small sample of alterations found in activities of daily living but they include common changes to musculoskeletal properties of the hand during the task such as muscle tendon length and muscle activation range that give insight into how the results would extend to a wider range of changes. We found that changes in context increase the error of offline BMI decoder predictions significantly for both kinematics (Figure 2-4) and muscle activations (Figure 2-3). This effect was larger for predicting muscle activations than for predicting kinematics. In online trials using a kinematic-based BMI, the monkeys were able to quickly adjust for context changes and achieved comparable performance to normal online trials. We tested this in two ways. First, we added context changes to the manipulandum during online trials (Figure 2-5), which resulted in almost no change in online performance. Second, we trained two decoders (one on normal trials and the other on off-context trials) and swapped between them for closed-loop control (Figure 2-6), which resulted in small but significant decreases in online performance for the model trained on off-context trials.

During the offline tasks, many channels changed neural activity with context, with 20.9–61.7% of tuned SBP channels modulating activity with context (Table 2-1). The magnitudes of these shifts were relatively small, especially when compared to the large changes in required muscle activation (Figures 2-2D and 2-2E), with weak trends to require greater activation for resisted flexion and lesser for assisted extension (Figures 2-7B and 2-7C). Additionally, the neural

manifolds underlying movements in each context were well aligned (Figure 2-7D). Using dPCA we found that while a large proportion of neural variance was explained by dPCA components that did not change with context, a significant proportion of the neural variance is associated with components that are context-dependent (Figure 2-8B). Visually, the context components are shifting the trajectories without changing the overall shape and the shift in neural activity is strongly correlated with muscle activations in new contexts (Figure 2-8C). This agrees with other studies which found lower variance activity may be related to the actual motor commands (Gallego et al., 2018; Russo et al., 2018; Saxena et al., 2022).

The similar online performance in each context, despite large offline mismatch, may be explained by a few possible factors. First would be if normal online trials are performed using a model that already does not capture the relationship between neural activity and intended finger movements well. In a control-systems perspective, online BMI control changes the 'plant' from native fingers to the virtual fingers on the screen. There is evidence that as a result of this, neural activity is different during online BMI control (Carmena et al., 2003; Fan et al., 2014; Ganguly et al., 2011; Gilja et al., 2015; Jarosiewicz et al., 2013; Orsborn et al., 2012; Taylor et al., 2002). Additionally, it is unlikely that a linear model like those used here robustly capture the relationship between motor cortex activity and kinematics. Due to the change in neural activity during online trials and inaccuracies in the decoding model, there is likely adjustment required by the monkey to use the BMI online during the normal setup. In this case, performing the online task in a new context is swapping one non-optimal decoder for a new one. In both BMI experiments, the initial BMI performance, that is the first five trials, was not worse for off-context trials as compared to normal online BMI trials, suggesting that both types of trials were of similar difficulty to adjust to (Figures 2-5C and 2-6C).

The similar online performance could also be observed if the context change does not have a large impact on task-relevant neural activity. Studies into neural plasticity have shown that during a session of online trials, subjects can adjust to decoder perturbations that are within the same intrinsic manifold (Sadtler et al., 2014). We found that individual channel activations change on up to 61.7% of channels that are important for decoding movements (Table 2-1), and this introduces error into model predictions. However, if the perturbations we introduced did not shift activity outside of the intrinsic manifold, then it may have been easy to adjust to the new context. Our data show a near instantaneous adaptation to the perturbations whereas Sadtler et al. found some within-manifold perturbations required on the order of hundreds of trials to adapt to, indicating that our perturbation was intuitive to adapt to. Analyzing the monkey's strategy during the BMI task revealed that they were able to do the BMI task with perturbations to the hand without adjusting their strategy (Figure 2-5D). This likely follows from the BMI task being driven by neural activity and visual feedback rather than movements of the hand itself. In the two decoder BMI task where off-context performance was often slightly worse, the monkeys did make small adjustments to perform the task (Figure 2-6D). For example, they tended to 'push' harder to flex the virtual hand during off-context trials. This re-aiming strategy is similar to what has been described in other work on short-term learning with motor BMIs (Golub et al., 2018a; Jarosiewicz et al., 2008). In this case re-aiming likely stems from the need to reproduce a higher or lower neural activation online in order to use a model trained on data where channel activation increased for flexion and decreased for extension for the spring context (Figures 2-7B and 2-7C).

The online BMI experiments in this study used a kinematic-based BMI decoder. BMI studies typically predict kinematic variables for applications such as prosthesis control (Hochberg et al., 2012; Wodlinger et al., 2015) and cursor or virtual movement control (Gilja et al., 2015;

Hochberg et al., 2006; Young et al., 2019). In the offline predictions using linear models, we found that neither kinematics nor muscle activations could be predicted at the same accuracy in new contexts. While significant, kinematics, specifically flexion velocity, did show a smaller decrease in offline performance between contexts (Figures 2-4B and 2-4C). These results suggest that when designing BMIs, using kinematic variables as a command signal may allow for better generalization when the biomechanics of the task are not important, such as virtual tasks.

However, in FES applications (Ajiboye et al., 2017; Bouton et al., 2016; Nason-Tomaszewski et al., 2022), biomechanics are important. The final outputs are stimulation parameters that cause a desired amount of muscle contraction. Importantly, the required stimulation parameters could change with context due to the change in required muscle activation. As a result, even if predictions of position or velocity generalize well to new contexts, the mapping from kinematics to stimulation parameters would no longer be accurate. Our results with an online BMI indicate that the monkeys are able to adapt by re-aiming with the BMI to restore some ability to do the virtual online task, which indicates they may also be able to re-aim in FES applications as well. However, in our task this adaptation occurred with a performance loss (Figure 2-6B). Instead it would be better to account for how context changes the biomechanics of the task with the BMI. This could be done either through incorporating a better control system into the BMI, for example developing a controller to update stimulation parameters to match the decoded joint angle or velocity, or by better estimating the intended muscle activations from neural activity. Decoded intended muscle activations can be mapped to stimulation parameters as done by some FES studies (Ethier et al., 2012; Hasse et al., 2022).

With regard to decoding intended muscle activations, non-prehensile finger movements are less studied than arm movements and grasping, partly due to experimental difficulty, with much

work coming from only a few data sets (Baker et al., 2009; Schieber, 1991). Although predictions of muscle activations from neural activity for muscles overlapping with those in this study have been done for movements of the wrist (Naufel et al., 2019; Oby et al., 2013) and grasp (Ethier et al., 2012), predicting finger related muscle activations during non-prehensile finger movements has to our knowledge not been attempted yet. Here we found that we could decode muscle activations during this individuated finger task with similar accuracy as decoding kinematics.

Predicting muscle activation also led to the poorest offline generalization. The off-context predictions of muscle activation had both a large unaccounted for magnitude change and a lower correlation. We observed that neural features change by a relatively small magnitude (Figures 2-7B and 2-7C) whereas the muscle activation changes by large amounts (Figures 2-2D and 2-2E), resulting in linear models failing to predict a large enough scaling for off-context muscle activation. This observation matches studies of wrist movements where predicting muscle activation also did not generalize well (Naufel et al., 2019). The lower correlation was partially driven by muscle activation patterns not observed in normal context training data, such as increased co-contracting flexor and extensor muscles during flexion trials to modulate stiffness when springs were present, as seen in Figure 2-3A where the predicted EDC activation does not increase for flexion in the spring condition. With a better model, it might be possible to pick out the relationship between neural activity and muscle activations. Determining for example that the intention is to activate EDC more, whether that is to co-contract with FDP or to extend the fingers may not matter as long as the intention can be accurately decoded. Based on these results, it's likely that linear models are not able to pick out this relationship. Additionally, some prediction generalization error can be associated with the muscle activations being a higher dimensional variable than kinematics, with evidence that motor cortex can selectively activate or inactivate

specific muscles (Schieber et al., 2009). In this study there was no effort to estimate lower dimensional muscle synergies that may be underlying the observed muscle activations, but it is possible that cortical activity would relate more linearly to muscle synergies than to individual muscle activations.

An alternative BMI design approach to decoding movements is to use task-specific features to augment decoder models (Schroeder et al., 2022). The context shifts studied here represent a small and discrete subset of the shifts found in activities of daily living, however they relate to continuous musculoskeletal properties that are shifting with the context, that is muscle length, co-contraction, or muscle activation magnitude. Identifying a feature in neural activity that accounts for the change in muscle activation across contexts would assist in decoder generalization. For example, the context-dependent neural activity that strongly correlated with muscle activations in new contexts (Figure 2-8C) could provide a feature for accounting for the scaling change while predicting muscle activation or allow models to modulate force or muscle activation while producing the same kinematics. More work is needed to understand if a neural feature like this would remain stable in different cognitive contexts, for example grasping or freely moving fingers as opposed to doing this virtual target acquisition task.

Nonlinear models could also improve predictions of intended muscle activation or kinematics from neural activity. Complex models are becoming more widely used in order to better model the relationship between motor cortex and intended movements (Glaser et al., 2020; Schwemmer et al., 2018; Sussillo et al., 2012; Willett et al., 2021). While a general concern for these nonlinear models is that they will overfit to the training data and not generalize well, given the correct training data they also may be able to identify less obvious trends that will distinguish between contexts and allow for better predictions. For example, Naufel et al. (2019) was able to

predict muscle activations in multiple wrist tasks after training an LSTM decoder on data from all of the tasks. This indicates that there may be enough information in our BMI features to distinguish between the different tasks. Our dPCA results indicate that around 24% of neural variance can be accounted for by context specific activity (Figure 2-8B), so it is likely that a neural network would be able to take advantage of that information to make predictions in multiple contexts. More work will be needed to characterize how much training data these nonlinear models need in order to generalize to all the contexts experienced during activities of daily living.

2.4 Methods

All procedures were approved by the University of Michigan Institutional Animal Care and Use Committee.

2.4.1 Implants

We implanted two male rhesus macaques (Monkey N age 8–9, Monkey W age 8–9) with Utah microelectrode arrays (Blackrock Neurotech, Salt Lake City, UT, USA) in the hand area of precentral gyrus, as described previously (Irwin et al., 2017; Nason et al., 2021; Vaskov et al., 2018). Two monkeys were chosen to ensure results are consistent between subjects. Monkey N was implanted with two 64-channel arrays in right hemisphere primary motor cortex and Monkey W was also implanted with two 96-channel arrays in right hemisphere primary motor cortex. Channels from both of Monkey N's motor cortex arrays and from Monkey W's lateral motor cortex array were used in this study, for a total of 96 channels from each monkey for analysis. The number of channels simultaneously recorded was limited to 96 due to the available recording hardware. Monkey N was between 511 and 1168 days post-cortical implant and Monkey W was between 254 and 411 days post-cortical implant during data collection.

Monkey N was also implanted with chronic bipolar intramuscular EMG recording electrodes (Synapse Biomedical, Inc, Oberlin, OH, USA) in a separate surgery as described previously (Nason et al., 2021). The list of muscles targeted along with their function are included in Table 2-2. Briefly, muscles were accessed via dorsal and ventral incisions on the left forearm and specific muscles were surgically identified with the assistance of intraoperative stimulation. Bipolar electrodes were inserted and sutured into the muscle belly near the point of innervation and then tunneled over the elbow and shoulder to an interscapular exit site. The percutaneous electrodes were connected to a 16-channel PermaLoc connector. Monkey N was between 120 and 496 days post-EMG electrode implant for all EMG data collected.

Table 2-2 List of muscles targeted during surgery with their associated function.

Muscle	Function
Extensor Indicis Proprius (EIP)	Index Finger Extensor
Flexor Digitorum Profundus, targeting MRS (FDP)	Finger Flexor
Extensor Digitorum Communis (EDC)	Finger Extensor
Extensor Carpi Radialis Brevis (ECRB)	Wrist Extensor
Flexor Carpi Ulnaris (FCU)	Wrist Flexor/Adductor
Flexor Carpi Radialis (FCR)	Wrist Flexor
Flexor Digitorum Profundus, targeting index, proximal and distal sites (FDPip, FDPid)	Index Finger Flexor

2.4.2 Feature Extraction

(TCFR and SBP) were recorded in real time during experiments using the Cerebus neural signal processor (Blackrock Neurotech). Threshold crossings were acquired by configuring the Cerebus to threshold each channel at –4.5 times the signal root-mean-square. For each threshold crossing, spike snippets were sent to a computer running xPC Target version 2012b (Mathworks)

which saved the channel and time for each threshold crossing. SBP is an estimate of power in the 300–1000 Hz frequency band and was acquired by configuring the Cerebus to bandpass filter the raw signals to 300–1000 Hz using the Digital Filter Editor feature in the Central Software Suite version 6.5.4 (Blackrock Neurotech), then sample at 2 kHz. The filtered 2 kHz recording was then sent to the computer running xPC Target, which rectified and summed the samples on each channel received in each 1 ms iteration and counted the quantity of samples received each 1 ms so that SBP could later be averaged within longer time bins. Both the threshold crossings and SBP were saved by xPC synchronized with other real-time experimental information. Artifacts were removed for TCFR by removing threshold crossing times if 20 or more channels had threshold crossings in the same millisecond. Features were binned into non-overlapping bins of length 32 ms for online and offline decoding, or bins with a length of 20 ms for calculating tuning and comparing features across trials. SBP is summed for every 1 ms in the time bin and then divided by the total number of raw 2 kHz samples in the bin. For TCFR the spike counts are summed within a bin and then divided by the bin size to get a threshold crossing rate.

EMG from Monkey N's eight bipolar electrodes was recorded for later offline synchronization. The percutaneous PermaLoc connector was connected to a CerePlex Direct (CPD) via a 64-channel splitter box and CerePlex A (Blackrock Neurotech) which converted the signals to the digital domain with unity gain. The CPD was configured to record 16 channels of raw signal at 10 kHz and for each bipolar pair the electrode implanted further inside the muscle was software referenced to the second electrode. These eight bipolar referenced channels are used in analyses. To synchronize EMG offline, we used the Sync Pulse functionality in Central to create unique pulses that were recorded by both the Cerebus and CPD and could later be used to align the Cerebus and CPD recordings. For offline analysis, muscle activations are estimated from the

10 kHz EMG recording by filtering with a second-order Butterworth bandpass filter between 100 and 500 Hz and then taking the mean absolute value of the filtered signal during every binning period.

2.4.3 Experimental Setup

During experiments the monkeys performed a virtual finger task while motor cortex activity and optionally arm muscle activity were recorded as described. Similar to previously described experiments (Irwin et al., 2017; Nason et al., 2021; Vaskov et al., 2018), we used xPC Target to coordinate the experiment in real time. The xPC Target computer acquired and stored task parameters and neural features in real time, coordinated target presentation, acquired finger positions from the flex sensors on each finger group (FS-L-0073-103-ST, Spectra Symbol, Salt Lake City, UT, USA), and sent finger positions and target locations to a computer simulating movements of a virtual monkey hand (MusculoSkeletal Modeling Software) (Davoodi et al., 2007). For online experiments, the xPC Target computer also binned threshold crossings and SBP in customizable bin sizes and evaluated the decoder model to predict finger positions in real time using an RFKF (see details below).

2.4.4 Behavioral Task

Monkeys N and W were trained to acquire virtual targets by moving their physical fingers in a manipulandum to control virtual fingers on a screen in front of them. All sessions took place in a shielded chamber with the monkey's head fixed and arms restrained at their side with elbows bent 90 degrees and hands resting on a table in front of them. The left hand was placed in a manipulandum described previously (Nason et al., 2021), with openings separating the index finger and the MRS finger group (Figure 2-1C). The monkeys were trained to move the index

finger independently of the MRS finger group (Figure 2-1B), that is 2-DOF, although in some trials they moved both finger groups as 1-DOF. Each trial began with spherical targets appearing for each active finger group with each target occupying 15% of the full range of motion of the fingers. In the 1-DOF task the target was presented to the index finger.

Target presentation followed a center-out-and-back pattern with every other target presented at a center position, equivalent to 50% on a scale from 0% (full extension) to 100% (full flexion). Additionally, center was presented after any failed trial. The non-center targets were randomly selected from a set of targets. For 2-DOF the targets included any combination of index flexion, rest, or extension, and MRS flexion, rest, or extension, with a randomly chosen magnitude of 20%, 30%, or 40% of the full movement range. The split movements (index flexion with MRS extension or vice versa) did not have a 40% movement magnitude because the monkeys had difficulty splitting the finger groups that far. The 1-DOF movements were also center-out with the fingers flexing or extending either 40% from rest or a randomly chosen magnitude of 20%, 30%, or 40% from rest depending on the session, the former generally being used for tuning analyses and offline comparisons and the latter being used for online experiments. In each trial the monkey had to hold their fingers within the target(s) for 750 ms. During online decoding experiments, the same center-out-and-back target presentation order was used but the hold time was reduced to 500 ms. In one session used in offline analysis and four online sessions, the hold time was 2 ms longer than expected due to a minor bug. In two online experiments with the manipulandum context changing BMI task, targets were presented in a random order instead of center-out. In this target presentation, a target separation up to 50% of the movement range and a center position were randomly generated and one target for each finger group was presented at the generated target separation from each other, equidistant from the generated center position.

Task context was altered through four potential task alterations. One alteration was the addition of torsional springs to both finger groups (180 degree deflection angle, 0.028 in or 0.04 in wire diameter, Gardner Spring Inc, Tulsa, OK, USA), referred to as the 'spring context'. The second alteration was the rotation of the manipulandum by 23 degrees in the flexion direction, referred to as the 'wrist context'. A third alteration was introduced by attaching rubber bands from the back of the manipulandum to the door for each finger group, thereby resisting flexion, referred to as the 'rubber band context'. A last alteration was addition of torsional springs and the rotation of the manipulandum by 23 degrees at the same time, referred to as the 'both context'. Trials performed with one of these alterations are referred to as 'off-context' trials, while trials performed without alterations are referred to as 'normal' trials. As the index finger alone is much weaker than the MRS finger group, the index finger used a smaller spring when applicable. The added springs increased the force required for full flexion by 9.5 N (for MRS) and 3.3 N (for index), while the rubber bands increased the force required for full flexion by 16.5 N. The rubber band context was only done by Monkey N and in a 1-DOF task due to task difficulty. For reference, full flexion required approximately 1.3 N of force without the springs or bands.

2.4.5 Comparison of Kinematics and Muscle Activation Between Contexts

Three representative sessions for both Monkey N and Monkey W, 1 day for each context – spring or wrist – were used to compare kinematics across contexts. During data collection, normal trials and off-context trials were interleaved by alternating context type every 175–350 trials in order to control for changes in behavior over time. During these representative days, there was an average of 1134 normal trials and 1118 off-context trials per day for Monkey N and 526 normal trials and 504 off-context trials per day for Monkey W. To compute how finger velocity changed between normal trials and off-context trials, the peak velocity of finger movements was

found for every trial. For every trial, the recorded finger flexions were downsampled to 20 ms and filtered with a second-order Savitzky-Golay FIR filter. Finger velocity was estimated from the downsampled and filtered finger positions and maximum finger speeds were found. The peak movement time was taken at the time of the largest peak in speed after trial start. Trials were then split by context and target direction (flexion vs. extension), and a two-sample t-test was used to compare peak speeds and compute a 99% confidence interval, once for flexion targets and again for extension targets. Comparisons were made only between trials to the same target, leaving about 281 trials per group and 129 trials per group for each comparison for Monkey N and Monkey W, respectively.

The same sessions for Monkey N used to compare kinematics were also used to compare muscle activations. The recorded EMG was filtered and the mean absolute value was taken in 20 ms bins as described previously. Binned muscle activations were then smoothed with a 100 ms Gaussian kernel. One value was obtained for every trial by taking the average muscle activation in a 420 ms window around peak movement, including 10 bins before peak movement, the bin that included peak movement, and 10 bins after peak movement. These muscle activation values were grouped by context and target, then compared with a two-sample t-test.

2.4.6 Computation of Neural Tuning and Context Modulation

During five representative experiments for each monkey, three that tested the spring context and two that tested the wrist context, we calculated the number of channels that were significantly modulated by any finger movement and the number of channels with a change in activity between normal trials and off-context trials. During these sessions, the monkeys performed the task with all fingers moving together (1-DOF), in a center-out task as described, to targets at either plus or minus 40% from center. Trials that were unsuccessful and trials following

unsuccessful trials were removed. Unsuccessful trials were rare, often only occurring on the first or last trial of a block of trials. There was an average of 1072 normal trials and 747 off-context trials for Monkey N and 544 normal trials and 387 off-context trials for Monkey W were used during these sessions.

Channel tuning and context modulation was calculated with both the SBP features and TCFR features. On each day, features and kinematics were averaged into non-overlapping 20 ms bins, data from normal trials and off-context trials were concatenated together, and the SBP and TCFR were each normalized to zero mean and unit standard deviation. An optimal lag was calculated for each channel by maximizing the L2-norm of regression coefficients between a feature and finger position and velocity. Features at that optimal lag were then regressed with finger position and velocity one at a time with an added effect for context following these equations:

$$X_n = [\hat{x}_n \quad c\hat{x}_n]$$

$$Y = B + X_n W_n$$

where $\hat{x}_n$ is the T x 1 vector of channel SBP or TCFR for channel n, c is an indicator variable that equals one if that sample was during an off-context trial or zero otherwise, Y is a T x 2 matrix containing finger position and velocity for each bin in T, B is the trained linear offset, and W_n is the 2 x 2 matrix of trained weights relating channel n's activity to finger position and velocity. A channel was called tuned if the regression coefficient between the neural feature and either finger position or velocity, i.e. $w_{1,1}$ or $w_{1,2}$, were significantly different from zero, via a t-test on the regression coefficient ($p < 0.001$). A channel was also called context modulated if either coefficient in the second row of W_n, which includes the effect of context, was significantly different from

zero, also via a t-test ($p < 0.001$), indicating a different slope relating neural activity and kinematics between normal trials and off-context trials.

To quantify the change in neural activity between contexts as in Figure 2-7, we used one representative session for Monkey N in which trials were done in the normal, spring, wrist, and rubber band contexts. An additional two representative sessions for Monkey W were used, one session comparing normal and spring trials and another session comparing normal and wrist trials, both performed with 1-DOF movements and with targets to 40% flexion or extension from rest only. Tuned channels were calculated as previously described using the SBP feature. For every trial, the SBP was binned into 20 ms bins and then smoothed with a 100 ms Gaussian kernel. Then the average activity in a window spanning 200 ms before and 200 ms after the bin containing peak movement was calculated for each tuned channel. The trials were then split by context and by target, and the trial SBP values were compared between contexts with a two-sample t-test.

2.4.7 Offline Predictions

Data from nine sessions with Monkey N, three for each context (springs, wrist, and both), were used for offline muscle activation and kinematic predictions, and three sessions for Monkey W, one for each context, were used for offline kinematic predictions. During these sessions, both monkeys performed the 2-DOF center-out task. Blocks of normal trials and off-context trials were interleaved by alternating context in order to control for changes in neural activity over time. Trials that were unsuccessful were removed before analysis. There was an average of 803 normal trials and 470 off-context trials for Monkey N and 737 normal trials and 329 off-context trials for Monkey W. To account for changes in monkey motivation, sessions chosen were those with consistent prediction accuracy between early and late normal trials within a session. These sessions

spanned 165 days starting 792 days post-cortical array implant and 120 days post-EMG electrode implant for Monkey N, and 63 days starting 285 days post-cortical array implant for Monkey W.

In each session, SBP and muscle activations or kinematics were binned into 32 ms bins and features were concatenated across trials of the same context. The SBP channels were masked to those with an average TCFR greater than 1 Hz across a session and 12 bins of history from each of these channels were used as additional features. Ridge regression relating SBP to muscle activations or kinematics was trained on normal trials and then tested on both normal trials and off-context trials with 10-fold cross-validation. To do this, the normal trials were split into 10 folds with an equivalent number of bins in each fold, a model was trained on nine folds, and then tested on the left-out fold as well as on data from off-context trials. We used two metrics to evaluate prediction accuracy. First we used the Pearson correlation coefficient between the predicted and measured muscle activations or kinematics to establish how well the predictions are linearly correlated with measurements. The second metric was MSE normalized by the variance of the measured data (MSE). Normalizing by the variance allows for better comparison across test datasets as they may have different variances. In this formulation, the MSE is the fraction of unexplained variance or one minus the variance accounted for or coefficient of determination used in previous studies (Fagg et al., 2009; Naufel et al., 2019). Values greater than one indicate that the predictions are introducing variance compared to the worst possible least-squares predictor, that is predicting the mean.

2.4.8 Online Decoding

We used either a KF or an RFKF (Gilja, Nuyujukian, Chestek, Cunningham, Yu, Fan, Churchland, et al., 2012) to predict intended finger movements for all BMI experiments, as done previously (Irwin et al., 2017; Nason et al., 2021; Vaskov et al., 2018). We performed two types

of online experiments. In the first experiments, an RFKF was trained on normal trials and then used during trials with context changes in the manipulandum or without any additions to the manipulandum. To train the model, monkeys first performed at least 300 trials of center-out manipulandum control with 750 ms hold time. Using these trials, we trained a position/velocity KF which the monkeys used online for at least 200 trials, with a 32 ms update rate and a 500 ms hold time. To use the KF, virtual finger position was updated by integrating the predicted velocity in the current time step to update the previous step's finger position. An RFKF was then trained, as done previously (Nason et al., 2021), by rotating incorrect velocities during online control with the KF to be toward the intended target represented in a two-dimensional space, setting finger velocity equal to zero when in the correct target, and then retraining regression coefficient matrices. The RFKF was used online for blocks of 100–200 trials with different context changes applied to the manipulandum, alternating between normal trials and other contexts. Multiple contexts could be tested in one session during these experiments by switching out the context manipulations present in the manipulandum.

In the second set of online experiments, two KFs were trained in one session and then used alternatingly in online control without any changes present in the manipulandum. During these sessions, the monkeys first performed at least 300 trials of center-out manipulandum control, followed by another 300 or more trials of center-out manipulandum control with a context change present. One model was trained using each set of trials. The monkeys then used these models in online control for sets of 100–200 trials, and then the models were alternated. Hold times and update rates were kept consistent between types of experiments and sessions.

2.4.9 Online Performance Measures

We estimated online performance with acquisition time, time to target, orbiting time, and path efficiency. Acquisition time was measured as the total time from target presentation to the end of the trial minus the hold time, therefore ending with the target being successfully acquired. Time to target was taken as the time from target presentation to the first time where all fingers with targets were in their targets. Orbiting time was then calculated as the time from all fingers first reaching their targets to the end of the trial minus the hold time. Trials where the fingers reached the targets and never left therefore had an orbiting time of 0 ms. Failed trials were excluded when comparing online performance between context but not for evaluating the monkeys adaptation within the first five trials. Path efficiency was calculated as the ratio of the shortest distance between the fingers' starting positions and the target positions projected onto a two-dimensional space, to the length of the path traveled by the fingers.

2.4.10 Online Neural Activity Patterns

To visualize neural activity during online trials, the normal offline training trials used to train the KF were used to train a new linear readout between neural activity and finger velocities. Neural activity from these trials was binned in 50 ms intervals, then neural activity in the current bin and the five most recent bins were regressed with the finger velocities during these trials to obtain one set of weights for that session. This model was then used to predict velocities from neural activity during the online trials. The predictions at the time point in the trial with the peak online velocity toward the target during the online trial were taken as the online neural activity patterns. To compare neural activity patterns across multiple targets in multiple sessions, the neural activity patterns for each trial were projected onto the target direction for each trial to obtain one 'pushing magnitude', or the velocity magnitude that they were pushing toward the target direction. Pushing magnitudes were collected for each trial, separated for flexion trials (IF, MF, IF+MF),

extension trials (IE, ME, IE+ME), and split trials (IF+ME, IE+MF), and then the pushing magnitudes for each set of trials were compared between normal trials and off-context trials using a two-sample t-test.

2.4.11 Dimensionality Reduction

To investigate changes in population neural activity due to changes in context, two sessions of 1-DOF center-out trials with targets of 40% flexion or extension from rest were used for each monkey. For Monkey N, both sessions included trials where the task was performed in the normal, spring, rubber band, and wrist contexts. For Monkey W, one session included trials in the normal and spring contexts, and the other session included trials in the normal and wrist contexts. SBP was binned into 20 ms bins, masked to only include channels with TCFR greater than 1 Hz, and then for each trial a time frame 400 ms before to 740 ms after the bin containing peak movement was taken from each trial. The neural activity for trials within a single context was concatenated and averaged across trials with the same context and target forming an $N \times T \times D$ data structure for each context, where N is the number of channels, T is the number of bins per trial used, and D is the number of targets. Neural data was then concatenated across targets to form an $N \times (T*D)$ matrix and then we used PCA to calculate a manifold for each context, keeping the top 16 components for Monkey N and eight components for Monkey W, which explained 86% of variance on average. Principal angles were found between the manifolds following methods used previously (Bjorck & Golub, 1973; Gallego et al., 2018). These principal angles are the minimal angles required to align the manifolds and serve as a measure for how well aligned two manifolds are. As a control, two sets of 50 trials were taken from the normal trials and used to calculate two manifolds in the same way. The principal angles between these manifolds were then calculated.

The sampling and angle calculations were repeated 100 times to obtain a control distribution of principal angles.

We also calculated one manifold spanning trials from all contexts tested in one session. This was done using dPCA (Kobak et al., 2016). This approach finds a single neural manifold that reduces the dimensionality of the data while maintaining a linear readout that can reconstruct the mean neural activation associated with manually chosen behavioral variables. In this instance, the behavioral parameters chosen were target, that is either flexion or extension, and which context the task was done in. MATLAB code for calculating dPCA components was downloaded from http://github.com/machenslab/dPCA, SBP was binned into 20 ms bins, masked to include only channels with TCFR greater than 1 Hz, and then concatenated into an N × C × D × T × n data structure where N, D, and T follow the same structure as the PCA calculations, n is the number of trials per condition, and C is the number of contexts tested in that session. SBP was averaged over the number of trials, n, to form the peristimulus-time-histograms for each target and context combination, after which dPCA components were calculated. Neural variance of a behavioral parameter was obtained by calculating the variance within the marginalization of neural data based on each behavioral parameter and taking the ratio of the total variance in a marginalization to the total variance in the neural data.

2.5 Acknowledgements

Cynthia A. Chestek and Parag G. Patil advised this work. Cortical surgeries were performed by Cynthia A. Chestek, Parag G. Patil and Matthew S. Willsey. Peripheral surgeries were performed by Theodore A. Kung and Nishant Ganesh Kumar. Samuel R. Nason-Tomaszewski, Hisham Temmar, Joseph T. Costello, and Dylan M. Wallace provided experimental support and assisted in collecting data. Eric Kennedy provided animal support.

We thank the University of Michigan Unit for Laboratory Animal Medicine for expert veterinary and surgical support. We appreciate Chris Andrew's expert statistical assistance and the support of the University of Michigan Biointerfaces Institute. This work was supported by NSF grant 1926576, NSF GRFP under grant 1841052, NIH grant F31HD0998804, NIH grant T32NS007222, NIH grant R01NS105132, the Dan and Betty Kahn Foundation Grant AWD011321, University of Michigan Robotics Institute, and A. Alfred Taubman Medical Research Institute.

Chapter 3 Functional Electrical Stimulation and Brain-Machine Interfaces for Simultaneous Control of Wrist and Finger Flexion

A subset of these results were presented as a poster at the 2023 Simian Collective Meeting

3.1 Introduction

Spinal cord injuries (SCI) impact a person's ability to perform activities of daily living and negatively impact quality of life, especially when hand function is affected. Almost 60% of SCI cases in the US are partial or complete injuries at the cervical level which typically decreases hand and or arm function (National Spinal Cord Injury Statistical Center, 2023). Restoration of hand function is a top priority for people with spinal cord injuries to improve quality of life (Anderson, 2004; Collinger, Boninger, et al., 2013). Functional electrical stimulation (FES) can restore hand movements after severe spinal cord injuries by electrically activating a person's own muscles. Stimulating electrodes are typically placed either at the nerves proximal to the muscles (epineural or intrafascicular) or at the muscles themselves. FES has been used to restore hand movements since the 1980s (Keith et al., 1989) and movements such as lateral and palmar grasps have been restored in more than 220 users with the Freehand System (Peckham et al., 2001) which was commercially available in the 2000s.

For restoring natural hand control, it is necessary to continuously control many degrees-of-freedom (DOF) in the hand simultaneously. The hand and wrist together have about 27 DOF (ElKoura & Singh, 2003). While some estimates of the dimensionality of functional hand movements have explained hand movements with as few as six synergies (Santello et al., 1998),

there is also evidence that many of the lower-variance synergies in the hand are important for natural movements (Yan et al., 2020). Intramuscular FES is a promising approach for restoring the many DOF required for dexterous hand movements. Whereas intrafascicular or nerve cuff stimulation can create functional grasps by evoking synergistic movements (Coste et al., 2022; Tigra et al., 2020), intramuscular FES allows targeting specific muscles or even portions of a muscle innervated by a single peripheral branch (neuromuscular compartments) (English et al., 1993). Stimulation at this most distal point more easily evokes selective movements at the expense of requiring more electrodes to cover all of the target muscles. Additionally, stimulation can be modulated to evoke different sized movements (Grandjean & Mortimer, 1986; Gruner & Mason, 1989; Singh et al., 2000), leading to graded control in many DOF.

Clinical trials with FES have focused on restoring specific grasps like the palmar or lateral grasps (Kilgore et al., 2018; Losanno et al., 2023). These studies have generally used prescribed stimulation or tasks that don't require graded control of grasping. An alternative to restoring discrete grasps is to restore graded control of multiple joints and let the user intuitively form the grasps. To do this, it will be important to understand how well we can achieve graded control of multiple DOF at the same time. Here we focus on simultaneous wrist flexion and finger flexion, which would enable grasping in different postures. Wrist posture plays an important role in grasp strength and grasp size (O'Driscoll et al., 1992). Studies have demonstrated continuous control of grasping, i.e. all fingers opening and closing, using intramuscular FES (Ajiboye et al., 2017; Nason-Tomaszewski et al., 2023). However, controlling multiple DOF continuously, such as both grasping and wrist flexion, has not been explored. While we can selectively activate muscles with intramuscular stimulation, joints in the hand and wrist are biomechanically linked. Many muscles that control the fingers cross through the wrist resulting in finger-related muscles with lengths, and

thus activation forces, that vary with wrist posture. Additionally, muscles can attach across multiple joints. For example, finger flexors cross the wrist and MCP joints so that their activation causes moments at both joints. This biomechanical linking increases the complexity of the control problem.

With respect to controlling continuous movements in multiple-DOF, intracortical brain-machine interfaces (BMI) are promising because they don't require residual movements and can provide an intuitive control signal. BMIs read out intended movements from cortical activity that can be used to control FES. Similar to intramuscular FES, BMIs have been used to decode continuous finger movements (Ajiboye et al., 2017; Nason et al., 2021) and wrist movements (Ajiboye et al., 2017). However, controlling multiple-DOF at the same time has been explored much less. Ajiboye et al. showed that they could decode the hand and elbow simultaneously (Ajiboye et al., 2017), and Nason et al. decoded multiple finger groups. However, simultaneously decoding continuous wrist and finger movements has not been demonstrated. Changes in wrist posture introduce errors to finger movement predictions, but users can re-aim to acquire targets with the BMI (Mender et al., 2023). This suggests a BMI that continuously controls wrist and finger flexion can produce a command signal to control FES.

Here we evaluate how well we can continuously control movements of the wrist and hand using intramuscular FES and standard control methods previously used in brain-controlled FES (Ajiboye et al., 2017; Nason-Tomaszewski et al., 2023). First we characterize the movements evoked in the wrist or fingers by stimulating muscles for each DOF independently. Then we show that by combining stimulation for both DOF we can evoke a large range of finger and wrist movements that is impacted by fatigue and an interaction between the two DOF. We can use these patterns to control stimulation and move the wrist and fingers simultaneously to continuously

acquire targets throughout the range of motion. We then test a BMI for predicting intended wrist and finger movements in real-time. We show that a linear 2-DOF BMI works well despite the lack of independent DOF. While the BMI stops working well after blocking sensory afferents, performance can be recovered by retraining the model.

3.2 Methods

All procedures were approved by the University of Michigan Animal Care and Use Committee.

3.2.1 Implants

We implanted two male Rhesus Macaques (Monkey N and Monkey R) with chronic bipolar intramuscular electrodes (Synapse Biomedical, Inc, Oberlin, OH, USA). Muscles were accessed via dorsal and ventral incisions on the left forearm, as described previously (Mender et al., 2023; Nason-Tomaszewski et al., 2023; Nason et al., 2021). In Monkey N, specific muscles were surgically identified and implant locations were selected based on intraoperative stimulation. With Monkey R, specific muscles were surgically identified and nerve entry points to the muscles were identified. Nerve entry points were targeted for implants and hand function was confirmed with intraoperative stimulation. Bipolar electrodes were inserted and sutured into the muscle belly at the target location and then tunneled to an interscapular exit site. Monkey N was implanted with 8 bipolar electrodes and Monkey R was implanted with 16 bipolar electrodes. Muscles targeted and evoked movements from intraoperative stimulation are described in Table 3-1. Electrodes are labeled based on the muscle that they are implanted in and their expected function. Monkey N had been previously implanted (22 months prior to FES electrode implant) with two 64 channel Utah microelectrode arrays (Blackrock Neurotech, Salt Lake City, UT, USA) in the right hemisphere

primary motor cortex. Arrays targeted the hand area of precentral gyrus, as described previously (Nason et al., 2021). Notably, these arrays were implanted 1577 days before the first BMI experiments presented here.

Table 3-1 Implant locations and expected function for each electrode

Monkey R Electrodes	Expected Function
Flexor Digitorum Superficialis (FDS)	All finger flexion
Flexor Digitorum Profundus, Ulnar Site (FDPr)	Ring finger flexion
Flexor Digitorum Profundus Radial Site (FDPi)	Index finger flexion
Flexor Digitorum Profundus Ulnar Site (FDPrs)	Ring and small finger flexion
Flexor Carpi Radialis Proximal Site (FCRp)	Wrist flexion
Flexor Carpi Radialis Distal Site (FCRd)	Wrist flexion
Flexor Carpi Ulnaris Proximal Site (FCUp)	Wrist flexion and adduction
Flexor Carpi Ulnaris Distal Site (FCUd)	Wrist flexion and adduction
Extensor Digitorum Communis Ulnar Site (EDCrs)	Ring and small finger extension
Extensor Digitorum Communis Radial Site (EDCi)	Index finger extension
Extensor Digitorum Communis Middle Site (EDCmrs)	Middle, ring, and small finger extension
Extensor Digitorum Communis Proximal Site (EDCim)	Index and middle finger extension
Extensor Indicis Proprius (EIP)	Index finger extension
Extensor Carpi Radialis Brevis Proximal Site (ECRBp)	Wrist extension
Extensor Carpi Radialis Brevis Distal Site (ECRBd)	Wrist extension
Extensor Carpi Ulnaris (ECU)	Wrist ulnar deviation
Monkey N Electrodes	Expected Function
Extensor Indicis Proprius (EIP)	Index finger extension
Flexor Digitorum Profundus, targeting MRS (FDP)	Middle, ring, and small finger flexion
Extensor Digitorum Communis (EDC)	All finger extension
Extensor Carpi Radialis Brevis (ECRB)	Wrist extension
Flexor Carpi Ulnaris (FCU)	Wrist flexion and adduction
Flexor Carpi Radialis (FCR)	Wrist flexion
Flexor Digitorum Profundus radial proximal site (FDPip)	Index finger flexion
Flexor Digitorum Profundus radial distal site (FDPid)	Index finger flexion

3.2.2 Experiment Overview

Both monkeys performed a virtual target acquisition task, moving their hands while finger and wrist posture were tracked with either a custom manipulandum and potentiometer, or with flex sensors (FS-L-0073-103-ST, Spectra Symbol, Salt Lake City, UT, USA) taped to the hand.

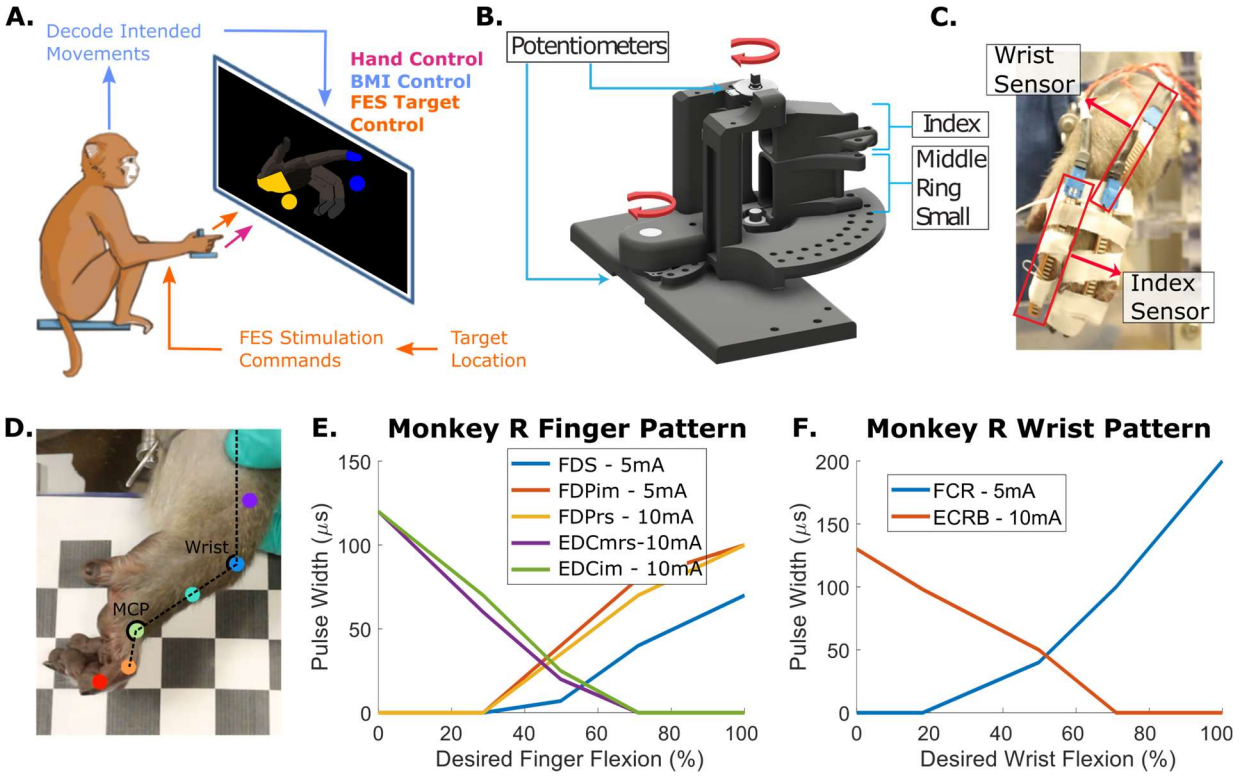

Figure 3-1 Experimental setup.
(A) Illustration of the three different types of closed-loop experiments performed, namely hand control, BMI control, and FES target control. (B) Design of the custom manipulandum used to measure finger groups (index and middle-ring-small grouped) and wrist angles during hand control and BMI experiments. Angles were measured with through-hole potentiometers at the axis of rotation. (C) Taped on flex sensors as used during closed-loop FES experiments. (D) Example angle measurements using markers identified with DLC. (E) Stimulation pattern for finger movements. Stimulation is controlled by specifying a desired finger flexion and the pattern acts as a look up table for stimulation parameters. Note that stimulation patterns were designed to acquire the extrema of the desired finger flexions and have smooth changes in pulse width rather than achieving intermediate desired finger flexions. (F) Stimulation pattern for wrist movements.

Monkey N did this task with hand control, BMI control, and target-guided FES control, whereas Monkey R only did this task with target-guided FES control. Figure 3-1A illustrates the control flow for hand control, BMI control, and FES target control. In hand control, the monkey's hand moved the manipulandum to control the virtual hand. In FES target control, the monkey's hand again moved the manipulandum to control the virtual hand, however the hand was temporarily paralyzed and moved due to stimulation. In BMI control, the monkey's movement intentions decoded from neural activity moved the virtual hand. We used xPC Target to coordinate the experiment in real time, storing task parameters, neural data, and hand kinematics while

coordinating target presentation, executing the decoder model to predict finger and wrist positions, and sending stimulation commands to the networked neuroprosthesis (NNP) (Smith et al., 2005) (Nason-Tomaszewski et al., 2023). The NNP system then stimulated through the implanted electrodes. Both monkeys also underwent open-loop stimulation, in which electrodes were used for stimulation and hand movements were recorded with video but not displayed on the screen in front of the monkey. Open-loop stimulation was controlled either by the experimenter to test the range of the movements evoked with stimulation patterns (as in Figures 3-2 and 3-3), or by xPC to sample stimulation from the patterns (as in Figure 3-4).

3.2.3 Neural Features

Motor-related spiking band power (SBP) (Nason et al., 2020) was recorded from 96 channels of Monkey N's Utah arrays in primary motor cortex. 96 channels were used due to available recording hardware. Briefly, we configured the Cerebus Neural Signal Processor (Blackrock Neurotech) to sample signals at 2000 Hz and band-pass filter the recorded signals between 300-1000 Hz. Continuous data was sent to the xPC computer which calculated the summed absolute value of neural data on each channel in each 1 ms iteration. For decoding, neural features were aggregated in non-overlapping 32 ms bins by calculating the mean absolute value of the neural feature on each channel. This mean absolute value of 300-1000 Hz bandpass filtered neural data on each channel is referred to as SBP. When decoding intended movements, neural channels were masked to only use channels that were not saturated with noise and that contained morphological spikes during the experiment or in the recent past.

3.2.4 Measuring Joint Angles

Joint angles were ultimately measured with four different methods. In both hand control and closed-loop FES experiments, joint angles were recorded as calibrated sensor values ranging from 0, fully extended, to 1, fully flexed. Sensors were calibrated to either a comfortable range of movement during hand control or to the range of movement over which FES patterns moved the hand during FES experiments. In hand control prior to BMI experiments, the monkeys moved their hand in a custom manipulandum (Figure 3-1B) while finger (all fingers grouped together) and wrist posture were tracked with potentiometers in the manipulandum (RH24PC, P3 America, Leander, TX, USA). The potentiometers connected to an Arduino Uno (Arduino, Somerville, MA, USA), which digitized the analog voltages and sent serial input to the xPC system. In closed loop FES experiments, due to the nerve block inactivating finger intrinsic muscles, the hand lacked rigidity and would slip out of the manipulandum during extension. Instead, flex sensors (FS-L-0073-103-ST, Spectra Symbol, Salt Lake City, UT, USA) were taped to the hand (Figure 3-1C). These flex sensors connected to a custom analog to digital converter circuit which sent serial input to the xPC system.

During open-loop experiments, such as testing stimulation patterns, movements were video recorded using a Canon Eos Rebel T3 SLR camera (Canon, Melville, NY). To ensure consistent video, the camera was mounted on a tripod and angled such that the forearm just proximal to the wrist was at the edge of the frame. The monkey's forearm was braced by an experimenter to keep the hand off the table and moving within the plane of the recorded video. Deeplabcut (DLC) models (Mathis et al., 2018; Nath et al., 2019) were trained to extract hand poses from the video. Briefly, 20 frames were extracted from up to three videos in an experiment. Frames were manually labeled using the DLC API and then the network model was trained. This work used the provided

ResNet-50 model and initiated network training with the provided pre-trained weights. Seven points were labeled in each frame: the forearm, wrist, back of the hand, index metacarpophalangeal (MCP) joint, index proximal interphalangeal (PIP) joint, and index distal interphalangeal (DIP) joint. Due to inconsistencies in recorded video each day, this process was done for each experiment where continuous joint angles were extracted. After evaluating models on videos, frames were filtered out if model certainty was not above 95% for at least two of the labels in the frame used to calculate angles. Wrist and index MCP angles were extracted from DLC labels using a custom MATLAB script. An example frame with wrist and MCP angles labeled is shown in Figure 3-1D. The wrist angle was defined as the angle between a vector from the forearm to the wrist label and a vector from the wrist label to the MCP label. Due to commonly occurring obstructions of the forearm marker (i.e. the edge of the frame, the arm restraint, or the experimenters), the edge of the frame at the forearm was used instead of the forearm marker (Figure 3-1D). The point was chosen such that the vector from the forearm to the wrist was perpendicular to the edge of the frame. The index MCP angle was defined as the angle between a vector from the wrist label to the MCP label and a vector from the MCP label to the PIP label. Extracted angles were then smoothed with a Gaussian-weighted moving average filter with a 0.5 second window.

In open-loop tests where continuous joint angles were not needed, single frames were extracted from videos and joint angles were measured using ImageJ (version 2.35). Wrist, MCP, and PIP joints were marked and angles were measured using the same vectors as when extracting angles from DLC. In some instances, where points were obfuscated, angles were also measured using vectors parallel to the back of the hand or the back of the finger. This angle was then averaged with an angle measured using an estimate of the joint markers.

3.2.5 FES Stimulation

Intramuscular electrodes were connected to a NNP evaluation system for stimulation. This system contained the same circuitry as the NNP used in humans (Clinical Trial NCT02329652) however was in a form more conductive to experimentation. The NNP system consisted of one power module and three pulse generator boards, each with four output channels. The return electrode of each bipolar pair connected to the same pulse generator board were electrically tied together to make one common return for each pulse generator board. During FES experiments, 8 of 12 output channels were used at a time and the remaining 4 outputs were used as LED indicators. All stimulation was current controlled and delivered at 32 ms inter-pulse intervals with either 5 mA or 10 mA amplitudes. Stimulation used charge-balanced biphasic pulses. The cathodic pulse was a square pulse and the subsequent anodic pulse had an exponential shape, falling from an initial anodic pulse back to zero, serving to balance charge and prevent anodic activation. Stimulation intensity was modulated by changing the width of the initial cathodic pulse, varying between 0 and 255 microseconds. Pulse width modulation was used due to the history of successful upper limb stimulation with it (Kilgore et al., 1989) and the potential to evoke the same movements with a lower amount of delivered charge (Crago et al., 1980).

Stimulation patterns were manually designed using anatomical knowledge and results from single electrode stimulation characterization experiments. During the characterization experiments, for each monkey, the median, radial, and ulnar nerves of the monkey's arm were blocked with a lidocaine epinephrine mix. Then, video was obtained while each electrode was stimulated at a range of pulse widths at either 5 mA or 10 mA pulse amplitudes. Some electrodes were tested at both 5 mA and 10 mA to determine if one resulted in more graded contractions. Video was used to determine pulse widths and amplitudes for use in stimulation patterns. Initial

patterns were made by setting the pulse width at maximal commands to the pulse width that evoked the largest movement in the desired DOF without evoking movements in additional DOF and the pulse width at the 50 percent command to the pulse width that caused the first movement in the desired DOF. The patterns then smoothly transitioned pulse widths between these two points. At the beginning of experiments, these established stimulation patterns were tested and then adjusted if necessary, typically by changing the amount of overlap for flexor and extensor muscle activations or by increasing or decreasing maximal pulse widths. As a result, patterns typically changed with each experiment. Example stimulation patterns for Monkey R can be found in Figures 3-1E and 3-1F.

3.2.6 Nerve Block

In order to achieve temporary hand and wrist paralysis, we performed an ultrasound guided nerve block of the median, radial, and ulnar nerves just proximal to the elbow prior to stimulation. First, lidocaine (2%) was injected subcutaneously near the planned injection sites to help prevent discomfort from injections. Then a solution of lidocaine (2%) and epinephrine (1:100 000) was injected into the perineural space surrounding the nerve under ultrasound guidance. In later experiments, the lidocaine dosing was reduced to 1% without a noticeable change in the efficacy of nerve block. Typical blocks involved injecting 1 mL to 1.5 mL around each of the three nerves. This blocked hand function for sufficient time to perform FES tests (about 2 hours) without re-dosing. Block effectiveness was first tested with a grasping task where we observed their motor capabilities while they attempted to grasp offered treats. Block effectiveness was further tested throughout experiments by inserting catch trials where stimulation was turned off and the monkey was allowed to attempt acquiring targets, thus earning juice, on their own.

3.2.7 Open-Loop FES Experiments

In order to investigate the range of movements that could be evoked in each DOF with FES, predetermined stimulation commands were sent, and then evoked movements were recorded on video. Joint angles were extracted later using DeepLabCut or ImageJ. Multiple types of datasets were recorded on these days, often on separate days due to fatigue. These included testing stimulation at multiple points along individual patterns, testing stimulation on the finger pattern with a constant wrist muscle activation maintaining a wrist posture, and testing stimulation at random points along both patterns. Stimulation at random points on the patterns was coordinated using xPC. The xPC selected random targets along the whole range of flexion for each DOF but did not present them on the screen. Instead, stimulation at the point in the patterns expected to reach that target were delivered and the evoked movements were recorded.

3.2.8 Closed-Loop FES Experiments

To investigate graded control of FES in 2-DOF, FES was used to move the monkey's fingers and wrist to acquire virtual targets. Wrist and finger angles were acquired with flex sensors taped to the back of the wrist and to the back of the index finger. At the beginning of the experiment, the monkey's wrist and hand were temporarily paralyzed using an ultrasound guided nerve block of the median, radial, and ulnar nerves. Before closed-loop tests began, stimulation patterns for both the wrist and the fingers were tested to ensure that they moved the desired joint through a large range of motion. If needed, patterns were adjusted to produce better movements and then retested. Flex sensor measurements were calibrated so that the virtual hand was fully flexed or extended at approximately the range of motion available from stimulation. Target amounts of flexion for both the wrist and the fingers were selected and then targets were presented on the screen. Target sizes were 22.5% and 24.9% of the movement range for the fingers and wrist

respectively. For a trial to be successful, both the fingers and the wrist had to remain in their respective targets for 500 ms. Trials resulted in failure if this took longer than 10 seconds. The stimulation was controlled with a simple algorithm that, every 32 ms, checked if the fingers and the wrist were in their targets, and if not would update the stimulation pulse width for the joint not in the target using the stimulation patterns by moving 1 command value (out of 255) on the corresponding joints pattern in the direction of stimulation needed to get to the target (i.e. flexion or extension).

3.2.9 BMI Experiments

To investigate whether Monkey N could use a BMI to control 2-DOF virtual wrist and finger movements before and after temporary paralysis, we implemented a position/velocity ReFit Kalman Filter (RKF) similar to what we have previously published with two finger-groups (Mender et al., 2023; Nason et al., 2021). To train the decoder, first Monkey N completed at least 300 trials with hand control, in the adapted finger and wrist manipulandum (Figure 3-1B). Then a position/velocity Kalman filter (KF) was trained using the hand control data and used in BMI control for at least 200 trials. This KF BMI control data was then used as training data for the RKF model. The RKF model was then used in BMI control for at least 150 trials to get an initial performance, after which the nerve block was performed. Once hand function was confirmed to be lost, the same RKF model was used in BMI control again for at least 150 trials. One more RKF model (Re-ReFIT model, ReRKF) was then trained using these post-nerve block RKF BMI control trials. The ReRKF model was then tested in BMI control for 130 or more trials.

Targets were presented in a center-out fashion requiring flexing or extending the fingers and or wrist, for a total of 8 movement combinations and to 3 different magnitudes of movement from center. The subsequent trial then required moving back to center, additionally the trial after

a failed trial required moving back to center. Targets presented were 16.9 to 18.8% of the movement range for the finger target and 18.7 to 20.8% of the movement range for the wrist target. Targets had to be held for 500 ms in BMI control and 750 ms in hand control. In one run of hand control trials the target hold time was mistakenly set to 500 ms instead of 750 ms. Trials were considered failed if targets were not reached and held within 10 seconds.

3.2.10 BMI Decoder Training

Decoder training matches training for a KF for two finger groups (Nason et al., 2021) but with updated parameters to use the wrist instead of a second finger group. The KF and RKF assume a kinematic state with one position and velocity for each degree of freedom. For the 2D finger and wrist task, there is one position and velocity for the wrist and one position and velocity for the fingers:

$$x_t = \begin{bmatrix} P_I \\ P_W \\ V_I \\ V_W \\ 1 \end{bmatrix}$$

Where x_t is the kinematic state at time t, P_I and V_I are position and velocity for the index finger, and P_W and V_W are position and velocity for the wrist. Note that the fingers were grouped together in visualizations by giving the rest of the fingers the same kinematics as the index finger. The KF updated the kinematic state at 32 ms intervals by combining a prediction of the state given the previous state ($\hat{x}_{t|t-1}$) with a state update gained from comparing the measured neural activity with the neural activity that was expected to be observed in this time step:

$$\hat{x}_{t|t-1} = A\hat{x}_{t-1}$$

$$\hat{x}_t = \hat{x}_{t|t-1} + K_t(y_t - C\hat{x}_{t|t-1})$$

where A is the kinematic trajectory model, C is the neural observation model, K_t is the Kalman gain and y_t is the measured neural SBP data for all active channels. The C matrix was computed by regression of kinematics to neural features. The A matrix contains scalars weighing how much each kinematic state variable contributes to the update of the kinematic state. This was trained by regression of the state at time t-1 to the state at time t, however the A matrix was constrained to have positions only updated by velocities, as expected of physical trajectories. To do this, the A matrix was given by:

$$A = \begin{bmatrix} 1 & 0 & 1 & 0 & 0 \\ 0 & 1 & 0 & 1 & 0 \\ 0 & 0 & A_{V_I V_I} & A_{V_W V_I} & 0 \\ 0 & 0 & A_{V_I V_W} & A_{V_W V_W} & 0 \\ 0 & 0 & 0 & 0 & 1 \end{bmatrix}.$$

The RKF and ReRKF models followed the same KF algorithm but used retrained model parameters. To train these models, the predicted velocities from the BMI trials used as training data were augmented by identifying timesteps with velocities in a direction away from the target and rotating the velocities to point towards the correct 2D target vector, but not rescaling the vector. This matches the assumption that the monkey intended to be moving towards the target during the online trials. New model parameters were then trained using the augmented velocities. During use of the RKF and ReRKF models, there was no further modification of the velocities.

3.2.11 Performance Metrics

We measured performance during FES closed-loop trials and BMI trials with success rate and acquisition time. In BMI control, trials were excluded if they were not entirely closed-loop (e.g. the first and last trial), or if a different target presentation style was used. Similarly, FES trials were excluded if stimulation was not turned on for the entire trial. FES trials were also excluded if both DOF started in their target, or if the taped-on flex sensors were noted as being out of place

and giving erroneous readings. Success rate was then measured as the ratio of successful FES or BMI trials to the number of valid FES or BMI trials. Acquisition time was measured as the time required to complete the trial, minus the hold time and was only measured for valid successful trials. In BMI trials, we also calculated an orbiting time, that is the time between first reaching both targets simultaneously, and successfully holding the targets, minus the hold time. Orbiting time was measured for all valid and successful BMI trials with a non-zero orbiting time.

3.3 Results

3.3.1 Coordinating Electrode Stimulation with Patterns

In order to restore dexterous hand movements, it is necessary to continuously control multiple DOF in the hand. A benefit of intramuscular stimulation is that stimulation on individual electrodes is expected to activate portions of individual muscles and therefore evoke more selective movements which can then be combined into functional movements. We first ask how well we can control individual DOF in the wrist and fingers using coordinated stimulation of multiple intramuscular FES electrodes. Two monkeys were implanted with bipolar intramuscular electrodes (Synapse Biomedical, Oberlin, OH). Monkey N was implanted with 8 bipolar leads targeting 6 different muscles, while Monkey R was implanted with 16 bipolar leads targeting 8 muscles. During the implantation for Monkey R, nerve entry points were specifically targeted to improve selectivity of evoked movements due to stimulation.

Following the conventional FES control methods (Kilgore et al., 1989), a stimulation pattern was defined for each DOF. Patterns were established using initial single electrode stimulation results and trial and error as described in the Methods, then minimally adjusted on each day. Figures 3-1E and 3-1F shows example finger and wrist patterns respectively for Monkey R. We first tested how well we could control one DOF at a time. During experimental sessions, we

measured step responses in evoked finger and wrist movements to stimulation at different points along the patterns. Figures 3-2A and 3-2C show example movements using the wrist pattern and the finger pattern respectively for one session with Monkey R. Qualitatively, the wrist pattern successfully moves the wrist through a large range of motion but sometimes recruits finger movements at the most flexed or extended commands where stimulation to wrist flexor or extensor muscles is high. Similarly, the finger pattern successfully moves the fingers through a large range of motion, however, it substantially moves the wrist as well.

To quantify the movements, we measured the joint flexion angles for the wrist joint and the index MCP joint during each evoked movement. More positive angles correspond to more extended joints with 180 degrees indicating straight extension and 90 degrees representing perpendicular flexion. Figures 3-2B and 3-2D illustrate example measurements for one session testing the wrist and finger pattern respectively. On three days for each monkey, we tested the range of evoked movement in finger and wrist joints for each pattern at the beginning of experiments (Figures 3-2E and 3-2F). The finger patterns moved the fingers through a large range for both monkeys, averaging 85 degrees for Monkey N and 91.4 degrees for Monkey R. The wrist patterns moved the wrist through an average of a 97 degree and 55.5 degree range for Monkey N and Monkey R respectively. Both patterns consistently moved both the wrist and fingers but the movements were significantly larger in the intended joint for that pattern. Across both monkeys, finger pattern evoked finger movement ranges were 36.5% larger than wrist movement ranges ($p<0.05$, one-sided paired t-test, n=6), whereas wrist pattern evoked wrist movement ranges were 326.5% larger than finger movement ranges ($p<0.01$, one-sided paired t-test, n=6). Additionally, wrist patterns evoked a 69.3% smaller range of finger movements compared to the finger patterns ($p<1e-4$, one-sided paired t-test, n=6), while wrist and finger patterns evoked the same range of

wrist movements ($p>0.05$, two-sided paired t-test, $n=6$). This indicates that stimulating wrist muscles in the wrist patterns more selectively evoked movements in the intended joint compared to stimulating the extrinsic hand muscles in the finger patterns.

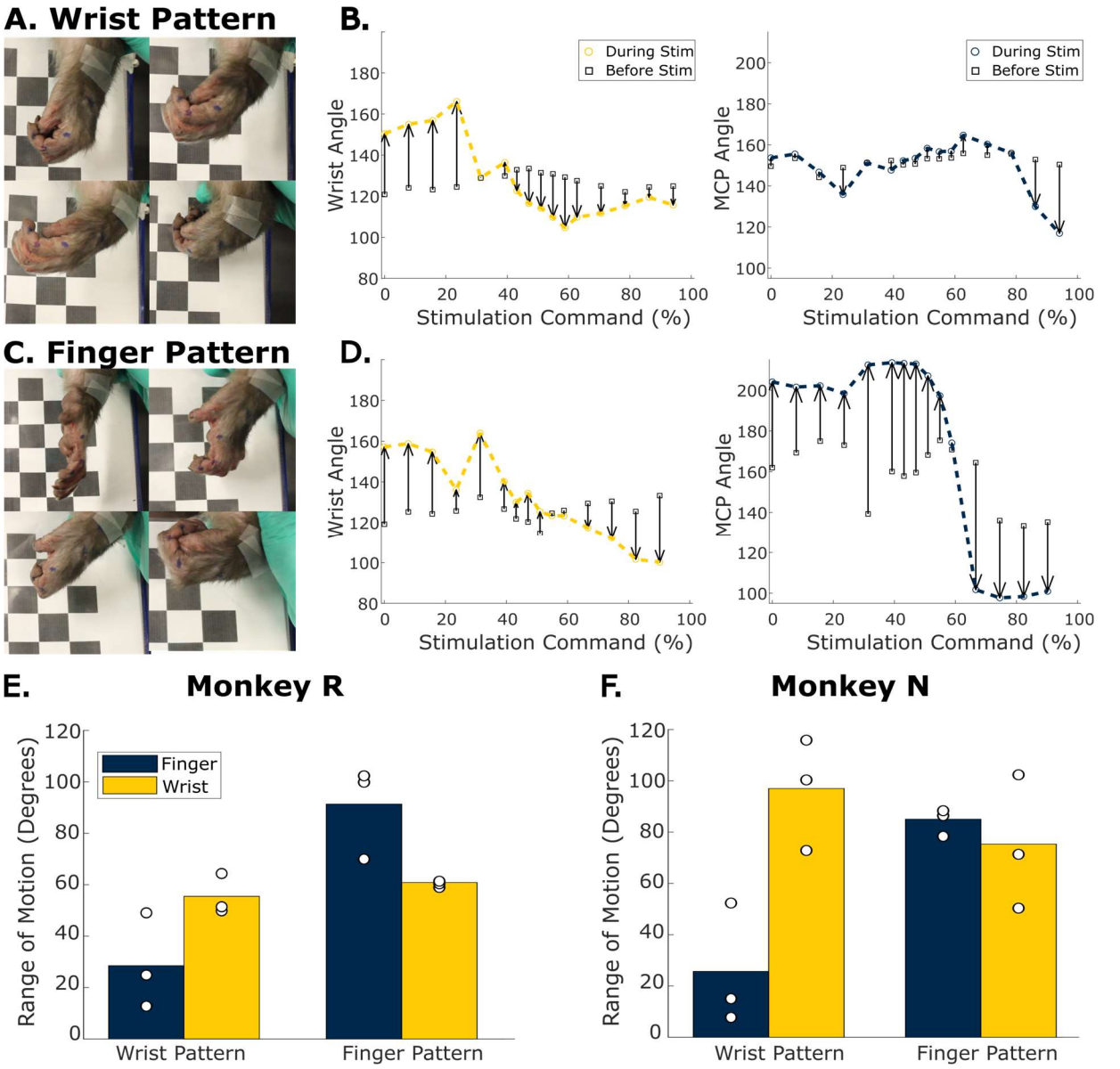

Figure 3-2 Range of movement using stimulation parameters independently.
(A) Example evoked movements from testing the wrist stimulation pattern on one example day with Monkey R 64 days after implant. (B) Measured wrist (left) and index MCP (right) angles from testing the wrist stimulation pattern on one day with Monkey R. Open squares indicate the resting position before the stimulation was stepped to the stimulation for the respective command. (C-D) Same as (A-B) but with stimulation from the finger pattern. (E-F) The range of evoked movements in the MCP joint (blue) and wrist joint (yellow) using the wrist pattern and finger pattern for Monkey R (E) and Monkey N (F) respectively. Open circles indicate measurements from different experiments where patterns were tested.

One concern with using these patterns is that they describe control of each DOF independently however they generally evoke movements both in the fingers and the wrist. We next asked what movements we would be able to elicit using these two patterns simultaneously. We first tested four specific postures, open or closed fingers with the wrist flexed or extended. These were tested by holding the wrist pattern constant at flexion or extension and then varying the finger pattern to move the fingers into the desired postures. Figure 3-3A and 3-3B show example movements during these tests for Monkey R and Monkey N respectively. This was done on two days for each monkey. Figure 3-3C and 3-3D illustrate the range of movement on each day for Monkey R and Monkey N respectively, by plotting the measured angles for each movement as a corner of the quadrilateral, resulting in one quadrilateral for each day. Measured angles were normalized by the range of movement that individual patterns moved the joints to on that day. For example, a wrist extension of 1 is the angle that the wrist pattern extended the wrist to on that day and a finger extension of 0 is the angle that the finger pattern flexed the fingers to on that day. With this normalization, a 2-DOF range of motion that matched the joint angles given by individual patterns would make a quadrilateral with an area of 1. When testing these four postures, the average area of the range of movements was 0.91 (std = 0.38). Both monkeys had one day with an area greater than 1 and one day with an area less than 1.

There are two effects due to biomechanical coupling that we expect to limit the range of movements available in 2-DOF stimulation. One is active coupling from the extrinsic finger muscles exerting a torque on the wrist when activated. The second is passive coupling where changes in wrist posture change the tendon length of extrinsic finger muscles making finger flexion or extension easier. We asked how large of an effect both of these types of biomechanical coupling

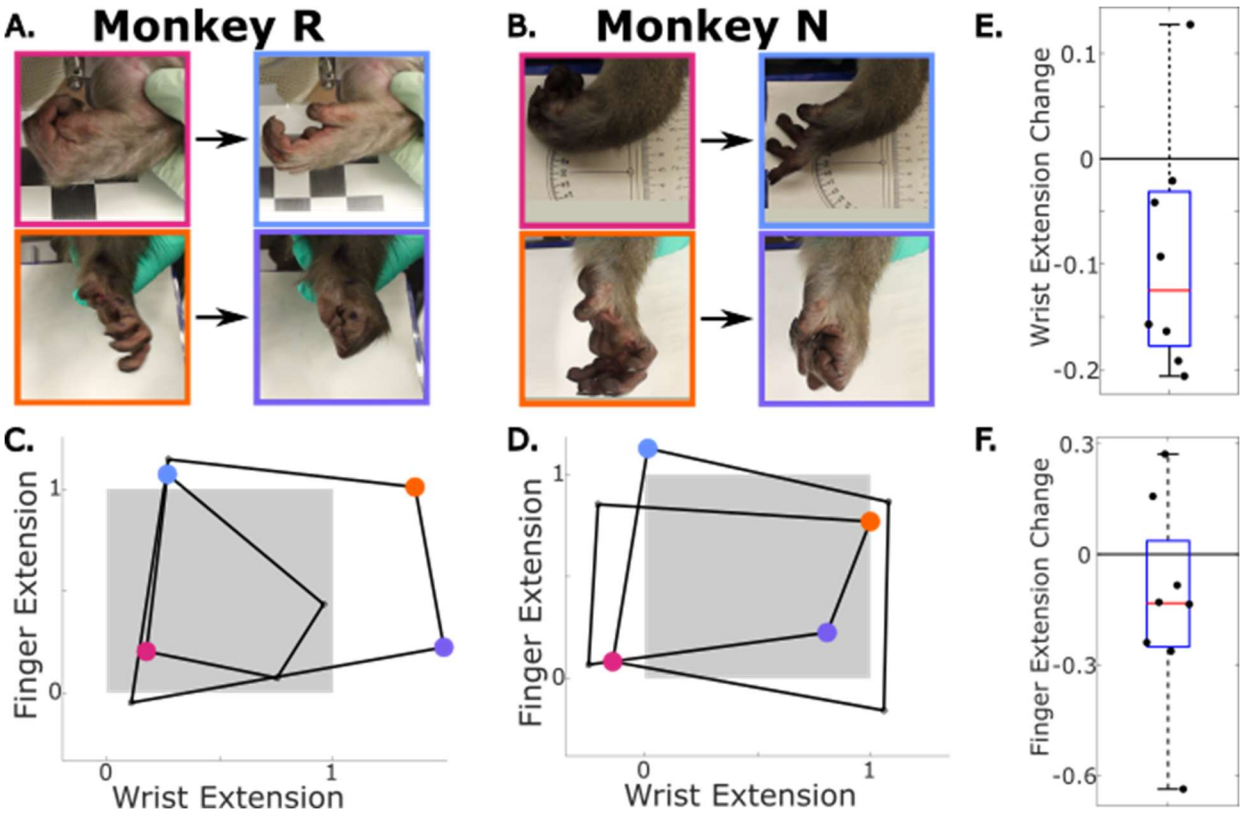

Figure 3-3 Range of movement using two-patterns simultaneously
(A) Example stimulated movements opening or closing the fingers with simultaneous stimulation holding the wrist in flexion (top) or extension (bottom). Results for Monkey R. (B) Same as (A) but for Monkey N. (C) Measured finger and wrist angles when opening and closing the fingers with the wrist held fully extended or fully flexed. Angles for postures on the same day are connected to make one quadrilateral. All four postures were tested on two days. Colored points correspond to the frames in (A). Extensions are calibrated to the range of movements available from stimulation with the corresponding pattern for that DOF. The grey box is a unit square corresponding to the calibration. (D) Same as (C) but for Monkey N. (E) Change in wrist extension (fraction of normalized range of movement) when the fingers are stimulated to flexion with stimulation holding the wrist either flexed or extended. (F) Change in finger extension (fraction of normalized range of movement) when the wrist is being held extended as opposed to being held flexed. Results include both when the fingers are open or closed.

had on our example movements. Figure 3-3E presents the change in wrist extension in movements with the fingers moving from extended to flexed while maintaining the same wrist posture. Flexing the fingers significantly flexed the wrist with a median change in wrist extension of -12.5% of the range ($p=0.027$). Figure 3-3F presents the change in finger extension when the fingers were at flexion or extension with the wrist extended as opposed to flexed. The fingers tended to be more flexed at wrist extension with a median change of -13.3% of the range, but there was a lot of variability between movements and the trend was not significant across all movements.

While these movement areas represent the edges of the range of movement, they didn't sample many combinations of the finger and wrist patterns together because the wrist pattern was held constant during the finger movements. We next asked what range of motion we could get by sampling along both patterns. To test this, we stepped stimulation between random points along the two patterns every three seconds and measured the resulting index MCP and wrist joint angles. This was done on two days for each monkey and then results were pooled for each monkey. Figure 3-4A and 3-4B illustrate the range of the resulting movements for each monkey. The enclosed area indicates a boundary on the measured movements in each joint with the red boundary indicating trials in the first three minutes (approximately 60 trials) and the black boundary indicating later trials in the last three minutes. Experiments were 8.37 and 7.95 minutes long for Monkey R and 6.15 and 9.92 minutes long for Monkey N. We observed initial movements through a large portion of the finger and wrist movement space for both monkeys that diminished over time, presumably due to fatigue. In the first three minutes, Monkey R's movement range area was 1.42 and Monkey N's movement range area was 0.84. Figure 3-4C presents the change in movement range area for each day, split by monkey. In the last three minutes, Monkey R's movement area was 48.1% smaller and Monkey N's movement area was 76.7% smaller than movements in the first three minutes. This fatigue effect was largest for wrist extension for both monkeys. We calculated the centroid for the movement area on each day and calculated how far (the fraction of the normalized range of movement) it moved between the first three minutes and last three minutes (Figure 3-4D). Across monkeys and days, the centroid shifts away from wrist extension by an average of 17.0% of the movement range. The centroids did not consistently shift away from or toward finger extension.

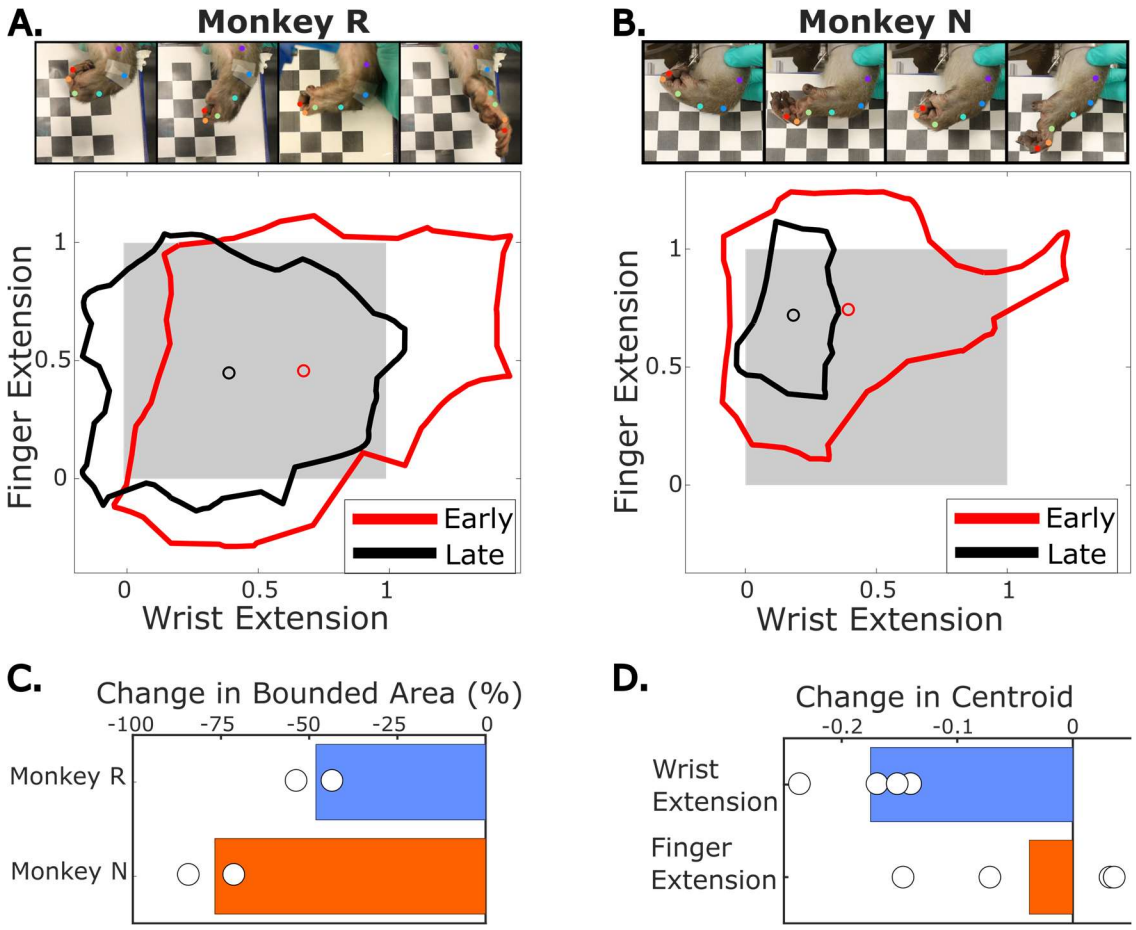

Figure 3-4 Movement range using graded stimulation on both patterns.
(A) (Top) Example frames from video of 2-DOF stimulation in Monkey R with markers estimated using DLC. (Bottom) Boundaries drawn containing measurements of each finger extension and wrist extension from video frames when stimulation was being administered in the first 3 minutes (red) or last 3 minutes (black). The frames at the highest and lowest 1% of measurements in each DOF are excluded. Angles are calibrated to the range of movements available from stimulation in the respective pattern. Grey box is a unit square corresponding to the calibration. (B) Same as (A) but with Monkey N. (C) Change in bounded area between the first 3 minutes and last 3 minutes using two experiments per monkey. (D) Change in centroid location of the bounded areas between the first 3 minutes and last 3 minutes, pooled across the 4 experiments in the 2 monkeys.

3.3.2 Continuous control of 2-DOF FES

With a large range of 2-DOF wrist and finger movements available using FES, we also will want to continuously control this stimulation to reach specific postures throughout the available range of movement. To test this, we used a virtual finger and wrist target acquisition task in which we presented targets on a screen and then used FES to control the monkey's nerve-blocked hand to acquire those targets as described in the Methods. Wrist and finger angles were measured with flex

sensors calibrated at the beginning of experiments to the range of movement available from the stimulation. Figure 3-5A shows finger and wrist extension as well as targets presented during an example run of FES trials for Monkey R, illustrating the fingers and wrist moving simultaneously to separate targets. This control strategy was moderately successful at acquiring targets throughout the range of movement, however, trials commonly failed at the edge of the range of movement, or by not being able to maintain wrist posture while moving the fingers. In an effort to maximize performance, we tested the ability to reach targets in a reduced range of movement consisting of the middle 50% of the range of movement for each joint. We repeated this FES control in four experiments, two for each monkey. Figures 3-5B and 3-5C show the probability of trial success given target locations, pooled across both days for each monkey. Both monkeys had some difficulty extending the wrist while the fingers flexed (50% success for Monkey R and 33.3% success for Monkey N in the most extreme wrist extension, finger flexion area) and Monkey R also had some difficulty extending fingers. However, in each experiment we obtained greater than 84% success using this reduced range of targets (Figure 3-5D). Figure 3-5E shows the acquisition time for each trial grouped by experiment and the dashed line indicates a representative acquisition time from Monkey N doing the task able bodied with the manipulandum (average from BMI experiment hand control). While success rates were high, acquisition times were much slower than able bodied control. Ultimately, this continuous control shows that we have fine enough control of FES to reach precise postures within a reduced range of motion.

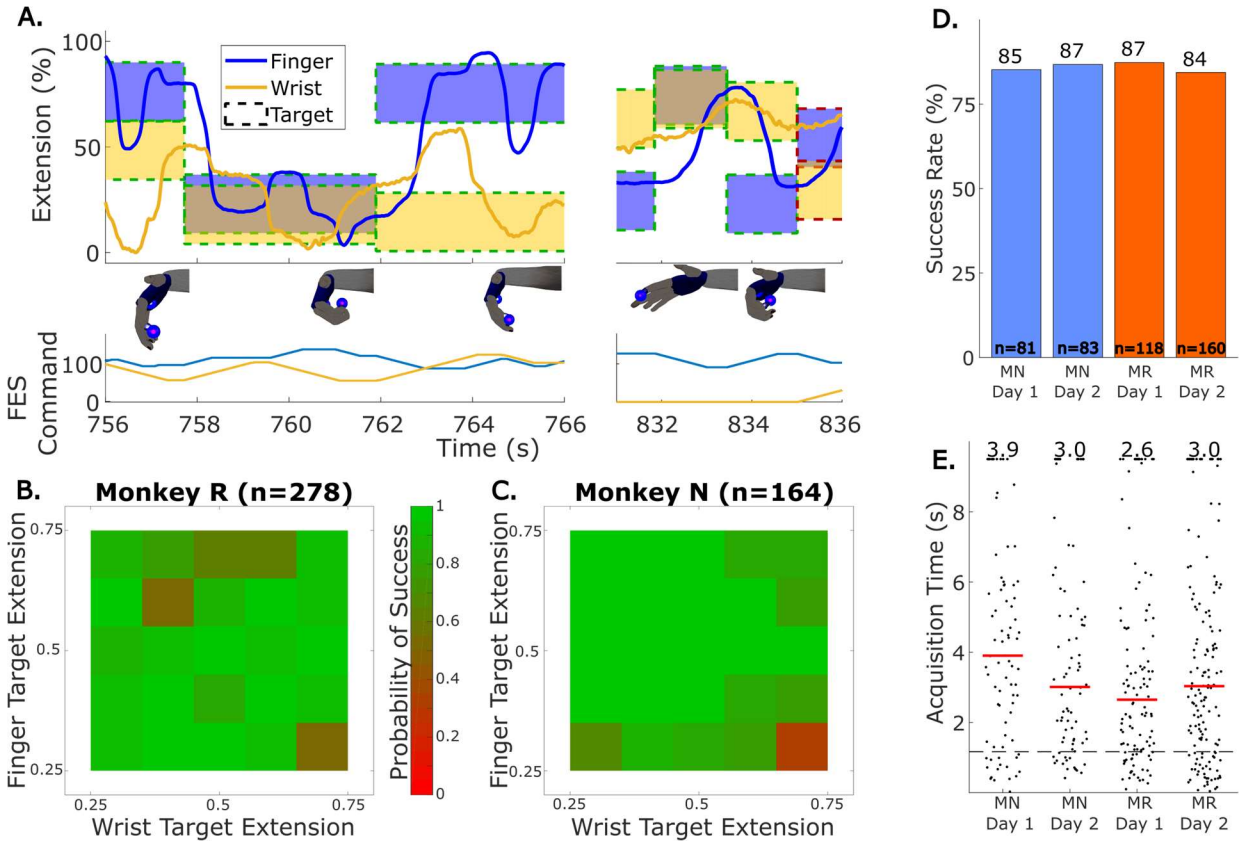

Figure 3-5 Closed-Loop control of two-DOF FES
(A) Example finger and wrist extension (top) and FES commands (bottom) from closed-loop FES control. Blue and yellow patches indicate targets; a green border indicates success while a red border indicates failure. Representative images of the virtual hand are included to illustrate the target movement at that time. (B) Probability of closed-loop FES trial success by target location, pooled across two experiments for Monkey R. (C) Same as (B) but for Monkey N. (D) Success rate for closed-loop FES in each session. MN=Monkey N, MR=Monkey R. (E) Acquisition times for successful trials using FES. Red bars and numbers above each column indicate the median acquisition time for that session. Dashed line indicates an example acquisition time from Monkey N using hand control.

3.3.3 BMI Control of Virtual Finger and Wrist Movements

Pattern based FES control simplifies the command signals down to one signal for each degree of freedom. This type of control is analogous to BMI control in which independent DOF are read out from the neural activity. We asked how well we can generate a command signal from brain activity to ultimately control this 2-DOF FES aimed at restoring finger and wrist flexion movements. We trained a monkey to do a 2-DOF finger and wrist task, moving their fingers grouped together in a manipulandum and flexing or extending their wrist in order to acquire targets on the screen in front of them. We then trained a ReFIT Kalman filter model (RKF) following the

procedure we have used previously (Mender et al., 2023; Nason et al., 2021) enabling the monkey to control the virtual hand with only their activity from implanted Utah arrays (Figure 3-1A, BMI control). While these experiments were done in the Monkey N (also described above) they were separated in time from FES due to brain signal quality. Monkey N was able to achieve high levels of success simultaneously controlling the wrist and finger flexion with a BMI. Figure 3-6A shows example decoded finger and wrist flexion from a real-time BMI session with Monkey N using the RKF model. The monkey acquired targets with 97% success with a median acquisition time of

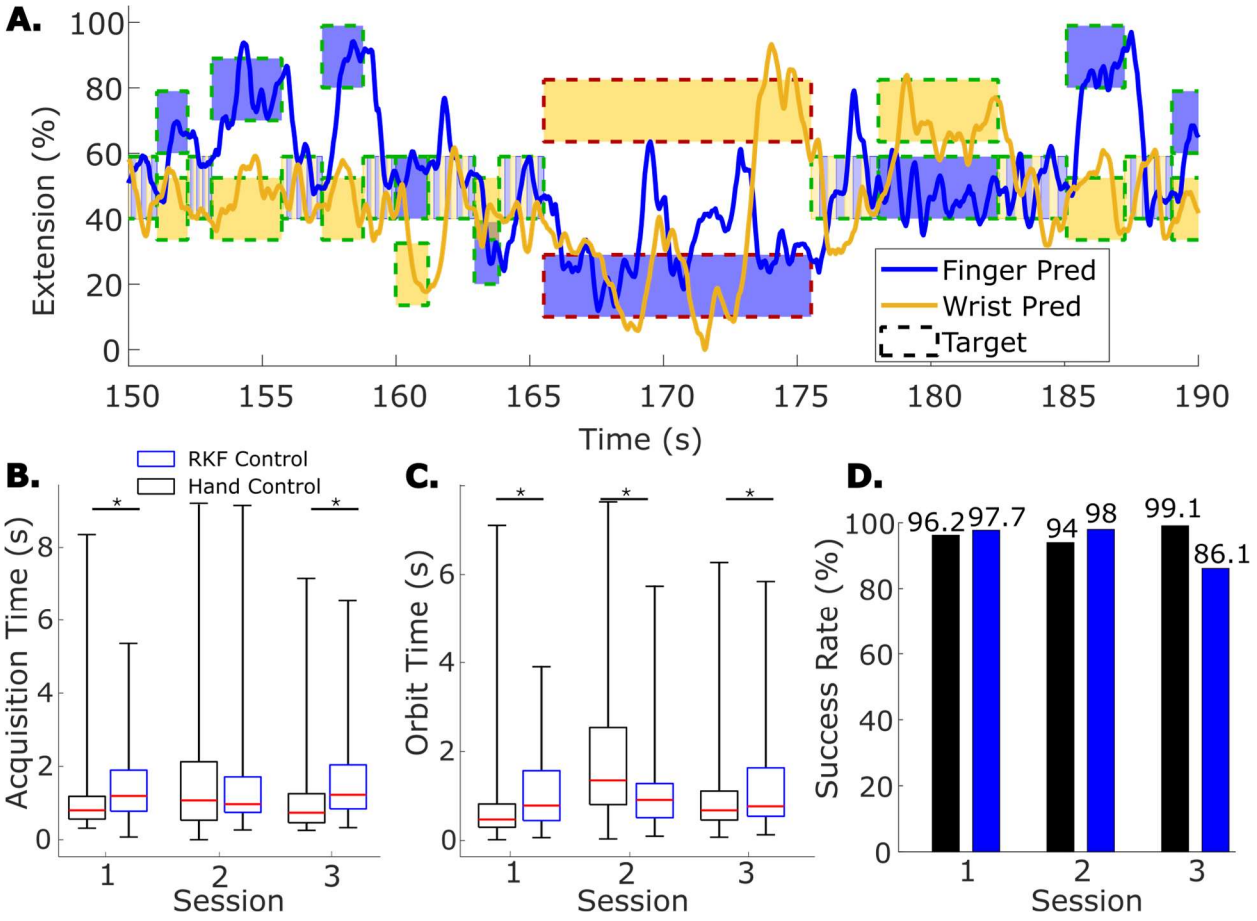

Figure 3-6 Two-DOF BMI control of virtual wrist and fingers
(A) Example decoded finger and wrist extension from a closed-loop BMI experiment. Green target boundary indicates trial success, and red target boundary indicates failure. (B) Box plot illustrating the distributions of acquisition time for all 3 sessions with RKF control in blue and hand control in black. Red bars indicate median, the box includes the 25th to 75th percentiles, and whiskers indicate the full range. * indicate significant difference between RKF and hand control ($p<0.05$ two-sample t-test). (C) Box plot of the distribution of orbit times for all three sessions, following the format in (B). (D) Success rate using hand control (black) or BMI control (blue) during each session.

1.0s during this session. We tested 2-DOF BMI control of the wrist and finger DOF on three experimental days. Performance was measured with acquisition time, orbit time, and success rate (Figures 3-6B to 3-6D). Performance with the RKF model was comparable to that of using the hand to control the manipulandum with only sessions 1 and 3 showing increases in median acquisition time (391 ms and 489 ms respectively, $p<1e-4$ two-sample t-test), and increases in median orbiting time (311.5 ms and 89.5 ms respectively, $p<0.05$ two-sample t-test). Due to the good performance we concluded that there is enough information in our array recording in hand area to decode command signals for two-DOF in real time with a linear Kalman filter.

For translational purposes, it will be important to decode intended movements in a patient with spinal cord injury whereas our monkey model is able-bodied. To this end, we tested whether the trained Kalman filter could still decode two-DOF of intended movements in a real-time BMI task after the same nerve block used in FES experiments, which eliminates movement and proprioception similar to a spinal cord injury. The order of BMI tests relative to the nerve block are illustrated in Figure 3-7A. First, a RKF model was trained and tested prior to the nerve block. Then the nerve block was performed and the same RKF model was tested again. Figure 3-7B and 3-7D show average acquisition time and success rate respectively during each set of trials in one example session. While using the same RKF model after nerve block, the RKF performance decreased, acquisition time increased from 994 ms to 1707 ms, and success rate decreased from 98% to 93%. Interestingly, some performance could be regained through an extra retraining step with the ReFIT method using the successful trials from BMI control after nerve block. In the example session, using the retrained RKF improved acquisition time to 1035 ms and success rate to 96.9%. We repeated the BMI task in three nerve block experiments. When testing the same RKF before and after nerve block, BMI performance consistently decreased after the nerve block.

Acquisition time increased on all three days ($p<7e-4$) with an average increase in acquisition time of 586.3 ms, meanwhile success rate decreased on days 1 and 2 ($p<0.04$ chi-squared test) by an average of 9.1%. Retraining the Kalman filter using ReFIT on BMI trials after the nerve block successfully regained performance in all three experiments, significantly improving acquisition time on days 1 and 2 ($P<7e-4$, two sample t-test) by an average of 695 ms, and improving success rate on days 1 and 3 by an average of 10.4% success. Performance after retraining was not significantly different from the RKF before nerve block for days 1 and 2, while day 3 had a higher

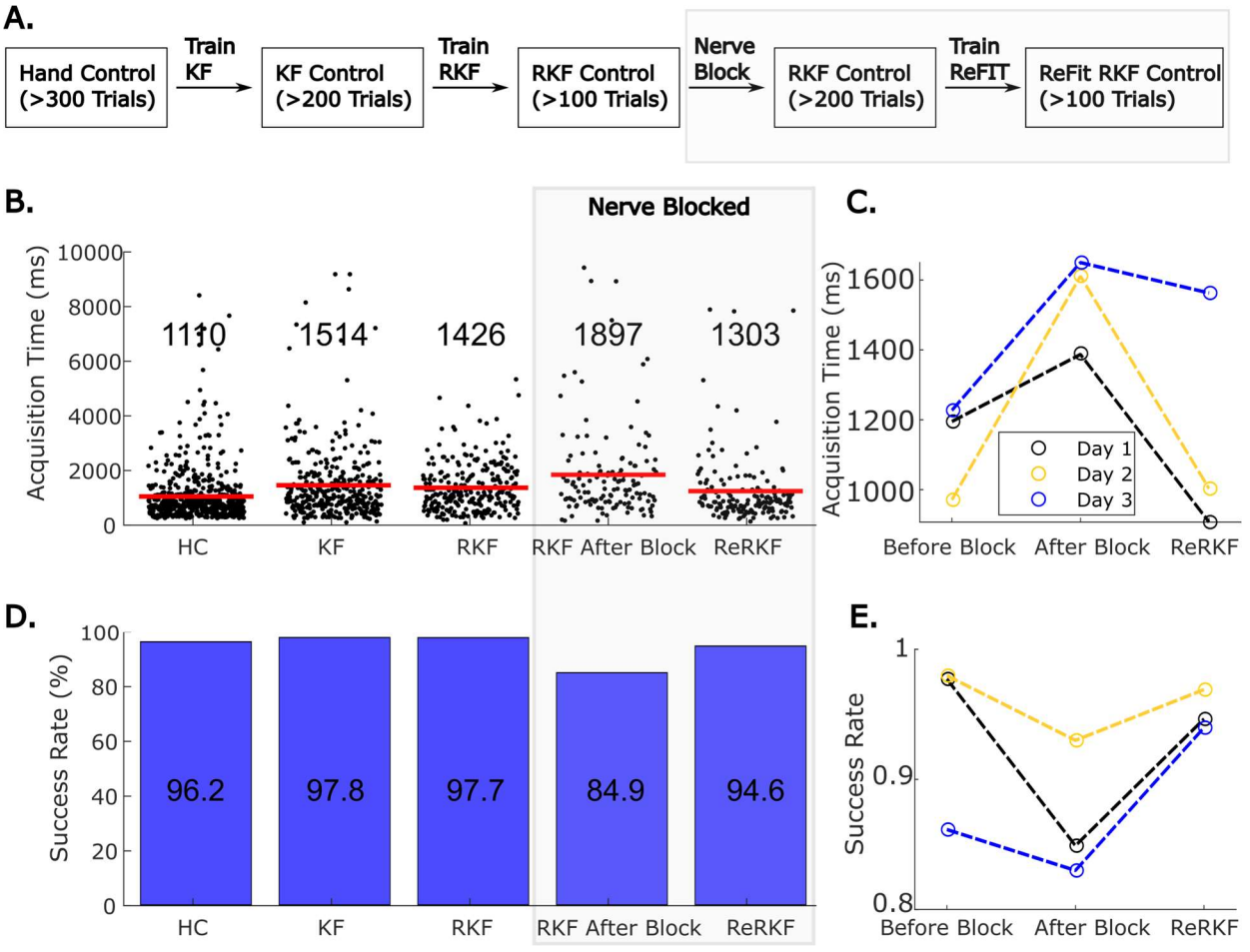

Figure 3-7 Recovering BMI performance after nerve block.
(A) Illustration of the model training process with respect to the nerve block. (B) Acquisition times during an example session. ReRKF is the decoder that was trained in a second ReFIT step after nerve block. Red lines and numbers near the top of each column indicate the median acquisition time for that set of trials. (C) Median acquisition time during 3 experiments where an RKF was tested before and after nerve block and then compared to the ReRKF. (D) Success rates during an example session. (E) Success rate during the 3 experiments where RKF was tested before and after nerve block and compared to ReRKF.

success rate (7.8% success, p=0.017 chi-squared test) but slower acquisition time (609ms, p=7e-4 two-sample t-test). Ultimately this shows that using a linear Kalman filter we can decode intended movements in 2-DOF after nerve block despite the loss of sensory information.

3.4 Discussion

Intramuscular FES is promising for restoring dexterous hand movements due to its ability to selectively activate portions of muscles and evoke selective movements. With more movements available, stimulating with multiple electrodes can cover a larger basis of hand movements. Here we characterize how well we can combine stimulation on two biomechanically linked DOF, that is the wrist and the fingers, simultaneously. We found that stimulation successfully evokes a large range of movements, similar in size to what would be expected from stimulating each DOF independently. However, the range is significantly impacted by interactions between evoked movements from stimulation on both patterns. For example, stimulating extrinsic finger muscles caused large wrist movements that limited the full 2-DOF range. Still, commanding stimulation for each DOF independently resulted in greater than 80% success when using the stimulation to reach target joint angles in the middle of the movement range.

Controlling the degree of flexion on independent DOF is analogous to BMI control in which independent joint angles are decoded from neural activity (Ajiboye et al., 2017; Nason-Tomaszewski et al., 2023). Previous works have decoded finger movements (Nason et al., 2021; Vaskov et al., 2018), or decoded wrist movements (Ajiboye et al., 2017). However, finger-related muscle activations change when moving the fingers in different wrist postures (Beringer et al., 2020), and this has an impact on neural activity and finger movement prediction accuracy (Mender et al., 2023). Here we show that Utah microelectrode arrays implanted in finger area of primary motor cortex of one animal can decode simultaneous finger flexion and wrist flexion. To our

knowledge, this is the first work showing continuous decoding of simultaneous finger and wrist movements. The success of this approach may be linked to the adaptable approach of the BMI decoding, which allows users to re-aim their intended control to successfully acquire targets (Golub et al., 2018b; Jarosiewicz et al., 2008; Mender et al., 2023).

Retraining BMI decoders with methods like ReFIT (Gilja, Nuyujukian, Chestek, Cunningham, Yu, Fan, Ryu, et al., 2012) is likely integral to improving online performance in clinical applications. For example, in our nerve block model of hand and wrist paralysis, we found that blocking motor output and sensory afferents significantly worsened decoder performance. These results suggest that motor cortex activity changed significantly after a change in sensory afferents, similar to what has been described previously (Nason-Tomaszewski et al., 2023). When we retrained the model using augmented training data, performance was restored to near pre-block levels. In clinical applications, these BMI methods will be applied to people with spinal cord injuries in which there are little sensory afferents and little to no motor output with which to train models. In these applications, training an initial model is difficult, but is generally achieved by relying on training data from attempting or observing the task. Retraining can then result in an accurate model for online use as long as there is some form of initial BMI control.

Throughout these experiments muscle fatigue has been a limiting factor. In intramuscular FES, fatigue is caused by a few factors. Large motor units that fatigue quickly are recruited before smaller fatigue resistant fibers, a phenomenon known as reverse recruitment. Fibers are also recruited at relatively high rates. In normal recruitment, fiber activations are offset and a fused contraction is formed by many overlapping twitches offset in time. In FES, all of the fibers are activated at once, so a fused contraction must be created by stimulating at a higher rate. Here, significant fatigue was observed in some muscles after as few as three minutes of stimulation.

More work is needed to identify stimulation paradigms that can alleviate fatigue. One promising route is through implanting electrodes in multiple motor points along the same muscles. Theoretically, this will activate different subsets of muscle fibers (Gruner & Mason, 1989) and stimulation can then be offset sequentially to lower the rate that any one subset of muscle fibers is activated and thus reduce fatigue (Peckham et al., 1970; Thomsen & Veltink, 1997).

Future work can aim to account for interactions between the DOF being controlled, both with respect to decoding accuracy and FES control. Ultimately, brain-controlled FES involves decoding an intended movement and a translation from intended movement to the stimulation parameters required to perform the movement. To predict intended movements, nonlinear methods such as neural networks have been increasingly successful in BMI applications (Glaser et al., 2020; Willsey et al., 2022). Importantly, these methods can model interactions between DOF, so given enough training data, more accurate decoders can be trained. Alternatively, feature engineering can be used to improve the decoding accuracy for specific approaches (Mender et al., 2023; Schroeder et al., 2022). With regards to stimulation protocols, optimization algorithms such as Bayesian optimization have shown promise in efficiently tuning stimulation parameters to evoke functional movements in FES (Bonizzato et al., 2023; Losanno et al., 2021). These algorithms optimize an objective function related to the movement using stimulation on each electrode as an input, which deviates from current control methods where one electrode contributes to movements in one DOF. Integrating optimization algorithms with BMI control hasn't been attempted yet, and will likely involve designing optimization functions that work with specific BMI control modalities.

3.5 Acknowledgements

Cynthia A. Chestek, Parag G. Patil, and Matthew S. Willsey advised the work and performed the cortical surgeries. Theodore A. Kung, Nishant Ganesh Kumar, Jordan Lam, and Ayobami L. Ward performed the peripheral surgeries. Luis H. Cubillos, Samuel R. Nason-Tomaszewski, Joseph T. Costello, Hisham Temmar, Dylan M. Wallace, Jake C. Joseph, and Madison Kelberman assisted in data collection. Edanjen Lin and Luis H. Cubillos assisted in designing the manipulandum. Jake C. Joseph assisted is extracting joint angles. Eric Kennedy performed the nerve block procedures and provided animal support.

We thank the University of Michigan Unit for Laboratory Animal Medicine for expert veterinary and surgical support. We appreciate the support of the University of Michigan Biointerfaces Institute. This work was supported by NSF grants 1926576 and 2223822, NSF GRFP under grant 1841052, NIH grant T32NS007222, NIH grant R01NS105132, the Dan and Betty Kahn Foundation Grant AWD011321, Agencia Nacional de Investigación y Desarrollo (ANID) of Chile, University of Michigan Robotics Institute, and A. Alfred Taubman Medical Research Institute.

Chapter 4 Targeting Nerve Entry Points for Selective FES

This chapter includes my contributions to a collaborative project establishing the surgical method described below and testing the efficacy of this method. A subset of these results were presented as a poster at the 2023 Simian Collective Meeting. A subset of these results were also presented by a neurosurgeon collaborator, Dr. Ayobami Ward, at the 2023 Society for Neuroscience Annual Meeting, and also by a plastic surgeon collaborator, Dr. Nishant Ganesh Kumar, at the 2024 American Society for Peripheral Nerve Annual Meeting

4.1 Introduction

Functional electrical stimulation (FES) can restore functional movements after spinal cord injury by stimulating intact muscles. Improved hand function in particular is important to improving quality of life for people with tetraplegia (Anderson, 2004; Collinger, Boninger, et al., 2013). Clinical FES devices have been able to restore specific grasps such as palmar and lateral grasps (Losanno et al., 2023; Peckham et al., 2001), doing so in over 250 patients. The hand however is a complex biomechanical system with 27 degrees-of-freedom (ElKoura & Singh, 2003) and over 30 muscles. These clinical devices so far are a long way from truly restoring dexterous hand movements. While much of the variance in hand movements can be explained by a few low-dimensional synergistic movements (Ingram et al., 2008; Santello et al., 2016; Yan et al., 2020), there is still important task dependent information in lower variance dimensions (Todorov & Ghahramani, 2004; Yan et al., 2020). Therefore, to restore natural dexterous hand control, we would need a stimulation paradigm that can restore many degrees-of-freedom.

Stimulating the nerve or the muscle shows promise in being able to restore fine movements in the hand (Badi et al., 2021; Kilgore et al., 2018; Losanno et al., 2023), however nerve stimulation tends to activate synergistic movements (Badi et al., 2021), which may limit the available hand movements. Intramuscular electrodes are well suited for selectively activating muscles because they can be placed directly in the muscle belly. Multiple electrodes can also be placed into the muscle belly in order to target different sections of the muscle. Most muscles can be subdivided into neuromuscular compartments, groupings of muscle fibers innervated by one peripheral nerve branch (English et al., 1993). These compartments can also have specific functions especially in the hand. For example, different compartments of flexor digitorum profundus will activate tension on different fingers (Schieber et al., 2001). Notably, there are not individual extrinsic finger muscles for each finger. Instead, motor units are activated together within compartments more so than between compartments, which contributes to individual finger control (Keen & Fuglevand, 2004; Mcisaac & Fuglevand, 2007; Reilly et al., 2004). As such, stimulating different compartments of extrinsic finger muscles may be necessary to improve individual finger movements. We aim to improve the selectivity of intramuscular FES by targeting the nerve entry points into muscles. Due to the spatial pattern of activation in intramuscular stimulation, it is expected that stimulation on electrodes at the nerve entry point would selectively activate muscle fibers in the neuromuscular compartment in which the electrode is implanted (Grandjean & Mortimer, 1986; Singh et al., 2000).

It has yet to be shown that we can target these nerve entry points intraoperatively and that we can stimulate them chronically to achieve selective movements in the hand. Here we show a proof of concept implantation in non-human primate of 16 electrodes targeting nerve entry points of 9 unique muscles in the forearm. We compare this to an FES implant using the standard

approach targeting each muscle belly once. After implantation, targeting nerve entry points led to stimulation on individual electrodes that selectively evoked movements on more individual fingers, more subgroups of fingers, and also the wrist.

4.2 Methods

4.2.1 Implants

Prior to surgery, ex-vivo exploration was used to determine a surgical plan. We performed an extensive anatomic dissection of one ex-vivo monkey arm, identifying flexor muscles, extensor muscles, and main nerve branches as they entered their respective targets. We identified multiple nerve entry points in each muscle, ranging up to 6 in flexor digitorum profundus, aligning with previous anatomic studies (Liu et al., 1996). We also found that entry points tended to be in more proximal locations of the target muscle belly, and relatively spread out (typically greater than 2 cm), indicating that one volar and one dorsal incision would allow access to the entry points of flexor muscle and extensor muscles respectively, and that there was enough space between points for individual nerve entry points to be targeted by single electrodes. While the exact number and distribution of nerve entry points varies by subject (Liu et al., 1996), this ex vivo procedure assisted in orienting the surgeons to the procedure and in developing a surgical plan.

Two monkeys, Monkey R and Monkey N, were implanted with chronic bipolar intramuscular electrodes (Synapse Biomedical, Inc., Oberlin, OH, USA). Monkey R was implanted after the ex vivo planning procedure and multiple nerve entry points were targeted per muscle. Monkey N was implanted about 2 years' prior with a similar surgical technique but only targeting one electrode per muscle. During the implantation procedure, a radial-volar incision was used to access flexor muscles of the deep and superficial compartments of the forearm, and a dorsal-ulnar incision was used to access the extensor muscles. Target muscles were identified

using anatomical landmarks and nerve entry points were identified. In Monkey N, intraoperative stimulation of the muscle was performed to isolate finger and wrist-related movements, then

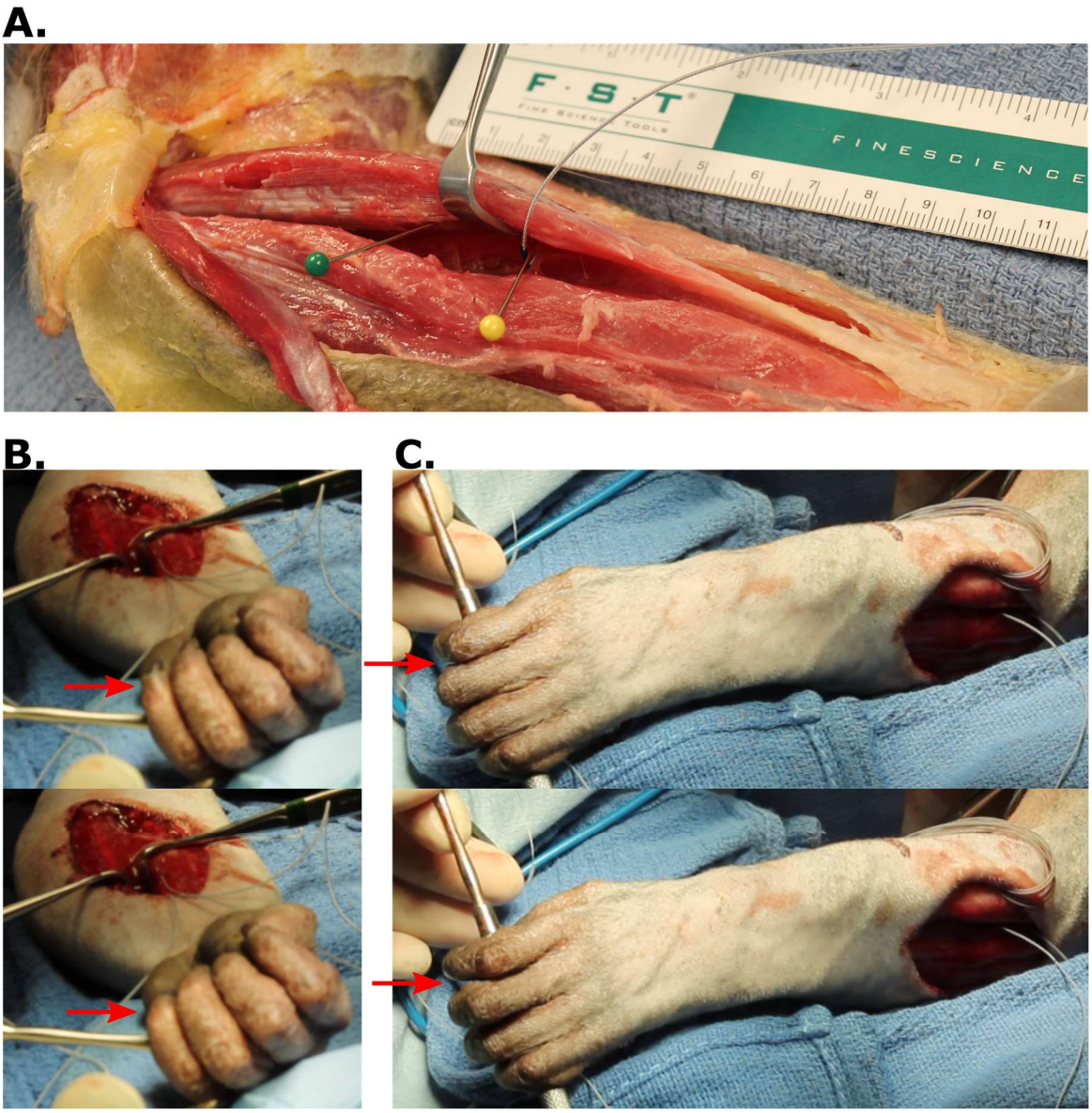

Figure 4-1 Ex Vivo surgical planning and intraoperative stimulation
(A) Example picture from the ex vivo exploration. Pins are placed where two nerve entry points were identified. An electrode is shown at one nerve entry point for scale. (B) Example intraoperative stimulation of the FDPrs electrode with Monkey R. Stimulation on this electrode intraoperatively evoked flexion on the small and ring fingers. Red arrows point to the small finger which is slightly flexed in the bottom image relative to the top. (C) Example intraoperative stimulation of the EDCim electrode with Monkey R. Stimulation on this electrode intraoperatively evoked extensions of the index and middle fingers. Red arrows point to the index and middle fingers which are slightly extended in the bottom image relative to the top.

electrodes were secured intramuscularly with suture in close proximity to a nerve entry point. In one muscle belly, better isolation of intended finger movement was identified by stimulation more distal from the nerve entry point and an additional electrode was implanted at that location. Through this method, 8 electrodes were placed on 7 muscles for Monkey N (Table 4-1). In Monkey R, nerve entry points were identified on the target muscle and electrodes were placed in close proximity. Intraoperative stimulation was then used to confirm finger or wrist related function by

Table 4-1 List of electrode targets and movements achieved by intraoperative stimulation

Monkey R Electrodes	Intraoperative Stimulation Result
Flexor Digitorum Superficialis (FDS)	Middle finger flexion
Flexor Digitorum Profundus, Ulnar Site (FDPr)	Ring finger flexion
Flexor Digitorum Profundus Radial Site (FDPi)	Index finger flexion
Flexor Digitorum Profundus Ulnar Site (FDPrs)	Ring and small finger flexion
Flexor Carpi Radialis Proximal Site (FCRp)	Wrist flexion
Flexor Carpi Radialis Distal Site (FCRd)	Wrist flexion
Flexor Carpi Ulnaris Proximal Site (FCUp)	Wrist flexion and adduction
Flexor Carpi Ulnaris Distal Site (FCUd)	Wrist flexion and adduction
Extensor Digitorum Communis Ulnar Site (EDCrs)	Ring and small finger extension
Extensor Digitorum Communis Radial Site (EDCi)	Index finger extension
Extensor Digitorum Communis Middle Site (EDCmrs)	Middle, ring, and small finger extension
Extensor Digitorum Communis Proximal Site (EDCim)	Index and middle finger extension
Extensor Indicis Proprius (EIP)	Index finger extension
Extensor Carpi Radialis Brevis Proximal Site (ECRBp)	Wrist extension
Extensor Carpi Radialis Brevis Distal Site (ECRBd)	Wrist extension
Extensor Carpi Ulnaris (ECU)	Wrist ulnar deviation
Monkey N Electrodes	**Intraoperative Stimulation Results**
Extensor Indicis Proprius (EIP)	Index finger extension
Flexor Digitorum Profundus, MRS muscle belly (FDP)	Middle, ring, and small finger flexion
Extensor Digitorum Communis (EDC)	All finger extension
Extensor Carpi Radialis Brevis (ECRB)	Wrist extension
Flexor Carpi Ulnaris (FCU)	Wrist flexion and adduction
Flexor Carpi Radialis (FCR)	Wrist flexion
Flexor Digitorum Profundus, index muscle belly proximal site (FDPip)	Index finger flexion
Flexor Digitorum Profundus, index muscle belly distal site (FDPid)	Index finger flexion

evoking finger or wrist twitches in the expected direction, before securing the electrode intramuscularly (Figures 4-1B and 4-1C). With this approach, 16 electrodes were placed on 8 muscles (Table 4-1). Electrodes were then tunneled proximally over the upper arm and to an interscapular incision where tunneled wires connected to the standard PermaLocTM connector.

4.2.2 FES System

Intramuscular electrodes were connected to a networked neuroprosthesis evaluation system (NNP) (Smith et al., 2005), similar to the system used in humans (NCT02329652) however in a form designed for experimentation rather than implantation. The NNP system consisted of one power module and three pulse generator boards, each containing four output channels and one return channel. In intraoperative stimulation, one stimulation output was used. The cathode electrode was connected to the stimulation output which was inserted near the nerve entry point, the anode electrode was placed in contact with the muscle belly approximately 1cm away and connected to the current return of the power module. For chronic stimulation, four output channels were used, connected to the cathode of four bipolar electrodes. The return electrodes of the four electrodes were tied together to one common return on the pulse generator. All stimulation was current controlled, charge-balanced biphasic pulses, delivered at 32 ms inter-pulse intervals, with 5 or 10 mA amplitudes and 1 to 255 microsecond pulse widths. Stimulation intensity was modulated by changing the pulse width of the leading cathodic pulse between 0 and 255 microseconds, and the amplitude of the pulse to either 5 or 10 mA.

4.2.3 Electrode Stimulation Characterization

To ensure recorded movements were due to stimulation, chronic electrode characterization was done either with the monkeys under propofol anesthesia or with the monkeys arm temporarily

paralyzed via nerve block. For propofol anesthesia, an IV catheter was placed in the cephalic vein distal to the monkey's right elbow (contralateral to electrodes). We then delivered a 2.5-3.0 mg/kg bolus of propofol to induce anesthesia and maintained light anesthesia with a constant rate infusion of propofol at 7.5 mg kg/h. Supplemental boluses of 0.2 mg/kg were used as needed to either induce anesthesia or maintain the desired level of anesthesia. For nerve blocks, the median, radial, and ulnar nerves were targeted just proximal to the elbow with ultrasound guidance. Then the monkeys arm was temporarily paralyzed with a solution of lidocaine (1% or 2%) and epinephrine (1:100000) injected into the space surrounding the nerve. Residual function was tested with a grasping task while offering enrichment.

Following nerve block or induction, the NNP was connected to the PermaLoc connector. One electrode was stimulated at a time in a stepwise fashion, turning stimulation on for 1-3 seconds then back off before trying a new intensity. Various stimulation intensities were tested in order to identify the threshold stimulation to cause a movement and then the stimulation intensities required to cause a plateau in movement or movement of additional joints. Pulse widths varied from 1 to 255 microseconds and amplitudes were either 5 mA or 10 mA. Each electrode was only stimulated at high enough intensities to determine that the recruited movement had plateaued, which typically occurred at less than 255 microsecond pulse widths. Video was recorded of evoked movements. To ensure consistent video, the camera was mounted on a tripod and angled such that the forearm just proximal to the wrist was at the edge of the frame. The monkeys forearm was braced by an experimenter to keep the hand off the table and moving within the plane of the recorded video. Joint angle measurements were later extracted from video frames. To measure angles, individual frames were selected from the video. Joints including the wrist, the metacarpaphalangeal (MCP) joint for index, middle and ring fingers, and the proximal interphalangeal (PIP) joint for index,

middle, and ring fingers, were marked. The angles for the wrist and index, middle, and ring MCP joints were measured in ImageJ (version 2.35). The wrist joint angle was measured as the angle between the vector from the forearm at the edge of the frame to the wrist marker (chosen to be perpendicular to the edge of the frame for consistency), and the vector from the wrist marker to the index MCP joint. The MCP joint angle for each finger was measured as the angle between the vector from the wrist marker to that finger's MCP marker and the vector from that finger's MCP marker to that finger's PIP marker, in the plane of the image. In frame's where there was an obstruction over a marker, a second measurement was made using vectors parallel to the back of the hand or parallel to the back of the finger. This second angle was then averaged together with an angle calculated from estimating the obstructed marker position. Note that the small finger's MCP joint angle was not measured due to the top down camera angle leading to it nearly always being obscured.

4.3 Results

4.3.1 Chronic Implant Stimulation

In order to investigate the ability to evoke selective movements with the chronic electrodes, we stimulated each electrode at different intensities. This was done 64 days post-operative for Monkey N and across two days, 27 and 41 days post-operative, for Monkey R. Figure 4-2A illustrates example movements captured from single electrode stimulation for Monkey R using the FDPim and EDCrs electrodes. For each electrode, we determined which finger movements they activated and in what order they evoked additional movements as stimulation increased. Figures 4-2B and 4-2C show the order that movements were recruited in as stimulation intensity (pulse width) was increased. For Monkey R, 6 of 9 electrodes targeting finger muscles produced initial movements in one or two fingers, all 6 electrodes were among those that evoked selective finger

movements intraoperatively. Additionally, 6 of 7 electrodes targeting wrist muscles produced selective wrist movements initially, and 5 of those electrodes only evoked wrist movements even at high levels of stimulation. For Monkey N, 3 electrodes out of 5 targeting finger muscles evoked movements in one or two fingers, and 3 electrodes out of 3 targeting wrist muscles evoked selective movements in the wrist initially.

We next asked how large the selective finger movements evoked by single electrodes were with Monkey R. Using the recorded video, we measured the wrist angle and MCP joint angle for index, middle, and ring-small grouped together during evoked movements. Figure 4-2D shows the

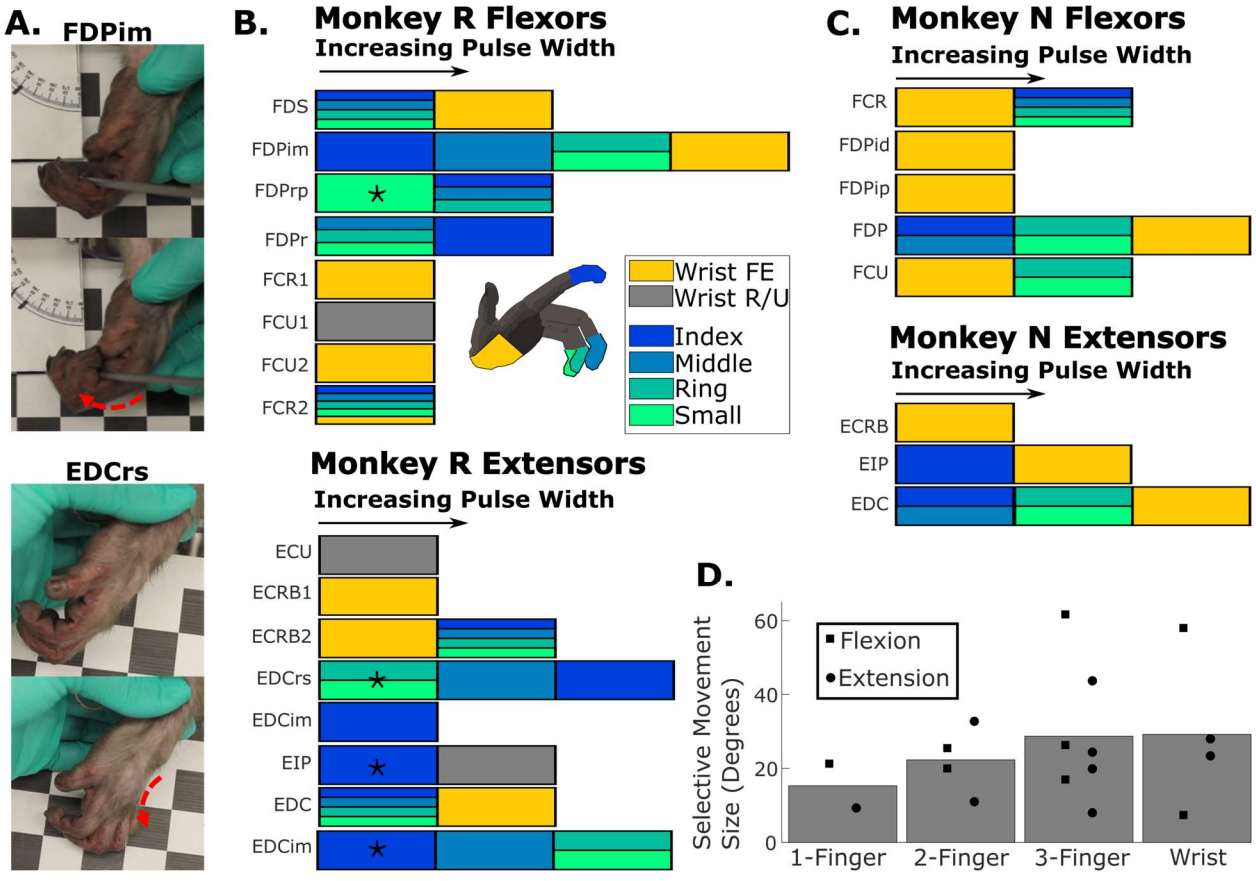

Figure 4-2 Order of movements recruited by stimulation on individual electrodes.
(A) Example movements evoked by single electrode stimulation. (B) Order that increasing stimulation intensity on Monkey R's individual electrodes recruited movements on different joints. (*) indicate movements that were only a twitch. (C) Same as (B) but from Monkey N. (D) Size of selective movements evoked grouped by whether it occurred on 1, 2 or 3 finger groups, or the wrist. Movement sizes were averaged across the actively moving joints. Bars indicate average movement size. Marked twitches in (B) are not included in (D).

largest size of selective movements (from rest) on single electrodes before increasing stimulation began recruiting movements on other joints, grouped by whether the movements were of the wrist or one, two, or all three measured finger groups. Notably, on four electrodes, the initial movement of 1 or 2 fingers was only a twitch (i.e. less than 5 degrees and not measured here). Not including the four twitches, selective movements of one or two fingers averaged 20.0 degrees (std = 8.83), while movements of all three finger groups averaged 28.7 degrees (std=18.2). Average movement sizes were not significantly different due to the large variance ($p=0.154$, one-tailed two-sample t-test). Pooling all of the movement sizes, only selective wrist and three finger group movements produced especially large movements (i.e. greater than one standard deviation above the mean).

When designing stimulation protocols, stimulation will be combined on multiple electrodes to evoke movements that are a combination of movements evoked from individual electrodes. To estimate the difference in functional movements that will be available with this approach, we next compared the unique movements evoked on individual electrodes (Table 4-2). Four finger muscles were targeted in Monkey R and three were targeted in Monkey N, the key difference being the number of electrodes. In Monkey R, we were able to evoke five unique combinations of finger flexions: index flexion into index-middle (IM) flexion at higher pulse widths, small flexion, middle-ring-small (MRS) flexion, and all finger flexion. We were also able to evoke five unique finger extensions: index extension, index extension into IM extension at higher pulse widths, ring-small (RS) extension, MRS extension, and all finger extension. With Monkey N, we were able to evoke only two finger flexions: IM flexion which transitioned into all fingers at higher pulse widths. There were also only three unique finger extensions: an isolated index extension and then IM extension which transitioned into all finger extension at higher pulse widths.

Table 4-2 Unique finger movements evoked from stimulating single electrodes

Monkey R		Monkey N	
Flexion	Extension	Flexion	Extension
I	I	IM	I
S	IM	IMRS	IM
IM	RS		IMRS
MRS	MRS		
IMRS	IMRS		

I – Index, M – Middle, R – Ring, S – Small

4.4 Discussion

In this study we piloted an approach to intramuscular FES specifically targeting nerve entry points into muscles in order to increase the repertoire of selective finger movements while targeting the same extrinsic finger muscles. In postoperative stimulation, the finger movements evoked by individual electrodes followed what was found intraoperatively. Movements evoked on one or two fingers spread to nearby fingers as stimulation increased. As a result, most single finger movements were small twitches, and larger movements were evoked on two fingers or more. This follows what is expected from previous studies analyzing the function of neuromuscular compartments in extrinsic finger muscles (Schieber et al., 2001), namely that a single neuromuscular compartment will cause tension on one finger primarily that will be distributed to neighboring fingers. These results suggest that when combining stimulation on multiple electrodes, movement sizes that will be useful will often be with two or more fingers. Movements of individual fingers will likely have to make use of both agonist and antagonist muscles in order to hold fingers still while moving the finger of interest, similar to how extrinsic finger muscles naturally produce individual finger movements (Schieber, 1995). As targeting nerve entry points led to more unique finger movements, this approach provides more possible movement combinations. It is therefore more likely to be able to generate single finger movements and unique functional hand movements.

An additional application of this implant approach will be to implement fatigue reducing stimulation protocols. Stimulation of different nerve entry points primarily activate non-overlapping groups of muscle fibers (Gruner & Mason, 1989). Stimulation can be designed to alternate stimulation on two electrodes and form a tetanic muscle activation by activating each group of muscle fibers at a reduced frequency. This approach has been shown to reduce fatigue in lower limb muscles (Peckham et al., 1970; Thomsen & Veltink, 1997).

Future work will need to determine how to combine stimulation on these electrodes to get graded contractions of individual fingers or groups of fingers. A first step is identifying a space where movements combine. For example, it is likely that forces will combine more predictably than kinematics evoked by single electrode stimulation. A second step will be identifying algorithms to efficiently explore combinations of stimulation. When targeting nerve points in the upper limb, there are many targets. One estimate in monkeys includes an average of 50 nerve entry points across 19 forearm muscles (Liu et al., 1996). With more nerve entry points targeted with electrodes, it becomes experimentally unfeasible to test all combinations of stimulation. Recent studies have instead used Bayesian optimization to optimize stimulation parameters for FES with kinematic or EMG based objectives (Bonizzato et al., 2023; Losanno et al., 2021). Efficient algorithms will be necessary to identify useful combinations of stimulation on electrodes implanted with this method, thereby increasing the probability of achieving dexterous finger movements.

4.5 Acknowledgements

Cynthia A. Chestek and Parag G. Patil advised this work. Theodore A. Kung, Nishant Ganesh Kumar, Jordan Lam, and Ayobami L. Ward performed the peripheral implant surgeries. Theodore A. Kung, Nishant Ganesh Kumar, and Ayobami L. Ward performed the ex vivo

exploratory procedure. Samuel R. Nason-Tomaszewski, Luis H. Cubillos, Joseph T. Costello, Hisham Temmar, Dylan M. Wallace, Madison Kelberman, and Jake C. Joseph assisted in data collection. Eric Kennedy performed the nerve block procedures and provided animal support.

We thank the University of Michigan Unit for Laboratory Animal Medicine for expert veterinary and surgical support. We appreciate the support of the University of Michigan Biointerfaces Institute. This work was supported by NSF grants 1926576 and 2223822, NSF GRFP under grant 1841052, NIH grant T32NS007222, NIH grant R01NS105132, the Dan and Betty Kahn Foundation Grant AWD011321, Agencia Nacional de Investigación y Desarrollo (ANID) of Chile, University of Michigan Robotics Institute, and A. Alfred Taubman Medical Research Institute.

Chapter 5 Discussion

5.1 Generalizable Decoding in Brain-Machine Interfaces

The field of intracortical brain-machine interfaces has greatly expanded in the past two decades. Among other things, these interfaces have restored function to people with paralysis by allowing them to control computer cursors (Dekleva et al., 2021; Gilja et al., 2015; Simeral et al., 2011), typing (Jarosiewicz et al., 2015; Pandarinath et al., 2017; Willett et al., 2021), generate speech (Metzger et al., 2023; Willett et al., 2023), control robotic arms (Flesher et al., 2021; Hochberg et al., 2012; Wodlinger et al., 2015), and restore function to their native arm (Ajiboye et al., 2017; Bouton et al., 2016; Herring et al., 2023). One factor slowing the clinical translation of these devices is the reliability of algorithms used to decode intended movements. Decoding algorithms can often fail to generalize to changes in a task when the underlying neural activity changes activation patterns. For example, BMI decoding efficacy decreases when grasping versus grasping during movements (Bouton et al., 2016; Dekleva et al., 2021), when swapping from native control to BMI control (Fan et al., 2014), and when changing the load on the wrist (Naufel et al., 2019). In Chapter 2, we similarly show that the accuracy of decoding intended finger movements decreases with changes to wrist posture or loading on the fingers. In natural hand control, changing wrist postures plays in role in grasp strength and grasping objects of different sizes (O'Driscoll et al., 1992). Our results suggest that when controlling FES with a BMI, decoder accuracy will be diminished when trying to grasp in different postures or loads on the fingers, especially if it is necessary to match the changes in muscle activations of the task.

Our results in Chapter 2 also indicate that a kinematic based decoder may generalize better than a muscle activation based decoder. We found large changes in muscle activations with the task changes but only small changes in neural activity. Additionally, the neural activity followed similar patterns of activations before and after task changes. Subsequently, a kinematic based BMI task, the NHP were still able to use the BMI decoder by re-aiming their control. Similarly, using a kinematic based decoder in Chapter 3, we were subsequently able to continuously control both wrist and finger movements in a virtual task. Taken together, our results suggest that the task changes shift the neural activity but in such a way that it is intuitive to re-aim intended movements when controlling a BMI. Therefore, kinematic based decoders may be a promising method for decoding in brain-controlled FES in a way that generalizes to different postures and loads. This approach would provide accurate predictions of intended movements, although it would not account for the change in mapping between intended movement and required muscle activation. An additional mechanism would be needed to modulate stimulation for the changes in muscle activation.

Accounting for the changes in muscle activations with the BMI decoders will require different algorithms or algorithm training in order to make models that make accurate predictions of desired muscle activations across tasks. There have been a few approaches suggested to modify decoding algorithms to be more generalizable. One method is to essentially engineer features that generalize well within the task for which that decoder is intended. An extreme example of this was implemented for forward and backward self-motion. A state-machine decoder was designed using only high variance neural features related to movement onset, rotational dynamics, and directional tuning (Schroeder et al., 2022). Other examples have classified cursor clicking using transient responses to grasp onset and offset (Dekleva et al., 2021), improved kinematic predictions by

modeling the evolution on neural dynamics or states (Kao et al., 2015, 2017), and generalized muscle activation predictions across tasks by identifying a task-independent subspace (Gallego et al., 2018). Similarly, in Chapter 2, we show that by characterizing the neural data during the context changes, we could identify a neural feature that correlated with the required muscle activations in different tasks. This result could subsequently be used to modulate muscle activation predictions or FES parameters, triggering an increased stimulation intensity when performing a task that requires more muscle activation. Alternatively, this feature could be ignored when predicting kinematics in order to improve the accuracy of kinematic predictions between tasks.

Recent BMI applications have veered towards implementing increasingly impressive machine learning methods to improve accuracy and generalization rather than hand selecting features (Costello et al., 2023; Glaser et al., 2020; Temmar et al., 2024; Ye & Pandarinath, 2021). Neural networks can be trained to identify and utilize useful and noise-robust features. However, neural networks can only find patterns of activity for the neural activity included in the training datasets. For example, subsequent analyses on the context changes presented in Chapter 2 show that a neural network trained on multiple contexts can perform as well as a neural network tested within context. A neural network tested on an unseen contexts though tended to be overfit and generalized worse than linear decoders (Temmar et al., 2024). Nevertheless, neural networks have a high capacity for learning, especially as technologies improve leading to more input channels (Costello et al., 2023; Willett et al., 2023). Ultimately, they are a promising solution for generalizable decoding as long as there is access to training data with the relevant patterns of neural activity and behavior represented.

5.2 Restoration of Dexterous Hand Movements with FES

In some regards, the dexterous hand movements available from BMIs have now outpaced what can be restored with FES. For example, in Chapter 3 we demonstrated continuous wrist and finger decoding and in Chapter 2 we demonstrated decoding for two finger groups in two wrist postures. Recent results have even extended BMI decoding to 4D finger movements (two finger groups and 2D thumb) (Willsey et al., 2024). With regards to FES, however, there have been no demonstrations of FES restoring graded control of individual finger groups, instead primarily restoring discrete grasps or single degree-of-freedom (DOF) movements. It is desirable to restore fine control of many DOFs in the hand instead. By controlling multiple DOFs, the user could form the same discrete grasps, and the control could also generalize to movements outside of the set of grasps, thereby improving the repertoire of restored movements. In chapter 3 we demonstrate graded control of two-DOFs in the hand, the wrist and fingers, for the first time. We were able to use a simple stimulation control scheme to reach targets throughout the available range of motion. In Chapter 4, we show evoked movements in individual fingers and in groups of fingers, illustrating a method to achieve movements in more fingers.

We also introduce considerations for restoring graded movements in multiple DOF of the hand at the same time. In Chapter 3, we show that the range of motion of evoked wrist and finger movements was impacted by interactions between evoked movements from stimulation targeting each DOF. For example, stimulation of extrinsic finger muscles causes a torque at the wrist that can pull the wrist out of the posture being held by stimulation of the wrist muscles. We expect that this effect will be present when extending to more DOF in the hand like individual fingers. In Chapter 4 we show a proof of concept selectively evoking movements in individual or groups of fingers. While stimulation could evoke small twitches on individual fingers, the larger movements

generally occurred on two or more fingers. This result matches studies examining the distribution of evoked tension over the five fingers due to activating individual neuromuscular compartments in FDP (Schieber et al., 2001). It seems unlikely that stimulation will be able to evoke individual finger movements large enough to be functional. Therefore, to evoke functional movements on individual fingers, it will be necessary to optimize stimulation to make use of the combined movements. Similar to the natural control of individual fingers (Schieber, 1995) individual finger movements will then be made by evoking agonist and antagonistic movements on different finger groups, with the net effect being to move one finger.

Our results also emphasize that muscle fatigue is likely to have a large impact on the efficacy of FES to restore movements. In Chapter 3 we show that within minutes some muscles, generally wrist extensors, will have a significant reduction in the amount that they contract due to stimulation, resulting in a large reduction in the range of motion that we can evoke with stimulation. This was tested in a paradigm similar to how FES could be used in active applications at home, and the effect size was on the order of a 48 to 76% decrease in movement area. Fatigue is a phenomenon commonly reported in FES studies (Ajiboye et al., 2017; Ethier et al., 2012), however the impact on functional movements, and methods to reduce fatigue are often not emphasized. Ajiboye et al., for example, reported 15% of single joint movements and 12% of multi-joint movements were failed due to fatigue, primarily in the elbow and wrist, but didn't include details related to how quickly it occurred or how large the reduction in movement was. There is evidence that fatigue can be reduced by sequentially stimulating different groups of muscle fibers at lower frequencies (Lou et al., 2017) or by stimulating on more electrodes to recruit more muscle fibers (Buckmire et al., 2018). Targeting nerve entry points for stimulation as described in Chapter 4 presents a promising implant approach where these methods to reduce

fatigue can be used. As these electrodes are targeting different nerve branches, they will activate largely separate groups of muscle fibers (Gruner & Mason, 1989; Singh et al., 2000). Therefore, sequential stimulation could activate alternating groups of muscle fibers and simultaneous stimulation could activate more of the muscle.

5.3 Future Directions

There are many potential next steps for this research. First, as Chapter 4 was a proof of concept, the procedure should be replicated in additional animals to show that this method is repeatable. After the proof of concept demonstration of selective finger movements in Chapter 4, this should be expanded to understand what DOF we can achieve graded movements for using this approach, what functional movements can then be generated, and an optimal number of implanted electrodes to achieve those movements. To assist in this, efficient algorithms are needed to better optimize stimulation protocols and achieve functional movements. When implanting multiple electrodes into each muscle, there can be dozens of electrodes in one arm alone. Current methods to determine stimulation protocols involve stimulating every electrode individually and then manually tuning a stimulation pattern based on how one expects the stimulated movements from multiple electrodes to combine (Ajiboye et al., 2017; Herring et al., 2023; Kilgore et al., 1989). More reliable and efficient methods to determine stimulation parameters could be informed by recorded muscle activations during natural movements (Hasse et al., 2022) or could use optimization methods (Bonizzato et al., 2023; Losanno et al., 2021)

In addition, future work can optimize the full control system. The brain-controlled FES system has two parts, estimating intended movements with a BMI and then restoring movements with FES. Current methods make the FES commands proportional to the BMI output and rely on the user to modulate or re-aim their control in order to compensate when movements are incorrect.

For example, NHP can voluntarily increase the stimulation command with BMI in order to compensate for fatigue (Ethier et al., 2012). Similarly, in Chapter 2 we informed BMI development to assist in controlling FES. However, to reduce the cognitive load on the user and improve usability, a closed-loop control system could be used with the FES intself to drive the stimulation parameters to achieve the intended movement. There has been substantial work developing closed loop systems for controlling FES (Chaikho et al., 2022; Lynch & Popovic, 2008). Feedback can be acquired using kinematic or inertial sensors, recorded muscle activations, or even sensory neural recordings (Bruns et al., 2013; Hwang et al., 2024). A FES system with feedback control could potentially adapt to varying loads and compensate for fatigue. This could then be combined with robust BMI algorithms that provide the intended kinematics.

Future FES systems could also combine multiple modalities of stimulation. Each stimulation approach to FES has different benefits related to the dexterity of restored movements and the potential for clinical translation. For example, peripheral nerve stimulation is able to efficiently generate larger movements with fewer electrodes, while intramuscular stimulation is able to recruit more selective movements but can require many electrodes. These approaches can be combined to restore more functional movements than peripheral nerve stimulation with less electrodes than intramuscular FES typically requires. For example, in the past 10 years, arm and hand movements have been restored using 36 intramuscular electrodes throughout the arm (Ajiboye et al., 2017), 9 nerve cuffs in the arm (Herring et al., 2023), or in the 2010s, two participants were implanted with nerve cuff electrodes to recruit arm movements and intramuscular electrodes to recruit hand and finger movements, for a total of 24 electrodes (Memberg et al., 2014). One could envision a future direction where multiple modalities of

stimulation are combined like this in order to improve the efficacy of the systems and move these devices closer to clinical translation (Shokur et al., 2021).

Appendices

Appendix A: Supplement to Chapter 2

Appendix Table A-1 Average prediction correlation when using a ridge regression model to predict muscle activations with the same or different test contexts. Results for Monkey N.

	Monkey N							
Test Context	**FCR**	**FDPid**	**FDPip**	**FDP**	**FCU**	**ECRB**	**EIP**	**EDC**
Normal	0.62	0.58	0.61	0.51	0.50	0.75	0.72	0.73
Wrist	0.62	0.54	0.60	0.49	0.51	0.68	0.66	0.66
Spring	0.65	0.62	0.61	0.60	0.71	0.71	0.71	0.75
Wrist + Spring	0.69	0.57	0.61	0.49	0.66	0.64	0.63	0.68
Wrist	0.59	0.49	0.57	0.43	0.47	0.65	0.63	0.59
Spring	0.56	0.25	0.49	0.35	0.55	0.64	0.61	0.66
Wrist + Spring	0.58	0.23	0.46	0.31	0.46	0.44	0.38	0.22

Appendix Table A-2 Average prediction correlation when using a ridge regression model to predict kinematics with the same or different test contexts.

	Monkey N				Monkey W			
Test Context	**Index Position**	**MRS Position**	**Index Velocity**	**MRS Velocity**	**Index Position**	**MRS Position**	**Index Velocity**	**MRS Velocity**
Normal	0.62	0.70	0.50	0.52	0.43	0.40	0.49	0.32
Wrist	0.55	0.71	0.51	0.52	0.39	0.41	0.48	0.30
Spring	0.69	0.73	0.46	0.58	0.59	0.34	0.51	0.44
Wrist + Spring	0.63	0.71	0.48	0.53	0.43	0.44	0.44	0.39
Wrist	0.51	0.66	0.49	0.48	0.37	0.38	0.49	0.28
Spring	0.53	0.57	0.37	0.46	0.53	0.15	0.47	0.29
Wrist + Spring	0.45	0.52	0.37	0.45	0.32	0.29	0.40	0.33

Appendix Table A-3 Average prediction mean-squared error (MSE) when using ridge regression models to predict muscle activations with the same or different test contexts. Results for Monkey N.

MSE		Monkey N							
Training Context	Test Context	FCR	FDPid	FDPip	FDP	FCU	ECRB	EIP	EDC
Normal	Normal	0.61	0.67	0.62	0.74	0.74	0.44	0.47	0.47
Wrist	Wrist	0.62	0.71	0.65	0.77	0.74	0.53	0.57	0.57
Spring	Spring	0.57	0.61	0.62	0.64	0.50	0.50	0.49	0.44
Wrist + Spring	Wrist + Spring	0.53	0.67	0.62	0.76	0.57	0.60	0.61	0.54
Normal	Wrist	0.70	0.87	0.78	0.95	0.88	0.83	0.84	1.00
Normal	Spring	0.89	1.89	1.26	2.78	1.18	1.14	1.26	0.68
Normal	Wrist + Spring	1.09	2.96	2.35	3.63	2.06	3.61	2.82	1.60

Appendix Table A-4 Average prediction mean-squared error (MSE) when using ridge regression models to predict kinematics with the same or different test contexts.

MSE		Monkey N				Monkey W			
Training Context	Test Context	Index Position	MRS Position	Index Velocity	MRS Velocity	Index Position	MRS Position	Index Velocity	MRS Velocity
Normal	Normal	0.61	0.50	0.75	0.73	0.81	0.84	0.76	0.90
Wrist	Wrist	0.69	0.50	0.74	0.73	0.85	0.84	0.78	0.92
Spring	Spring	0.53	0.46	0.79	0.67	0.65	0.89	0.75	0.81
Wrist + Spring	Wrist + Spring	0.60	0.49	0.78	0.72	0.82	0.81	0.82	0.86
Normal	Wrist	0.76	0.68	0.76	0.77	0.94	0.89	0.77	0.92
Normal	Spring	0.92	0.94	0.90	0.82	2.46	1.16	0.91	0.92
Normal	Wrist + Spring	1.45	0.92	0.88	1.00	1.67	1.09	1.00	0.90

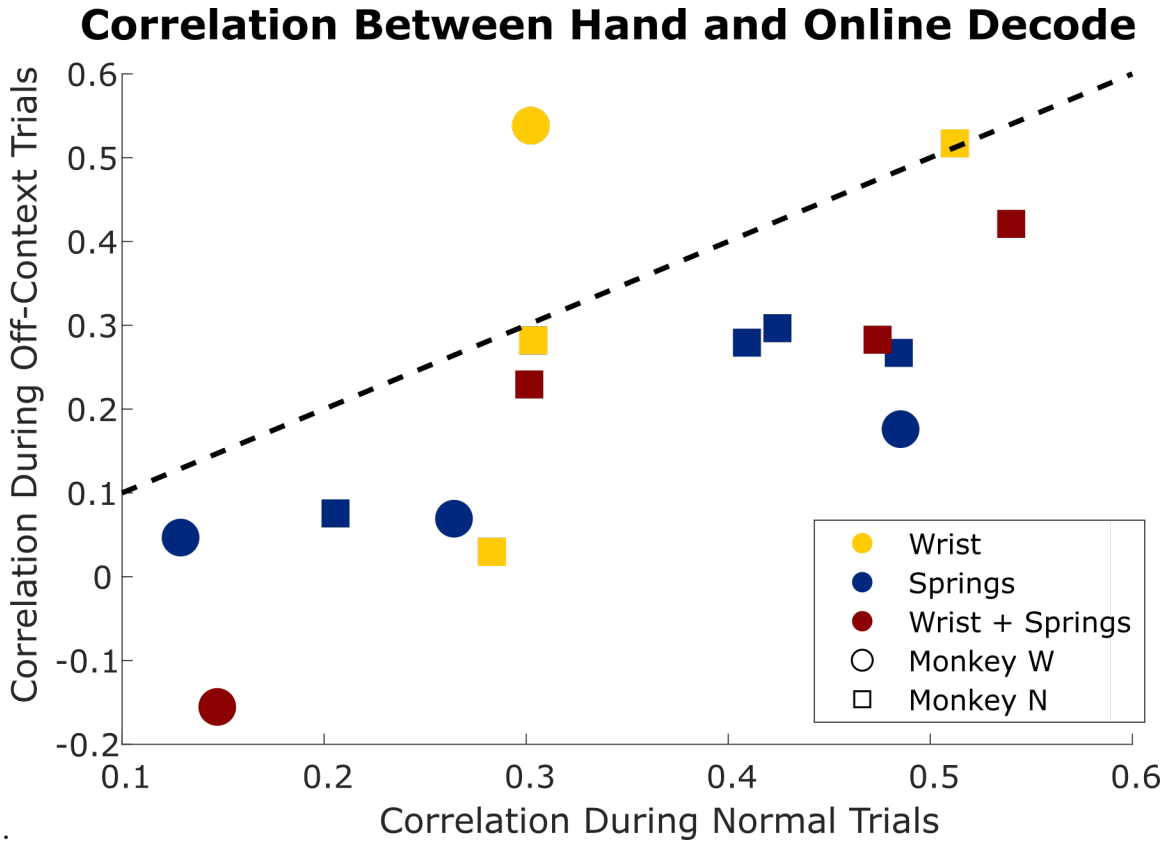

.

Appendix Figure A-1 The correlation between hand position and online decode during the trials for each online comparison in Figure 2-5B.
Colors represent the type of context change (yellow – wrist, blue – springs, red – both wrist and springs), and shape indicates which monkey the session was with. Dotted line indicates equal hand-decode correlation in both types of trial

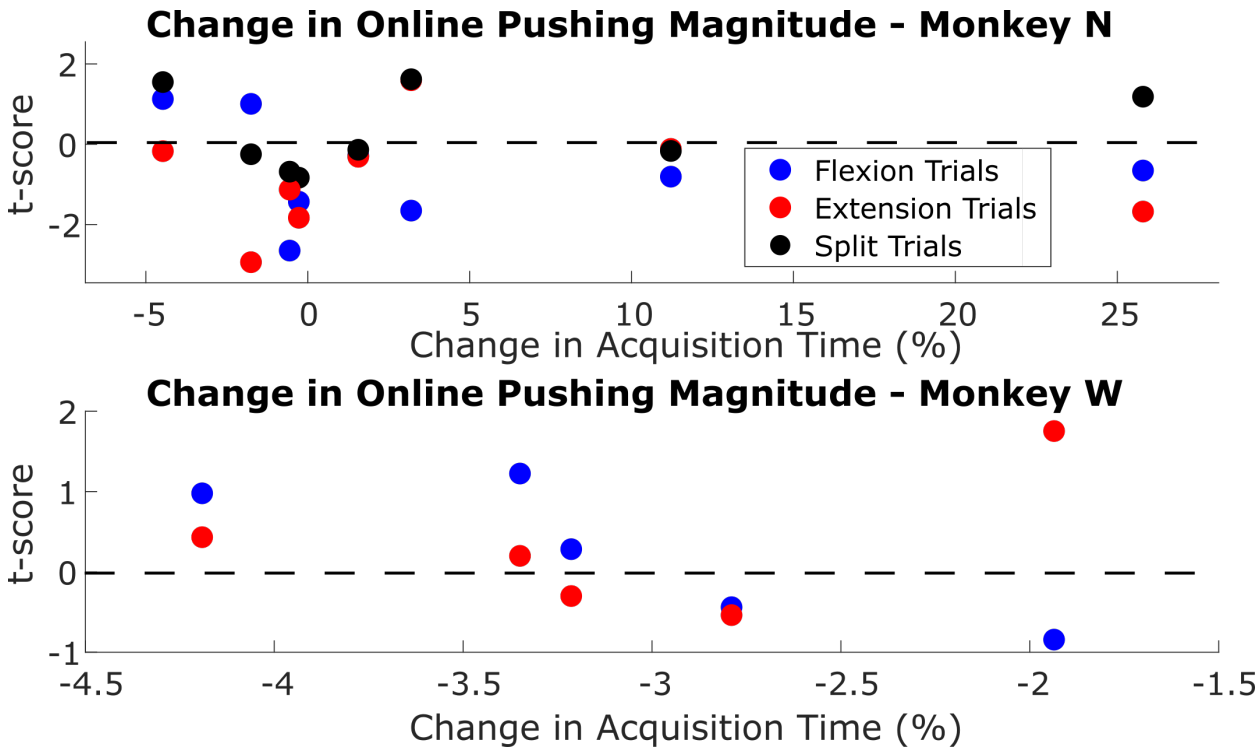

Appendix Figure A-2 Change in online 'pushing' magnitude during BMI with manipulandum context changed. Pushing magnitude is the predicted velocity along the target direction, with predictions made by a linear regression model. This was trained on normal trials offline and evaluated on neural data during online trials at the time point of peak movement. The change is between trials during normal online control and trials with a context changed added during online control. One dot indicates the two-sample t-score of this change calculated using all trials of one type (blue – flexion, red – extension, or black – split) in one session for Monkey N (top) or Monkey W (bottom). A change greater than 0 indicates a larger magnitude during the off-context trials, that is pushing harder.

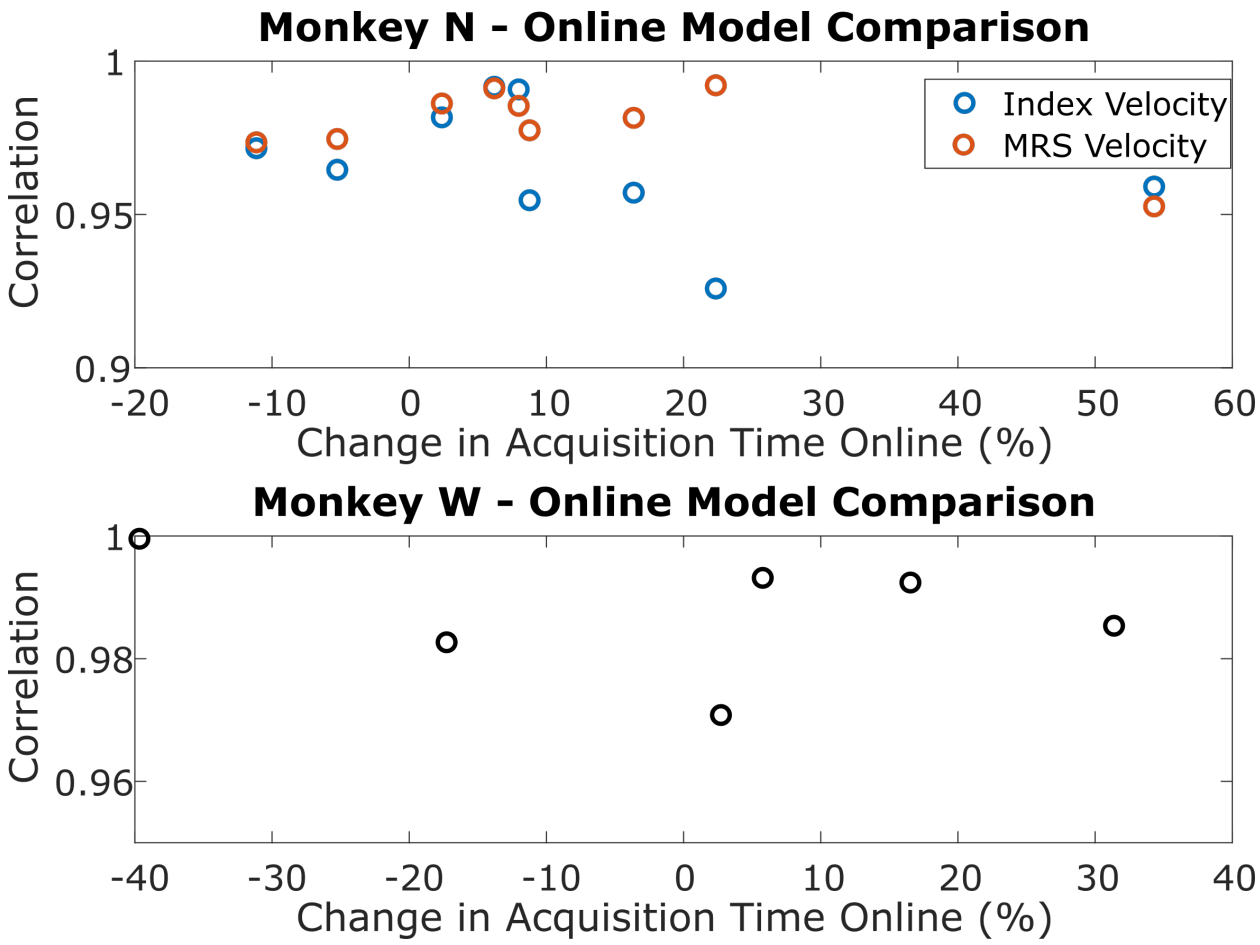

Appendix Figure A-3 Correlation between the velocity predictions made with each Kalman filter used in the two-model brain-machine interface (BMI) experiments for Monkey N.
Each Kalman filter was evaluated on all online trials in a session. One point indicates the correlation between these predictions with both Kalman filters used in one session.

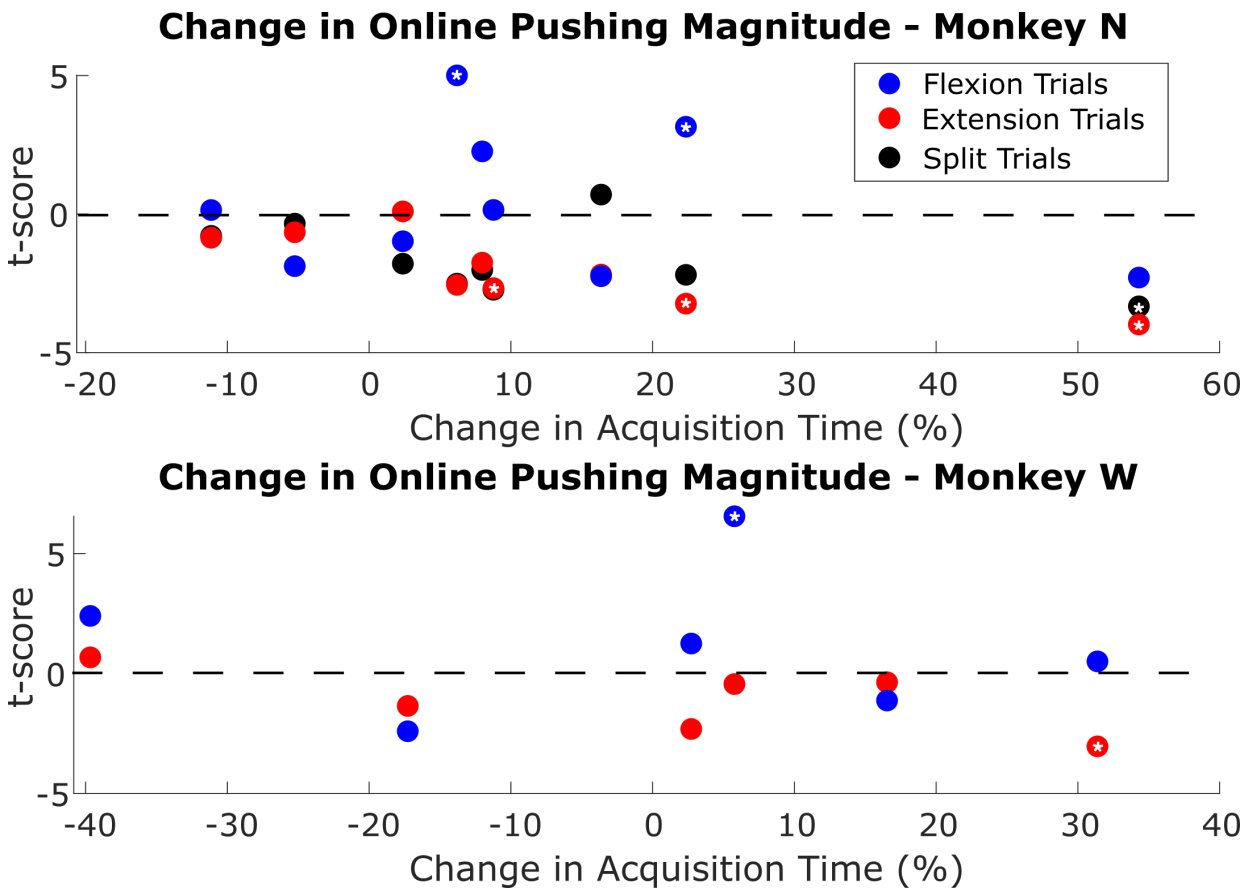

Appendix Figure A-4 Change in 'pushing' magnitude during two-model BMI tasks.
Pushing magnitude is the predicted velocity along the target direction, with predictions made by a linear regression model. This was trained on normal trials offline and evaluated on neural data during online trials at the time point of peak movement. The change is between trials during normal online control and trials with a context changed added during online control. One dot indicates the two-sample t-score of this change calculated using all trials of one type (blue – flexion, red – extension, or black – split) in one session for Monkey N (top) or Monkey W (bottom). A change greater than 0 indicates a larger magnitude during the off-context trials, that is pushing harder. White asterisks indicate significant changes.

Bibliography

Aggarwal, V., Acharya, S., Tenore, F., Shin, H. C., Etienne-Cummings, R., Schieber, M. H., & Thakor, N. V. (2008). Asynchronous decoding of dexterous finger movements using M1 neurons. *IEEE Transactions on Neural Systems and Rehabilitation Engineering*, *16*(1), 3–14. https://doi.org/10.1109/TNSRE.2007.916289

Ajiboye, A. B., Willett, F. R., Young, D. R., Memberg, W. D., Murphy, B. A., Miller, J. P., Walter, B. L., Sweet, J. A., Hoyen, H. A., Keith, M. W., Peckham, P. H., Simeral, J. D., Donoghue, J. P., Hochberg, L. R., & Kirsch, R. F. (2017). Restoration of reaching and grasping movements through brain-controlled muscle stimulation in a person with tetraplegia: a proof-of-concept demonstration. *The Lancet*, *389*(10081), 1821–1830. https://doi.org/10.1016/S0140-6736(17)30601-3

Al-Quraishi, M. S., Elamvazuthi, I., Daud, S. A., Parasuraman, S., & Borboni, A. (2018). Eeg-based control for upper and lower limb exoskeletons and prostheses: A systematic review. *Sensors (Switzerland)*, *18*(10). https://doi.org/10.3390/s18103342

Ali, M. A., Hu, C., Jahan, S., Yuan, B., Saleh, M. S., Ju, E., Gao, S. J., & Panat, R. (2021). Sensing of COVID-19 Antibodies in Seconds via Aerosol Jet Nanoprinted Reduced-Graphene-Oxide-Coated 3D Electrodes. *Advanced Materials*, *33*(7). https://doi.org/10.1002/adma.202006647

Ames, K. C., & Churchland, M. M. (2019). Motor cortex signals for each arm are mixed across hemispheres and neurons yet partitioned within the population response. *ELife*, *8*. https://doi.org/10.7554/eLife.46159

Anderson, K. D. (2004). Targeting recovery: Priorities of the spinal cord-injured population. In *Journal of Neurotrauma* (Vol. 21, Issue 10, pp. 1371–1383). J Neurotrauma. https://doi.org/10.1089/neu.2004.21.1371

Angeli, C. A., Boakye, M., Morton, R. A., Vogt, J., Benton, K., Chen, Y., Ferreira, C. K., & Harkema, S. J. (2018). Recovery of Over-Ground Walking after Chronic Motor Complete Spinal Cord Injury. *New England Journal of Medicine*, *379*(13), 1244–1250. https://doi.org/10.1056/nejmoa1803588

Badi, M., Wurth, S., Scarpato, I., Roussinova, E., Losanno, E., Bogaard, A., Delacombaz, M., Borgognon, S., Cvancara, P., Fallegger, F., Su, D. K., Schmidlin, E., Courtine, G., Bloch, J., Lacour, S. P., Stieglitz, T., Rouiller, E. M., Capogrosso, M., & Micera, S. (2021). Intrafascicular peripheral nerve stimulation produces fine functional hand movements in primates. *Science Translational Medicine*, *13*(617), 6463. https://doi.org/10.1126/SCITRANSLMED.ABG6463

Baker, J., Bishop, W., Kellis, S., Levy, T., House, P., & Greger, B. (2009). Multi-scale recordings

for neuroprosthetic control of finger movements. *Proceedings of the 31st Annual International Conference of the IEEE Engineering in Medicine and Biology Society: Engineering the Future of Biomedicine, EMBC 2009*, *2009*, 4573–4577. https://doi.org/10.1109/IEMBS.2009.5332692

Bao, X., Zhou, Y., Wang, Y., Zhang, J., Lü, X., & Wang, Z. (2018). Electrode placement on the forearm for selective stimulation of finger extension/ flexion. *PLoS ONE*, *13*(1). https://doi.org/10.1371/journal.pone.0190936

Barra, B., Conti, S., Perich, M. G., Zhuang, K., Schiavone, G., Fallegger, F., Galan, K., James, N. D., Barraud, Q., Delacombaz, M., Kaeser, M., Rouiller, E. M., Milekovic, T., Lacour, S., Bloch, J., Courtine, G., & Capogrosso, M. (2022). Epidural electrical stimulation of the cervical dorsal roots restores voluntary upper limb control in paralyzed monkeys. *Nature Neuroscience*, *25*(7), 924–934. https://doi.org/10.1038/s41593-022-01106-5

Beisteiner, R., Windischberger, C., Lanzenberger, R., Edward, V., Cunnington, R., Erdler, M., Gartus, A., Streibl, B., Moser, E., & Deecke, L. (2001). Finger somatotopy in human motor cortex. *NeuroImage*, *13*(6), 1016–1026. https://doi.org/10.1006/nimg.2000.0737

Beringer, C. R., Mansouri, M., Fisher, L. E., Collinger, J. L., Munin, M. C., Boninger, M. L., & Gaunt, R. A. (2020). The effect of wrist posture on extrinsic finger muscle activity during single joint movements. *Scientific Reports*, *10*(1). https://doi.org/10.1038/s41598-020-65167-x

Bernshteĭn, N. A. (1967). The Co-ordination and Regulation of Movements. *Pergamon Press*.

Bicchi, A., Gabiccini, M., & Santello, M. (2011). Modelling natural and artificial hands with synergies. *Philosophical Transactions of the Royal Society B: Biological Sciences*, *366*(1581), 3153–3161. https://doi.org/10.1098/rstb.2011.0152

Bickel, C. S., Gregory, C. M., & Dean, J. C. (2011). Motor unit recruitment during neuromuscular electrical stimulation: A critical appraisal. *European Journal of Applied Physiology*, *111*(10), 2399–2407. https://doi.org/10.1007/s00421-011-2128-4

Bishop, W., Chestek, C. C., Gilja, V., Nuyujukian, P., Foster, J. D., Ryu, S. I., Shenoy, K. V., & Yu, B. M. (2014). Self-recalibrating classifiers for intracortical brain-computer interfaces. *Journal of Neural Engineering*, *11*(2). https://doi.org/10.1088/1741-2560/11/2/026001

Bizzi, E., & Cheung, V. C. K. (2013). The neural origin of muscle synergies. *Frontiers in Computational Neuroscience*, *7*, 1–6. https://doi.org/10.3389/fncom.2013.00051

Bizzi, E., Mussa-Ivaldi, F. A., & Giszter, S. (1991). Computations underlying the execution of movement: A biological perspective. *Science*, *253*(5017), 287–291. https://doi.org/10.1126/science.1857964

Bjorck, A., & Golub, G. H. (1973). Numerical Methods for Computing Angles Between Linear Subspaces. *Mathematics of Computation*, *27*(123), 579. https://doi.org/10.2307/2005662

Boles, C. A., Kannam, S., & Cardwell, A. B. (2000). The forearm: Anatomy of muscle compartments and nerves. *American Journal of Roentgenology*, *174*(1), 151–159.

https://doi.org/10.2214/ajr.174.1.1740151

Bollini, C. A., & Wikinski, J. A. (2006). Anatomical review of the brachial plexus. *Techniques in Regional Anesthesia and Pain Management*, *10*(3), 69–78. https://doi.org/10.1053/j.trap.2006.07.006

Bonizzato, M., Guay Hottin, R., Côté, S. L., Massai, E., Choinière, L., Macar, U., Laferrière, S., Sirpal, P., Quessy, S., Lajoie, G., Martinez, M., & Dancause, N. (2023). Autonomous optimization of neuroprosthetic stimulation parameters that drive the motor cortex and spinal cord outputs in rats and monkeys. *Cell Reports Medicine*, *4*(4), 101008. https://doi.org/10.1016/J.XCRM.2023.101008

Bouton, C. E., Shaikhouni, A., Annetta, N. V., Bockbrader, M. A., Friedenberg, D. A., Nielson, D. M., Sharma, G., Sederberg, P. B., Glenn, B. C., Mysiw, W. J., Morgan, A. G., Deogaonkar, M., & Rezai, A. R. (2016). Restoring cortical control of functional movement in a human with quadriplegia. *Nature*, *533*(7602), 247–250. https://doi.org/10.1038/nature17435

Bruns, T. M., Wagenaar, J. B., Bauman, M. J., Gaunt, R. A., & Weber, D. J. (2013). Real-time control of hind limb functional electrical stimulation using feedback from dorsal root ganglia recordings. *Journal of Neural Engineering*, *10*(2), 26020–26033. https://doi.org/10.1088/1741-2560/10/2/026020

Buckmire, A. J., Arakeri, T. J., Reinhard, J. P., & Fuglevand, A. J. (2018). Mitigation of excessive fatigue associated with functional electrical stimulation. *Journal of Neural Engineering*, *15*(6). https://doi.org/10.1088/1741-2552/aade1c

Bullard, A. J., Hutchison, B. C., Lee, J., Chestek, C. A., & Patil, P. G. (2020). Estimating Risk for Future Intracranial, Fully Implanted, Modular Neuroprosthetic Systems: A Systematic Review of Hardware Complications in Clinical Deep Brain Stimulation and Experimental Human Intracortical Arrays. *Neuromodulation*, *23*(4), 411–426. https://doi.org/10.1111/ner.13069

Bullock, I. M., Zheng, J. Z., De La Rosa, S., Guertler, C., & Dollar, A. M. (2013). Grasp frequency and usage in daily household and machine shop tasks. *IEEE Transactions on Haptics*, *6*(3), 296–308. https://doi.org/10.1109/TOH.2013.6

Buzśaki, G., & Wang, X. J. (2012). Mechanisms of gamma oscillations. *Annual Review of Neuroscience*, *35*, 203–225. https://doi.org/10.1146/annurev-neuro-062111-150444

Capogrosso, M., Wenger, N., Raspopovic, S., Musienko, P., Beauparlant, J., Luciani, L. B., Courtine, G., & Micera, S. (2013). A computational model for epidural electrical stimulation of spinal sensorimotor circuits. *Journal of Neuroscience*, *33*(49), 19326–19340. https://doi.org/10.1523/JNEUROSCI.1688-13.2013

Carmena, J. M., Lebedev, M. A., Crist, R. E., O'Doherty, J. E., Santucci, D. M., Dimitrov, D. F., Patil, P. G., Henriquez, C. S., & Nicolelis, M. A. L. (2003). Learning to control a brain-machine interface for reaching and grasping by primates. *PLoS Biology*, *1*(2). https://doi.org/10.1371/journal.pbio.0000042

Carpaneto, J., Raos, V., Umiltà, M. A., Fogassi, L., Murata, A., Gallese, V., & Micera, S. (2012). Continuous decoding of grasping tasks for a prospective implantable cortical neuroprosthesis. *Journal of NeuroEngineering and Rehabilitation*, *9*(1). https://doi.org/10.1186/1743-0003-9-84

Chaikho, L., Clark, E., & Raison, M. (2022). Transcutaneous Functional Electrical Stimulation Controlled by a System of Sensors for the Lower Limbs: A Systematic Review. In *Sensors* (Vol. 22, Issue 24). https://doi.org/10.3390/s22249812

Chestek, C. A., Gilja, V., Blabe, C. H., Foster, B. L., Shenoy, K. V., Parvizi, J., & Henderson, J. M. (2013). Hand posture classification using electrocorticography signals in the gamma band over human sensorimotor brain areas. *Journal of Neural Engineering*, *10*(2), 026002. https://doi.org/10.1088/1741-2560/10/2/026002

Chung, J. E., Joo, H. R., Fan, J. L., Liu, D. F., Barnett, A. H., Chen, S., Geaghan-Breiner, C., Karlsson, M. P., Karlsson, M., Lee, K. Y., Liang, H., Magland, J. F., Pebbles, J. A., Tooker, A. C., Greengard, L. F., Tolosa, V. M., & Frank, L. M. (2019). High-Density, Long-Lasting, and Multi-region Electrophysiological Recordings Using Polymer Electrode Arrays. *Neuron*, *101*(1), 21-31.e5. https://doi.org/10.1016/j.neuron.2018.11.002

Churchland, M. M., Cunningham, J. P., Kaufman, M. T., Foster, J. D., Nuyujukian, P., Ryu, S. I., Shenoy, K. V., & Shenoy, K. V. (2012). Neural population dynamics during reaching. *Nature*, *487*(7405), 51–56. https://doi.org/10.1038/nature11129

Churchland, M. M., & Shenoy, K. V. (2007). Temporal complexity and heterogeneity of single-neuron activity in premotor and motor cortex. *Journal of Neurophysiology*, *97*(6), 4235–4257. https://doi.org/10.1152/jn.00095.2007

Colachis, S. C., Bockbrader, M. A., Zhang, M., Friedenberg, D. A., Annetta, N. V., Schwemmer, M. A., Skomrock, N. D., Mysiw, W. J., Rezai, A. R., Bresler, H. S., & Sharma, G. (2018). Dexterous control of seven functional hand movements using cortically-controlled transcutaneous muscle stimulation in a person with tetraplegia. *Frontiers in Neuroscience*, *12*(APR). https://doi.org/10.3389/fnins.2018.00208

Collinger, J. L., Boninger, M. L., Bruns, T. M., Curley, K., Wang, W., & Weber, D. J. (2013). Functional priorities, assistive technology, and brain-computer interfaces after spinal cord injury. *Journal of Rehabilitation Research and Development*, *50*(2), 145–160. https://doi.org/10.1682/JRRD.2011.11.0213

Collinger, J. L., Wodlinger, B., Downey, J. E., Wang, W., Tyler-Kabara, E. C., Weber, D. J., McMorland, A. J. C., Velliste, M., Boninger, M. L., & Schwartz, A. B. (2013). High-performance neuroprosthetic control by an individual with tetraplegia. *The Lancet*, *381*(9866), 557–564. https://doi.org/10.1016/S0140-6736(12)61816-9

Coste, C. A., William, L., Fonseca, L., Hiairrassary, A., Andreu, D., Geffrier, A., Teissier, J., Fattal, C., & Guiraud, D. (2022). Activating effective functional hand movements in individuals with complete tetraplegia through neural stimulation. *Scientific Reports*, *12*(1), 1–17. https://doi.org/10.1038/s41598-022-19906-x

Costello, J. T., Temmar, H., Cubillos, L. H., Mender, M. J., Wallace, D. M., Willsey, M. S., Patil, P. G., & Chestek, C. A. (2023). Balancing Memorization and Generalization in RNNs for High Performance Brain-Machine Interfaces. *BioRxiv*, 2023.05.28.542435. https://doi.org/10.1101/2023.05.28.542435

Crago, P. E., Peckham, P. H., & Thrope, G. B. (1980). Modulation of Muscle Force by Recruitment During Intramuscular Stimulation. *IEEE Transactions on Biomedical Engineering*, *BME-27*(12), 679–684. https://doi.org/10.1109/TBME.1980.326592

Cunningham, J. P., & Yu, B. M. (2014). Dimensionality reduction for large-scale neural recordings. *Nature Neuroscience*, *17*(11), 1500–1509. https://doi.org/10.1038/nn.3776

Dali, M., Rossel, O., Andreu, D., Laporte, L., Hernández, A., Laforet, J., Marijon, E., Hagège, A., Clerc, M., Henry, C., & Guiraud, D. (2018). Model based optimal multipolar stimulation without a priori knowledge of nerve structure: Application to vagus nerve stimulation. *Journal of Neural Engineering*, *15*(4). https://doi.org/10.1088/1741-2552/aabeb9

Davoodi, R., Urata, C., Hauschild, M., Khachani, M., & Loeb, G. E. (2007). Model-based development of neural prostheses for movement. *IEEE Transactions on Biomedical Engineering*, *54*(11), 1909–1918. https://doi.org/10.1109/TBME.2007.902252

De Freitas, R. M., Capogrosso, M., Nomura, T., & Milosevic, M. (2022). Preferential activation of proprioceptive and cutaneous sensory fibers compared to motor fibers during cervical transcutaneous spinal cord stimulation: A computational study. *Journal of Neural Engineering*, *19*(3). https://doi.org/10.1088/1741-2552/ac6a7c

Dechent, P., & Frahm, J. (2003). Functional somatotopy of finger representations in human primary motor cortex. *Human Brain Mapping*, *18*(4), 272–283. https://doi.org/10.1002/hbm.10084

Dekleva, B. M., Weiss, J. M., Boninger, M. L., & Collinger, J. L. (2021). Generalizable cursor click decoding using grasp-related neural transients. *Journal of Neural Engineering*, *18*(4), 0460e9. https://doi.org/10.1088/1741-2552/ac16b2

Delgado-Martínez, I., Badia, J., Pascual-Font, A., Rodríguez-Baeza, A., & Navarro, X. (2016). Fascicular topography of the human median nerve for neuroprosthetic surgery. *Frontiers in Neuroscience*, *10*(JUL), 1–13. https://doi.org/10.3389/fnins.2016.00286

Downey, J. E., Brane, L., Gaunt, R. A., Tyler-Kabara, E. C., Boninger, M. L., & Collinger, J. L. (2017). Motor cortical activity changes during neuroprosthetic-controlled object interaction. *Scientific Reports*, *7*(1), 1–10. https://doi.org/10.1038/s41598-017-17222-3

ElKoura, G., & Singh, K. (2003). Handrix: Animating the human hand. *Proceedings of the 2003 ACM SIGGRAPH/Eurographics Symposium on Computer Animation, SCA 2003*.

English, A. W., Wolf, S. L., & Segal, R. L. (1993). Compartmentalization of muscles and their motor nuclei: The partitioning hypothesis. *Physical Therapy*, *73*(12), 857–867. https://doi.org/10.1093/ptj/73.12.857

Ethier, C., Gallego, J. A., & Miller, L. E. (2015). Brain-controlled neuromuscular stimulation to

drive neural plasticity and functional recovery. *Current Opinion in Neurobiology*, *33*, 95–102. https://doi.org/10.1016/j.conb.2015.03.007

Ethier, C., Oby, E. R., Bauman, M. J., & Miller, L. E. (2012). Restoration of grasp following paralysis through brain-controlled stimulation of muscles. *Nature*, *485*(7398), 368–371. https://doi.org/10.1038/nature10987

Evarts, E. V. (1968). Relation of pyramidal tract activity to force exerted during voluntary movement. *Journal of Neurophysiology*, *31*(1), 14–27. https://doi.org/10.1152/jn.1968.31.1.14

Even-Chen, N., Muratore, D. G., Stavisky, S. D., Hochberg, L. R., Henderson, J. M., Murmann, B., & Shenoy, K. V. (2020). Power-saving design opportunities for wireless intracortical brain–computer interfaces. *Nature Biomedical Engineering*, *4*(10), 984–996. https://doi.org/10.1038/s41551-020-0595-9

Fagg, A. H., Ojakangas, G. W., Miller, L. E., & Hatsopoulos, N. G. (2009, October). *Kinetic trajectory decoding using motor cortical ensembles*. IEEE Transactions on Neural Systems and Rehabilitation Engineering. https://doi.org/10.1109/TNSRE.2009.2029313

Fan, J. M., Nuyujukian, P., Kao, J. C., Chestek, C. A., Ryu, S. I., & Shenoy, K. V. (2014). Intention Estimation in Brain Machine Interfaces. In *J Neural Eng* (Vol. 11, Issue 1).

Fang, Z.-P., & Mortimer, J. T. (1991). Alternate excitation of large and small axons with different stimulation waveforms: an application to muscle activation. *Medical & Biological Engineering & Computing*, *29*(5), 543–547. https://doi.org/10.1007/BF02442328

Feix, T., Romero, J., Schmiedmayer, H. B., Dollar, A. M., & Kragic, D. (2016). The GRASP Taxonomy of Human Grasp Types. *IEEE Transactions on Human-Machine Systems*, *46*(1), 66–77. https://doi.org/10.1109/THMS.2015.2470657

Flesher, S. N., Downey, J. E., Weiss, J. M., Hughes, C. L., Herrera, A. J., Tyler-Kabara, E. C., Boninger, M. L., Collinger, J. L., & Gaunt, R. A. (2021). A brain-computer interface that evokes tactile sensations improves robotic arm control. *Science*, *372*(6544), 831–836. https://doi.org/10.1126/science.abd0380

Flint, R. D., Rosenow, J. M., Tate, M. C., & Slutzky, M. W. (2017). Continuous decoding of human grasp kinematics using epidural and subdural signals. *Journal of Neural Engineering*, *14*(1). https://doi.org/10.1088/1741-2560/14/1/016005

Flint, R. D., Tate, M. C., Li, K., Templer, J. W., Rosenow, J. M., Pandarinath, C., & Slutzky, M. W. (2020). The representation of finger movement and force in human motor and premotor cortices. *ENeuro*, *7*(4), 1–15. https://doi.org/10.1523/ENEURO.0063-20.2020

Frewin, C. L., Bernardin, E. E., Deku, F., Everly, R., Hassan, J., Pancrazio, J. J., & Saddow, S. E. (2016). (Invited) Silicon Carbide as a Robust Neural Interface. *ECS Transactions*, *75*(12), 39–45. https://doi.org/10.1149/07512.0039ecst

Friedenberg, D. A., Schwemmer, M. A., Landgraf, A. J., Annetta, N. V., Bockbrader, M. A., Bouton, C. E., Zhang, M., Rezai, A. R., Mysiw, W. J., Bresler, H. S., & Sharma, G. (2017).

Neuroprosthetic-enabled control of graded arm muscle contraction in a paralyzed human. *Scientific Reports*, *7*(1), 1–10. https://doi.org/10.1038/s41598-017-08120-9

Fugl Meyer, A. R., Jaasko, L., & Leyman, I. (1975). The post stroke hemiplegic patient. I. A method for evaluation of physical performance. *Scandinavian Journal of Rehabilitation Medicine*, *7*(1), 13–31. https://doi.org/10.2340/1650197771331

Gallego, J. A., Perich, M. G., Miller, L. E., & Solla, S. A. (2017). Neural Manifolds for the Control of Movement. In *Neuron* (Vol. 94, Issue 5, pp. 978–984). Cell Press. https://doi.org/10.1016/j.neuron.2017.05.025

Gallego, J. A., Perich, M. G., Naufel, S. N., Ethier, C., Solla, S. A., & Miller, L. E. (2018). Cortical population activity within a preserved neural manifold underlies multiple motor behaviors. *Nature Communications*, *9*(1). https://doi.org/10.1038/s41467-018-06560-z

Ganguly, K., Dimitrov, D. F., Wallis, J. D., & Carmena, J. M. (2011). Reversible large-scale modification of cortical networks during neuroprosthetic control. *Nature Neuroscience*, *14*(5), 662–669. https://doi.org/10.1038/nn.2797

Gant, K., Guerra, S., Zimmerman, L., Parks, B. A., Prins, N. W., & Prasad, A. (2018). EEG-controlled functional electrical stimulation for hand opening and closing in chronic complete cervical spinal cord injury. *Biomedical Physics and Engineering Express*, *4*(6). https://doi.org/10.1088/2057-1976/aabb13

Gaunt, R. A., Prochazka, A., Mushahwar, V. K., Guevremont, L., & Ellaway, P. H. (2006). Intraspinal microstimulation excites multisegmental sensory afferents at lower stimulus levels than local α-motoneuron responses. *Journal of Neurophysiology*, *96*(6), 2995–3005. https://doi.org/10.1152/jn.00061.2006

Georgopoulos, A. P., Kalaska, J. F., Caminiti, R., & Massey, J. T. (1982). On the relations between the direction of two-dimensional arm movements and cell discharge in primate motor cortex. *Journal of Neuroscience*, *2*(11), 1527–1537. https://doi.org/10.1523/jneurosci.02-11-01527.1982

Georgopoulos, A. P., Schwartz, A. B., & Kettner, R. E. (1986). Neuronal population coding of movement direction. *Science*, *233*(4771), 1416–1419. https://doi.org/10.1126/science.3749885

Giat, Y., Mizrahi, J., & Levy, M. (1993). A Musculotendon Model of the Fatigue Profiles of Paralyzed Quadriceps Muscle Under FES. *IEEE Transactions on Biomedical Engineering*, *40*(7), 664–674. https://doi.org/10.1109/10.237696

Gilja, V., Nuyujukian, P., Chestek, C. A., Cunningham, J. P., Yu, B. M., Fan, J. M., Churchland, M. M., Kaufman, M. T., Kao, J. C., Ryu, S. I., & Shenoy, K. V. (2012). A high-performance neural prosthesis enabled by control algorithm design. *Nature Neuroscience*, *15*(12), 1752–1757. https://doi.org/10.1038/nn.3265

Gilja, V., Nuyujukian, P., Chestek, C. A., Cunningham, J. P., Yu, B. M., Fan, J. M., Ryu, S. I., & Shenoy, K. V. (2012). A brain machine interface control algorithm designed from a feedback

control perspective. *Proceedings of the Annual International Conference of the IEEE Engineering in Medicine and Biology Society, EMBS*, 1318–1322. https://doi.org/10.1109/EMBC.2012.6346180

Gilja, V., Pandarinath, C., Blabe, C. H., Nuyujukian, P., Simeral, J. D., Sarma, A. A., Sorice, B. L., Perge, J. A., Jarosiewicz, B., Hochberg, L. R., Shenoy, K. V., & Henderson, J. M. (2015). Clinical translation of a high-performance neural prosthesis. *Nature Medicine*, *21*(10), 1142–1145. https://doi.org/10.1038/nm.3953

Gill, M. L., Grahn, P. J., Calvert, J. S., Linde, M. B., Lavrov, I. A., Strommen, J. A., Beck, L. A., Sayenko, D. G., Van Straaten, M. G., Drubach, D. I., Veith, D. D., Thoreson, A. R., Lopez, C., Gerasimenko, Y. P., Edgerton, V. R., Lee, K. H., & Zhao, K. D. (2018). Neuromodulation of lumbosacral spinal networks enables independent stepping after complete paraplegia. *Nature Medicine*, *24*(11), 1677–1682. https://doi.org/10.1038/s41591-018-0175-7

Glaser, J. I., Benjamin, A. S., Chowdhury, R. H., Perich, M. G., Miller, L. E., & Kording, K. P. (2020). Machine learning for neural decoding. *ENeuro*, *7*(4), 1–16. https://doi.org/10.1523/ENEURO.0506-19.2020

Golabchi, A., Woeppel, K. M., Li, X., Lagenaur, C. F., & Cui, X. T. (2020). Neuroadhesive protein coating improves the chronic performance of neuroelectronics in mouse brain. *Biosensors and Bioelectronics*, *155*. https://doi.org/10.1016/j.bios.2020.112096

Golub, M. D., Sadtler, P. T., Oby, E. R., Quick, K. M., Ryu, S. I., Tyler-Kabara, E. C., Batista, A. P., Chase, S. M., & Yu, B. M. (2018a). Learning by neural reassociation/631/378/1595/631/378/2629 article. *Nature Neuroscience*, *21*(4), 607–616. https://doi.org/10.1038/s41593-018-0095-3

Golub, M. D., Sadtler, P. T., Oby, E. R., Quick, K. M., Ryu, S. I., Tyler-Kabara, E. C., Batista, A. P., Chase, S. M., & Yu, B. M. (2018b). Learning by neural reassociation. *Nature Neuroscience*, *21*(4), 607–616. https://doi.org/10.1038/s41593-018-0095-3

Goodman, J. M., Tabot, G. A., Lee, A. S., Suresh, A. K., Rajan, A. T., Hatsopoulos, N. G., & Bensmaia, S. (2019). Postural Representations of the Hand in the Primate Sensorimotor Cortex. *Neuron*, *104*(5), 1000-1009.e7. https://doi.org/10.1016/j.neuron.2019.09.004

Gracia-Ibáñez, V., Sancho-Bru, J. L., & Vergara, M. (2018). Relevance of grasp types to assess functionality for personal autonomy. *Journal of Hand Therapy*, *31*(1), 102–110. https://doi.org/10.1016/j.jht.2017.02.003

Grandjean, P. A., & Mortimer, J. T. (1986). Recruitment properties of monopolar and bipolar epimysial electrodes. *Annals of Biomedical Engineering*, *14*(1), 53–66. https://doi.org/10.1007/BF02364648

Graziano, M. (2006). The organization of behavioral repertoire in motor cortex. *Annual Review of Neuroscience*, *29*, 105–134. https://doi.org/10.1146/annurev.neuro.29.051605.112924

Greiner, N., Barra, B., Schiavone, G., Lorach, H., James, N., Conti, S., Kaeser, M., Fallegger, F., Borgognon, S., Lacour, S., Bloch, J., Courtine, G., & Capogrosso, M. (2021). Recruitment of

upper-limb motoneurons with epidural electrical stimulation of the cervical spinal cord. *Nature Communications*, *12*(1), 1–19. https://doi.org/10.1038/s41467-020-20703-1

Gruner, J. A., & Mason, C. P. (1989). Nonlinear muscle recruitment during intramuscular and nerve stimulation. *Journal of Rehabilitation Research and Development*, *26*(2), 1–16.

Gu, J., Wang, Z., Kuen, J., Ma, L., Shahroudy, A., Shuai, B., Liu, T., Wang, X., Wang, G., Cai, J., & Chen, T. (2018). Recent advances in convolutional neural networks. *Pattern Recognition*, *77*, 354–377. https://doi.org/10.1016/j.patcog.2017.10.013

Guitchounts, G., Markowitz, J. E., Liberti, W. A., & Gardner, T. J. (2013). A carbon-fiber electrode array for long-term neural recording. *Journal of Neural Engineering*, *10*(4). https://doi.org/10.1088/1741-2560/10/4/046016

Haghi, B., Kellis, S., Shah, S., Ashok, M., Bashford, L., Kramer, D., Lee, B., Liu, C., Andersen, R. A., & Emami, A. (2019). Deep multi-state dynamic recurrent neural networks operating on wavelet based neural features for robust brain machine interfaces. In *Advances in Neural Information Processing Systems* (Vol. 32). https://proceedings.neurips.cc/paper_files/paper/2019/file/1e0feeaff84a19bf3936e693311fa66d-Paper.pdf

Hamed, S. Ben, Schieber, M. H., & Pouget, A. (2007). Decoding M1 neurons during multiple finger movements. *Journal of Neurophysiology*, *98*(1), 327–333. https://doi.org/10.1152/jn.00760.2006

Hanson, T. L., Diaz-Botia, C. A., Kharazia, V., Maharbiz, M. M., & Sabes, P. N. (2019). The "sewing machine" for minimally invasive neural recording. *BioRxiv*, 578542. https://doi.org/10.1101/578542

Harkema, S., Gerasimenko, Y., Hodes, J., Burdick, J., Angeli, C., Chen, Y., Ferreira, C., Willhite, A., Rejc, E., Grossman, R. G., & Edgerton, V. R. (2011). Effect of epidural stimulation of the lumbosacral spinal cord on voluntary movement, standing, and assisted stepping after motor complete paraplegia: A case study. *The Lancet*, *377*(9781), 1938–1947. https://doi.org/10.1016/S0140-6736(11)60547-3

Hart, R. L., Kilgore, K. L., & Peckham, P. H. (1998). A comparison between control methods for implanted FES hand-grasp systems. *IEEE Transactions on Rehabilitation Engineering*, *6*(2), 208–218. https://doi.org/10.1109/86.681187

Hasse, B. A., Sheets, D. E. G., Holly, N. L., Gothard, K. M., & Fuglevand, A. J. (2022). Restoration of complex movement in the paralyzed upper limb. *Journal of Neural Engineering*, *19*(4), 046002. https://doi.org/10.1088/1741-2552/ac7ad7

Heald, E., Hart, R., Kilgore, K., & Peckham, P. H. (2017). Characterization of Volitional Electromyographic Signals in the Lower Extremity after Motor Complete Spinal Cord Injury. *Neurorehabilitation and Neural Repair*, *31*(6), 583–591. https://doi.org/10.1177/1545968317704904

Henneman, E. (1957). Relation between size of neurons and their susceptibility to discharge.

Science, *126*(3287), 1345–1347. https://doi.org/10.1126/science.126.3287.1345

Herring, E. Z., Graczyk, E. L., Memberg, W. D., Adams, R., Fernandez Baca-Vaca, G., Hutchison, B. C., Krall, J. T., Alexander, B. J., Conlan, E. C., Alfaro, K. E., Bhat, P., Ketting-Olivier, A. B., Haddix, C. A., Taylor, D. M., Tyler, D. J., Sweet, J. A., Kirsch, R. F., Ajiboye, A. B., & Miller, J. P. (2023). Reconnecting the Hand and Arm to the Brain: Efficacy of Neural Interfaces for Sensorimotor Restoration After Tetraplegia. *Neurosurgery*. https://doi.org/10.1227/neu.0000000000002769

Hochberg, L. R., Bacher, D., Jarosiewicz, B., Masse, N. Y., Simeral, J. D., Vogel, J., Haddadin, S., Liu, J., Cash, S. S., Van Der Smagt, P., & Donoghue, J. P. (2012). Reach and grasp by people with tetraplegia using a neurally controlled robotic arm. *Nature*, *485*(7398), 372–375. https://doi.org/10.1038/nature11076

Hochberg, L. R., Serruya, M. D., Friehs, G. M., Mukand, J. A., Saleh, M., Caplan, A. H., Branner, A., Chen, D., Penn, R. D., & Donoghue, J. P. (2006). Neuronal ensemble control of prosthetic devices by a human with tetraplegia. *Nature*, *442*(7099), 164–171. https://doi.org/10.1038/nature04970

Hofstoetter, U. S., Freundl, B., Binder, H., & Minassian, K. (2018). Common neural structures activated by epidural and transcutaneous lumbar spinal cord stimulation: Elicitation of posterior root-muscle reflexes. *PLoS ONE*, *13*(1). https://doi.org/10.1371/journal.pone.0192013

Holly, N. L., Hasse, B. A., Gothard, K. M., & Fuglevand, A. J. (2022). Large-scale intramuscular electrode system for chronic electromyography and functional electrical stimulation. *Journal of Neurophysiology*, *128*(5), 1011–1024. https://doi.org/10.1152/JN.00325.2022/ASSET/IMAGES/LARGE/JN.00325.2022_F009.JPEG

Hong, G., & Lieber, C. M. (2019). Novel electrode technologies for neural recordings. *Nature Reviews Neuroscience*, *20*(6), 330–345. https://doi.org/10.1038/s41583-019-0140-6

Hotson, G., McMullen, D. P., Fifer, M. S., Johannes, M. S., Katyal, K. D., Para, M. P., Armiger, R., Anderson, W. S., Thakor, N. V., Wester, B. A., & Crone, N. E. (2016). Individual finger control of a modular prosthetic limb using high-density electrocorticography in a human subject. *Journal of Neural Engineering*, *13*(2). https://doi.org/10.1088/1741-2560/13/2/026017

Hwang, Y. C. E., Long, L., Filho, J. S., Genov, R., & Zariffa, J. (2024). Closed-Loop Control of Functional Electrical Stimulation Using a Selectively Recording and Bidirectional Nerve Cuff Interface. *IEEE Transactions on Neural Systems and Rehabilitation Engineering*, *32*, 504–513. https://doi.org/10.1109/TNSRE.2024.3355063

Ingram, J. N., Körding, K. P., Howard, I. S., & Wolpert, D. M. (2008). The statistics of natural hand movements. *Experimental Brain Research*, *188*(2), 223–236. https://doi.org/10.1007/s00221-008-1355-3

Ioffe, S., & Szegedy, C. (2015). Batch normalization: Accelerating deep network training by

reducing internal covariate shift. *32nd International Conference on Machine Learning, ICML 2015*, *1*, 448–456.

Irwin, Z. T., Schroeder, K. E., Vu, P. P., Bullard, A. J., Tat, D. M., Nu, C. S., Vaskov, A., Nason, S. R., Thompson, D. E., Bentley, J. N., Patil, P. G., & Chestek, C. A. (2017). Neural control of finger movement via intracortical brain-machine interface. *Journal of Neural Engineering*, *14*(6). https://doi.org/10.1088/1741-2552/aa80bd

Iturrate, I., Chavarriaga, R., Pereira, M., Zhang, H., Corbet, T., Leeb, R., & Millán, J. del R. (2018). Human EEG reveals distinct neural correlates of power and precision grasping types. *NeuroImage*, *181*, 635–644. https://doi.org/10.1016/j.neuroimage.2018.07.055

Jabaley, M. E., Wallace, W. H., & Heckler, F. R. (1980). Internal topography of major nerves of the forearm and hand: A current view. *Journal of Hand Surgery*, *5*(1), 1–18. https://doi.org/10.1016/S0363-5023(80)80035-9

Jain, N. B., Ayers, G. D., Peterson, E. N., Harris, M. B., Morse, L., O'Connor, K. C., & Garshick, E. (2015). Traumatic spinal cord injury in the United States, 1993-2012. *JAMA*, *313*(22), 2236–2243. https://doi.org/10.1001/JAMA.2015.6250

Jarosiewicz, B., Chase, S. M., Fraser, G. W., Velliste, M., Kass, R. E., & Schwartz, A. B. (2008). Functional network reorganization during learning in a brain-computer interface paradigm. *Proceedings of the National Academy of Sciences of the United States of America*, *105*(49), 19486–19491. https://doi.org/10.1073/pnas.0808113105

Jarosiewicz, B., Masse, N. Y., Bacher, D., Cash, S. S., Eskandar, E., Friehs, G., Donoghue, J. P., & Hochberg, L. R. (2013). Advantages of closed-loop calibration in intracortical brain-computer interfaces for people with tetraplegia. *Journal of Neural Engineering*, *10*(4). https://doi.org/10.1088/1741-2560/10/4/046012

Jarosiewicz, B., Sarma, A. A., Bacher, D., Masse, N. Y., Simeral, J. D., Sorice, B., Oakley, E. M., Blabe, C., Pandarinath, C., Gilja, V., Cash, S. S., Eskandar, E. N., Friehs, G., Henderson, J. M., Shenoy, K. V., Donoghue, J. P., & Hochberg, L. R. (2015). Virtual typing by people with tetraplegia using a self-calibrating intracortical brain-computer interface. *Science Translational Medicine*, *7*(313), 1–11. https://doi.org/10.1126/scitranslmed.aac7328

Jochumsen, M., Niazi, I. K., Dremstrup, K., & Kamavuako, E. N. (2016). Detecting and classifying three different hand movement types through electroencephalography recordings for neurorehabilitation. *Medical and Biological Engineering and Computing*, *54*(10), 1491–1501. https://doi.org/10.1007/s11517-015-1421-5

Jorge, A., Royston, D. A., Tyler-Kabara, E. C., Boninger, M. L., & Collinger, J. L. (2020). Classification of individual finger movements using intracortical recordings in human motor cortex. *Neurosurgery*, *87*(4), 630–638. https://doi.org/10.1093/neuros/nyaa026

Jun, J. J., Steinmetz, N. A., Siegle, J. H., Denman, D. J., Bauza, M., Barbarits, B., Lee, A. K., Anastassiou, C. A., Andrei, A., Aydin, Ç., Barbic, M., Blanche, T. J., Bonin, V., Couto, J., Dutta, B., Gratiy, S. L., Gutnisky, D. A., Häusser, M., Karsh, B., … Harris, T. D. (2017). Fully integrated silicon probes for high-density recording of neural activity. *Nature*,

551(7679), 232–236. https://doi.org/10.1038/nature24636

Kakei, S., Hoffman, D. S., & Strick, P. L. (1999). Muscle and movement representations in the primary motor cortex. *Science*, *285*(5436), 2136–2139. https://doi.org/10.1126/science.285.5436.2136

Kalaska, J. F. (2009). From intention to action: Motor cortex and the control of reaching movements. *Advances in Experimental Medicine and Biology*, *629*, 139–178. https://doi.org/10.1007/978-0-387-77064-2_8

Kalaska, J. F. (2019). Emerging ideas and tools to study the emergent properties of the cortical neural circuits for voluntary motor control in non-human primates. *F1000Research*, *8*. https://doi.org/10.12688/f1000research.17161.1

Kao, J. C., Nuyujukian, P., Ryu, S. I., Churchland, M. M., Cunningham, J. P., & Shenoy, K. V. (2015). Single-trial dynamics of motor cortex and their applications to brain-machine interfaces. *Nature Communications*, *6*(1), 1–12. https://doi.org/10.1038/ncomms8759

Kao, J. C., Nuyujukian, P., Ryu, S. I., & Shenoy, K. V. (2017). A High-Performance Neural Prosthesis Incorporating Discrete State Selection with Hidden Markov Models. *IEEE Transactions on Biomedical Engineering*, *64*(4), 935–945. https://doi.org/10.1109/TBME.2016.2582691

Kapadia, N., Zivanovic, V., & Popovic, M. R. (2013). Restoring voluntary grasping function in individuals with incomplete chronic spinal cord injury: Pilot study. *Topics in Spinal Cord Injury Rehabilitation*, *19*(4), 279–287. https://doi.org/10.1310/sci1904-279

Kaufman, M. T., Churchland, M. M., Ryu, S. I., & Shenoy, K. V. (2014). Cortical activity in the null space: Permitting preparation without movement. *Nature Neuroscience*, *17*(3), 440–448. https://doi.org/10.1038/nn.3643

Keen, D. A., & Fuglevand, A. J. (2004). Common Input to Motor Neurons Innervating the Same and Different Compartments of the Human Extensor Digitorum Muscle. *Journal of Neurophysiology*, *91*(1), 57–62. https://doi.org/10.1152/jn.00650.2003

Keith, M. W., Peckham, P. H., Thrope, G. B., Stroh, K. C., Smith, B., Buckett, J. R., Kilgore, K. L., & Jatich, J. W. (1989). Implantable functional neuromuscular stimulation in the tetraplegic hand. *Journal of Hand Surgery*, *14*(3), 524–530. https://doi.org/10.1016/S0363-5023(89)80017-6

Kilbreath, S. L., & Heard, R. C. (2005). Frequency of hand use in healthy older persons. *Australian Journal of Physiotherapy*, *51*(2), 119–122. https://doi.org/10.1016/S0004-9514(05)70040-4

Kilgore, K. L., Bryden, A., Keith, M. W., Hoyen, H. A., Hart, R. L., Nemunaitis, G. A., & Peckham, P. H. (2018). Evolution of neuroprosthetic approaches to restoration of upper extremity function in spinal cord injury. *Topics in Spinal Cord Injury Rehabilitation*, *24*(3), 252–264. https://doi.org/10.1310/sci2403-252

Kilgore, K. L., Hoyen, H. A., Bryden, A. M., Hart, R. L., Keith, M. W., & Peckham, P. H. (2008). An Implanted Upper-Extremity Neuroprosthesis Using Myoelectric Control. *Journal of Hand*

Surgery, *33*(4), 539–550. https://doi.org/10.1016/j.jhsa.2008.01.007

Kilgore, K. L., Peckham, P. H., & Keith, M. W. (2009). Twenty year experience with implanted neuroprostheses. *Proceedings of the 31st Annual International Conference of the IEEE Engineering in Medicine and Biology Society: Engineering the Future of Biomedicine, EMBC 2009*, 7212–7215. https://doi.org/10.1109/IEMBS.2009.5335272

Kilgore, K. L., Peckham, P. H., Keith, M. W., Montague, F. W., Hart, R. L., Gazdik, M. M., Bryden, A. M., Snyder, S. A., & Stage, T. C. (2003). Durability of implanted electrodes and leads in an upper-limb neuroprosthesis. *Journal of Rehabilitation Research and Development*, *40*(6), 457–468. https://doi.org/10.1682/JRRD.2003.11.0457

Kilgore, K. L., Peckham, P. H., Thrope, G. B., Keith, M. W., & Gallaher-Stone, K. A. (1989). Synthesis of Hand Grasp Using Functional Neuromuscular Stimulation. *IEEE Transactions on Biomedical Engineering*, *36*(7), 761–770. https://doi.org/10.1109/10.32109

Kim, S. P., Simeral, J. D., Hochberg, L. R., Donoghue, J. P., & Black, M. J. (2008). Neural control of computer cursor velocity by decoding motor cortical spiking activity in humans with tetraplegia. *Journal of Neural Engineering*, *5*(4), 455–476. https://doi.org/10.1088/1741-2560/5/4/010

Koutsou, A. D., Moreno, J. C., Del Ama, A. J., Rocon, E., & Pons, J. L. (2016). Advances in selective activation of muscles for non-invasive motor neuroprostheses. *Journal of NeuroEngineering and Rehabilitation*, *13*(1). https://doi.org/10.1186/s12984-016-0165-2

Kuhn, A., Keller, T., Lawrence, M., & Morari, M. (2010). The influence of electrode size on selectivity and comfort in transcutaneous electrical stimulation of the forearm. *IEEE Transactions on Neural Systems and Rehabilitation Engineering : A Publication of the IEEE Engineering in Medicine and Biology Society*, *18*(3), 255–262. https://doi.org/10.1109/TNSRE.2009.2039807

Ledbetter, N. M., Ethier, C., Oby, E. R., Hiatt, S. D., Wilder, A. M., Ko, J. H., Agnew, S. P., Miller, L. E., & Clark, G. A. (2013). Intrafascicular stimulation of monkey arm nerves evokes coordinated grasp and sensory responses. *Journal of Neurophysiology*, *109*(2), 580–590. https://doi.org/10.1152/jn.00688.2011

Lee, J., Leung, V., Lee, A. H., Huang, J., Asbeck, P., Mercier, P. P., Shellhammer, S., Larson, L., Laiwalla, F., & Nurmikko, A. (2021). Neural recording and stimulation using wireless networks of microimplants. *Nature Electronics*, *4*(8), 604–614. https://doi.org/10.1038/s41928-021-00631-8

Lee, S., Cortese, A. J., Gandhi, A. P., Agger, E. R., McEuen, P. L., & Molnar, A. C. (2018). A 250 μm × 57 μm Microscale Opto-electronically Transduced Electrodes (MOTEs) for Neural Recording. *IEEE Transactions on Biomedical Circuits and Systems*, *12*(6), 1256–1266. https://doi.org/10.1109/TBCAS.2018.2876069

Lemay, M. A., & Grill, W. M. (2004). Modularity of Motor Output Evoked by Intraspinal Microstimulation in Cats. *Journal of Neurophysiology*, *91*(1), 502–514. https://doi.org/10.1152/jn.00235.2003

Lemon, R. N. (2008). An enduring map of the motor cortex. *Experimental Physiology*, *93*(7), 798–802. https://doi.org/10.1113/expphysiol.2007.039081

Li, Y., Wei, C., & Ma, T. (2019). Towards explaining the regularization effect of initial large learning rate in training neural networks. *Advances in Neural Information Processing Systems*, *32*(NeurIPS), 1–12.

Lim, J., Moon, E., Barrow, M., Nason, S. R., Patel, P. R., Patil, P. G., Oh, S., Lee, I., Kim, H. S., Sylvester, D., Blaauw, D., Chestek, C. A., Phillips, J., & Jang, T. (2020). A 0.19×0.17mm2 Wireless Neural Recording IC for Motor Prediction with Near-Infrared-Based Power and Data Telemetry. *Digest of Technical Papers - IEEE International Solid-State Circuits Conference*, *2020-Febru*, 416–418. https://doi.org/10.1109/ISSCC19947.2020.9063005

Liu, J., Fu, T. M., Cheng, Z., Hong, G., Zhou, T., Jin, L., Duvvuri, M., Jiang, Z., Kruskal, P., Xie, C., Suo, Z., Fang, Y., & Lieber, C. M. (2015). Syringe-injectable electronics. *Nature Nanotechnology*, *10*(7), 629–635. https://doi.org/10.1038/nnano.2015.115

Liu, J., Lau, H. K., Pereira, B. P., Kumar, V. P., & Pho, R. W. H. (1996). Terminal Nerve Branch Entries (Motor Points) of Forearm Muscles: A Comparative Study between Monkey and Human. *Cells Tissues Organs*, *155*(1), 41–49. https://doi.org/10.1159/000147788

Liu, J., & Zhou, P. (2013). A novel myoelectric pattern recognition strategy for hand function restoration after incomplete cervical spinal cord injury. *IEEE Transactions on Neural Systems and Rehabilitation Engineering*, *21*(1), 96–103. https://doi.org/10.1109/TNSRE.2012.2218832

Lorach, H., Galvez, A., Spagnolo, V., Martel, F., Karakas, S., Intering, N., Vat, M., Faivre, O., Harte, C., Komi, S., Ravier, J., Collin, T., Coquoz, L., Sakr, I., Baaklini, E., Hernandez-Charpak, S. D., Dumont, G., Buschman, R., Buse, N., … Courtine, G. (2023). Walking naturally after spinal cord injury using a brain–spine interface. *Nature*, *618*(7963), 126–133. https://doi.org/10.1038/s41586-023-06094-5

Losanno, E., Badi, M., Roussinova, E., Bogaard, A., Delacombaz, M., Shokur, S., & Micera, S. (2022). Validation of manifold-based direct control for a brain-to-body neural bypass. *BioRxiv*, 2022.07.25.501351. https://doi.org/10.1101/2022.07.25.501351

Losanno, E., Badi, M., Wurth, S., Borgognon, S., Courtine, G., Capogrosso, M., Rouiller, E. M., & Micera, S. (2021). Bayesian optimization of peripheral intraneural stimulation protocols to evoke distal limb movements. *Journal of Neural Engineering*, *18*(6). https://doi.org/10.1088/1741-2552/ac3f6c

Losanno, E., Mender, M., Chestek, C., Shokur, S., & Micera, S. (2023). Neurotechnologies to restore hand functions. *Nature Reviews Bioengineering*, *1*(6), 390–407. https://doi.org/10.1038/s44222-023-00054-4

Lou, J. W. H., Bergquist, A. J., Aldayel, A., Czitron, J., & Collins, D. F. (2017). Interleaved neuromuscular electrical stimulation reduces muscle fatigue. *Muscle and Nerve*, *55*(2), 179–189. https://doi.org/10.1002/mus.25224

Lu, D. C., Edgerton, V. R., Modaber, M., Auyong, N., Morikawa, E., Zdunowski, S., Sarino, M. E., Sarrafzadeh, M., Nuwer, M. R., Roy, R. R., & Gerasimenko, Y. (2016). Engaging Cervical Spinal Cord Networks to Reenable Volitional Control of Hand Function in Tetraplegic Patients. *Neurorehabilitation and Neural Repair*, *30*(10), 951–962. https://doi.org/10.1177/1545968316644344

Lu, Z., Stampas, A., Francisco, G. E., & Zhou, P. (2019). Offline and online myoelectric pattern recognition analysis and real-time control of a robotic hand after spinal cord injury. *Journal of Neural Engineering*, *16*(3). https://doi.org/10.1088/1741-2552/ab0cf0

Luan, L., Wei, X., Zhao, Z., Siegel, J. J., Potnis, O., Tuppen, C. A., Lin, S., Kazmi, S., Fowler, R. A., Holloway, S., Dunn, A. K., Chitwood, R. A., & Xie, C. (2017). Ultraflexible nanoelectronic probes form reliable, glial scar–free neural integration. *Science Advances*, *3*(2). https://doi.org/10.1126/sciadv.1601966

Lynch, C. L., & Popovic, M. R. (2008). Functional Electrical Stimulation. *IEEE Control Systems*, *28*(2), 40–50. https://doi.org/10.1109/MCS.2007.914689

Mangold, S., Keller, T., Curt, A., & Dietz, V. (2005). Transcutaneous functional electrical stimulation for grasping in subjects with cervical spinal cord injury. *Spinal Cord*, *43*(1), 1–13. https://doi.org/10.1038/sj.sc.3101644

Marquez-Chin, C., & Popovic, M. R. (2020). Functional electrical stimulation therapy for restoration of motor function after spinal cord injury and stroke: A review. *BioMedical Engineering Online*, *19*(1). https://doi.org/10.1186/s12938-020-00773-4

Marshall, N. J., Glaser, J. I., Trautmann, E. M., Amematsro, E. A., Perkins, S. M., Shadlen, M. N., Abbott, L. F., Cunningham, J. P., & Churchland, M. M. (2022). Flexible neural control of motor units. *Nature Neuroscience*, *25*(11), 1492–1504. https://doi.org/10.1038/s41593-022-01165-8

Martin, J. R., Zatsiorsky, V. M., & Latash, M. L. (2011). Multi-finger interaction during involuntary and voluntary single finger force changes. *Experimental Brain Research*, *208*(3), 423–435. https://doi.org/10.1007/s00221-010-2492-z

Mason, C. R., Gomez, J. E., & Ebner, T. J. (2001). Hand synergies during reach-to-grasp. *Journal of Neurophysiology*, *86*(6), 2896–2910. https://doi.org/10.1152/jn.2001.86.6.2896

Mathis, A., Mamidanna, P., Cury, K. M., Abe, T., Murthy, V. N., Mathis, M. W., & Bethge, M. (2018). DeepLabCut: markerless pose estimation of user-defined body parts with deep learning. *Nature Neuroscience*, *21*(9), 1281–1289. https://doi.org/10.1038/s41593-018-0209-y

McCallum, G. A., Sui, X., Qiu, C., Marmerstein, J., Zheng, Y., Eggers, T. E., Hu, C., Dai, L., & Durand, D. M. (2017). Chronic interfacing with the autonomic nervous system using carbon nanotube (CNT) yarn electrodes. *Scientific Reports*, *7*(1), 1–14. https://doi.org/10.1038/s41598-017-10639-w

McDonnall, D., Clark, G. A., & Normann, R. A. (2004). Selective motor unit recruitment via

intrafascicular multielectrode stimulation. *Canadian Journal of Physiology and Pharmacology*, *82*(8–9), 599–609. https://doi.org/10.1139/Y04-047

McFarland, D. J., Anderson, C. W., Müller, K. R., Schlögl, A., & Krusienski, D. J. (2006). BCI Meeting 2005 - Workshop on BCI signal processing: Feature extraction and translation. *IEEE Transactions on Neural Systems and Rehabilitation Engineering*, *14*(2), 135–138. https://doi.org/10.1109/TNSRE.2006.875637

McFarland, D. J., & Wolpaw, J. R. (2017). EEG-based brain–computer interfaces. *Current Opinion in Biomedical Engineering*, *4*, 194–200. https://doi.org/10.1016/j.cobme.2017.11.004

McIntosh, J. R., Joiner, E. F., Goldberg, J. L., Murray, L. M., Yasin, B., Mendiratta, A., Karceski, S. C., Thuet, E., Modik, O., Shelkov, E., Lombardi, J. M., Sardar, Z. M., Lehman, R. A., Mandigo, C., Riew, K. D., Harel, N. Y., Virk, M. S., & Carmel, J. B. (2023). Intraoperative electrical stimulation of the human dorsal spinal cord reveals a map of arm and hand muscle responses. *Journal of Neurophysiology*, *129*(1), 66–82. https://doi.org/10.1152/jn.00235.2022

Mcisaac, T. L., & Fuglevand, A. J. (2007). Motor-Unit Synchrony Within and Across Compartments of the Human Flexor Digitorum Superficialis. *J Neuro-Physiol*, *97*, 550–556. https://doi.org/10.1152/jn.01071.2006

McNaughton, B. L., O'Keefe, J., & Barnes, C. A. (1983). The stereotrode: A new technique for simultaneous isolation of several single units in the central nervous system from multiple unit records. *Journal of Neuroscience Methods*, *8*(4), 391–397. https://doi.org/10.1016/0165-0270(83)90097-3

Mehrotra, P., Dasgupta, S., Robertson, S., & Nuyujukian, P. (2018). An open-source realtime computational platform (short WIP paper). *ACM SIGPLAN Notices*, *53*(6), 109–112. https://doi.org/10.1145/3299710.3211344

Memberg, W. D., Polasek, K. H., Hart, R. L., Bryden, A. M., Kilgore, K. L., Nemunaitis, G. A., Hoyen, H. A., Keith, M. W., & Kirsch, R. F. (2014). Implanted neuroprosthesis for restoring arm and hand function in people with high level tetraplegia. In *Archives of Physical Medicine and Rehabilitation* (Vol. 95, Issue 6, pp. 1201-1211.e1). Arch Phys Med Rehabil. https://doi.org/10.1016/j.apmr.2014.01.028

Mender, M. J., Nason-Tomaszewski, S. R., Temmar, H., Costello, J. T., Wallace, D. M., Willsey, M. S., Kumar, N. G., Kung, T. A., Patil, P., & Chestek, C. A. (2023). The impact of task context on predicting finger movements in a brain-machine interface. *ELife*, *12*. https://doi.org/10.7554/eLife.82598

Metzger, S. L., Littlejohn, K. T., Silva, A. B., Moses, D. A., Seaton, M. P., Wang, R., Dougherty, M. E., Liu, J. R., Wu, P., Berger, M. A., Zhuravleva, I., Tu-Chan, A., Ganguly, K., Anumanchipalli, G. K., & Chang, E. F. (2023). A high-performance neuroprosthesis for speech decoding and avatar control. *Nature*, *620*(7976), 1037–1046. https://doi.org/10.1038/s41586-023-06443-4

Miller, K. J., Zanos, S., Fetz, E. E., Den Nijs, M., & Ojemann, J. G. (2009). Decoupling the cortical power spectrum reveals real-time representation of individual finger movements in humans. *Journal of Neuroscience*, *29*(10), 3132–3137. https://doi.org/10.1523/JNEUROSCI.5506-08.2009

Miri, A., Warriner, C. L., Seely, J. S., Elsayed, G. F., Cunningham, J. P., Churchland, M. M., & Jessell, T. M. (2017). Behaviorally Selective Engagement of Short-Latency Effector Pathways by Motor Cortex. *Neuron*, *95*(3), 683-696.e11. https://doi.org/10.1016/j.neuron.2017.06.042

Moineau, B., Myers, M., Ali, S. S., Popovic, M. R., & Hitzig, S. L. (2021). End-user and clinician perspectives on the viability of wearable functional electrical stimulation garments after stroke and spinal cord injury. *Disability and Rehabilitation: Assistive Technology*, *16*(3), 241–250. https://doi.org/10.1080/17483107.2019.1668974

Moran, D. W., & Schwartz, A. B. (1999). Motor cortical representation of speed and direction during reaching. *Journal of Neurophysiology*, *82*(5), 2676–2692. https://doi.org/10.1152/jn.1999.82.5.2676

Moraud, E. M., Capogrosso, M., Formento, E., Wenger, N., DiGiovanna, J., Courtine, G., & Micera, S. (2016). Mechanisms Underlying the Neuromodulation of Spinal Circuits for Correcting Gait and Balance Deficits after Spinal Cord Injury. *Neuron*, *89*(4), 814–828. https://doi.org/10.1016/J.NEURON.2016.01.009

Moritz, C. T., Lucas, T. H., Perlmutter, S. I., & Fetz, E. E. (2007). Forelimb movements and muscle responses evoked by microstimulation of cervical spinal cord in sedated monkeys. *Journal of Neurophysiology*, *97*(1), 110–120. https://doi.org/10.1152/JN.00414.2006

Moritz, C. T., Perlmutter, S. I., & Fetz, E. E. (2008). Direct control of paralysed muscles by cortical neurons. *Nature*, *456*(7222), 639–642. https://doi.org/10.1038/nature07418

Mortimer, J. T. (2011). Motor prostheses. In R. Terjung (Ed.), *Comprehensive Physiology*. https://doi.org/10.1002/cphy.cp010205

Mrachacz-Kersting, N., Kristensen, S. R., Niazi, I. K., & Farina, D. (2012). Precise temporal association between cortical potentials evoked by motor imagination and afference induces cortical plasticity. *Journal of Physiology*, *590*(7), 1669–1682. https://doi.org/10.1113/jphysiol.2011.222851

Muller-Putz, G. R., Ofner, P., Pereira, J., Pinegger, A., Schwarz, A., Zube, M., Eck, U., Hessing, B., Schneiders, M., & Rupp, R. (2019). Applying intuitive EEG-controlled grasp neuroprostheses in individuals with spinal cord injury: Preliminary results from the MoreGrasp clinical feasibility study. In *Proceedings of the Annual International Conference of the IEEE Engineering in Medicine and Biology Society, EMBS* (pp. 5949–5955). https://doi.org/10.1109/EMBC.2019.8856491

Musk, E. (2019). An integrated brain-machine interface platform with thousands of channels. *Journal of Medical Internet Research*, *21*(10). https://doi.org/10.2196/16194

Nagai, M. K., Cesar Marquez-Chin, C., & R., P. M. (2016). Why Is Functional Electrical Stimulation Therapy Capable of Restoring Motor Function Following Severe Injury to the Central Nervous System? In M. H. Tuszynski (Ed.), *Translational Neuroscience: Fundamental Approaches for Neurological Disorders* (pp. 479–498). Springer US. https://doi.org/10.1007/978-1-4899-7654-3

Nanayakkara, V. K., Cotugno, G., Vitzilaios, N., Venetsanos, D., Nanayakkara, T., & Sahinkaya, M. N. (2017). The Role of Morphology of the Thumb in Anthropomorphic Grasping: A Review. *Frontiers in Mechanical Engineering*, *3*, 252454. https://doi.org/10.3389/fmech.2017.00005

Napier, J. R. (1956). The prehensile movements of the human hand. *The Journal of Bone and Joint Surgery. British Volume*, *38 B*(4), 902–913. https://doi.org/10.1302/0301-620x.38b4.902

Nason-Tomaszewski, S. R., Mender, M. J., Kennedy, E., Lambrecht, J. M., Kilgore, K. L., Chiravuri, S., Ganesh Kumar, N., Kung, T. A., Willsey, M. S., Chestek, C. A., & Patil, P. G. (2023). Restoring continuous finger function with temporarily paralyzed nonhuman primates using brain-machine interfaces. *Journal of Neural Engineering*, *20*(3). https://doi.org/10.1088/1741-2552/accf36

Nason-Tomaszewski, S. R., Mender, M. J., Kennedy, E., Lambrecht, J. M., Kilgore, K. L., Chiravuri, S., Kumar, N. G., Kung, T. A., Willsey, M. S., Chestek, C. A., & Patil, P. G. (2022). Brain-Controlled Electrical Stimulation Restores Continuous Finger Function. *BioRxiv*. https://doi.org/10.1101/2022.06.15.496349

Nason, S. R., Mender, M. J., Vaskov, A. K., Willsey, M. S., Ganesh Kumar, N., Kung, T. A., Patil, P. G., & Chestek, C. A. (2021). Real-time linear prediction of simultaneous and independent movements of two finger groups using an intracortical brain-machine interface. *Neuron*, *109*(19), 3164-3177.e8. https://doi.org/10.1016/j.neuron.2021.08.009

Nason, S. R., Vaskov, A. K., Willsey, M. S., Welle, E. J., An, H., Vu, P. P., Bullard, A. J., Nu, C. S., Kao, J. C., Shenoy, K. V., Jang, T., Kim, H. S., Blaauw, D., Patil, P. G., & Chestek, C. A. (2020). A low-power band of neuronal spiking activity dominated by local single units improves the performance of brain–machine interfaces. *Nature Biomedical Engineering*, *4*(10), 973–983. https://doi.org/10.1038/s41551-020-0591-0

Nath, T., Mathis, A., Chen, A. C., Patel, A., Bethge, M., & Mathis, M. W. (2019). Using DeepLabCut for 3D markerless pose estimation across species and behaviors. *Nature Protocols*, *14*(7), 2152–2176. https://doi.org/10.1038/s41596-019-0176-0

National Spinal Cord Injury Statistical Center. (2023). *Traumatic Spinal Cord Injury Facts and Figures at a Glance*. https://www.nscisc.uab.edu/public/Facts and Figures 2023 - Final.pdf

Naufel, S., Glaser, J. I., Kording, K. P., Perreault, E. J., & Miller, L. E. (2019). A muscle-activity-dependent gain between motor cortex and emg. *Journal of Neurophysiology*, *121*(1), 61–73. https://doi.org/10.1152/jn.00329.2018

Nicolelis, M. A. L., Dimitrov, D., Carmena, J. M., Crist, R., Lehew, G., Kralik, J. D., & Wise, S. P. (2003). Chronic, multisite, multielectrode recordings in macaque monkeys. *Proceedings*

of the National Academy of Sciences of the United States of America, *100*(19), 11041–11046. https://doi.org/10.1073/pnas.1934665100

Nordhausen, C. T., Maynard, E. M., & Normann, R. A. (1996). Single unit recording capabilities of a 100 microelectrode array. *Brain Research*, *726*(1–2), 129–140. https://doi.org/10.1016/0006-8993(96)00321-6

Normann, R. A., Dowden, B. R., Frankel, M. A., Wilder, A. M., Hiatt, S. D., Ledbetter, N. M., Warren, D. A., & Clark, G. A. (2012). Coordinated, multi-joint, fatigue-resistant feline stance produced with intrafascicular hind limb nerve stimulation. *Journal of Neural Engineering*, *9*(2). https://doi.org/10.1088/1741-2560/9/2/026019

Normann, R. A., & Fernandez, E. (2016). Clinical applications of penetrating neural interfaces and Utah Electrode Array technologies. *Journal of Neural Engineering*, *13*(6). https://doi.org/10.1088/1741-2560/13/6/061003

O'Driscoll, S. W., Horii, E., Ness, R., Cahalan, T. D., Richards, R. R., & An, K. N. (1992). The relationship between wrist position, grasp size, and grip strength. *The Journal of Hand Surgery*, *17*(1), 169–177. https://doi.org/10.1016/0363-5023(92)90136-D

Obaid, A., Hanna, M. E., Wu, Y. W., Kollo, M., Racz, R., Angle, M. R., Müller, J., Brackbill, N., Wray, W., Franke, F., Chichilnisky, E. J., Hierlemann, A., Ding, J. B., Schaefer, A. T., & Melosh, N. A. (2020). Massively parallel microwire arrays integrated with CMOS chips for neural recording. *Science Advances*, *6*(12). https://doi.org/10.1126/sciadv.aay2789

Oby, E. R., Ethier, C., & Miller, L. E. (2013). Movement representation in the primary motor cortex and its contribution to generalizable EMG predictions. *Journal of Neurophysiology*, *109*(3), 666–678. https://doi.org/10.1152/jn.00331.2012

Oby, E. R., Golub, M. D., Hennig, J. A., Degenhart, A. D., Tyler-Kabara, E. C., Yu, B. M., Chase, S. M., & Batista, A. P. (2019). New neural activity patterns emerge with long-term learning. *Proceedings of the National Academy of Sciences of the United States of America*, *116*(30), 15210–15215. https://doi.org/10.1073/pnas.1820296116

Ofner, P., Schwarz, A., Pereira, J., Wyss, D., Wildburger, R., & Müller-Putz, G. R. (2019). Attempted Arm and Hand Movements can be Decoded from Low-Frequency EEG from Persons with Spinal Cord Injury. *Scientific Reports*, *9*(1). https://doi.org/10.1038/s41598-019-43594-9

Orsborn, A. L., Dangi, S., Moorman, H. G., & Carmena, J. M. (2012). Closed-loop decoder adaptation on intermediate time-scales facilitates rapid BMI performance improvements independent of decoder initialization conditions. *IEEE Transactions on Neural Systems and Rehabilitation Engineering*, *20*(4), 468–477. https://doi.org/10.1109/TNSRE.2012.2185066

Orsborn, A. L., Moorman, H. G., Overduin, S. A., Shanechi, M. M., Dimitrov, D. F., & Carmena, J. M. (2014). Closed-loop decoder adaptation shapes neural plasticity for skillful neuroprosthetic control. *Neuron*, *82*(6), 1380–1393. https://doi.org/10.1016/j.neuron.2014.04.048

Osuagwu, B. A. C., Whicher, E., & Shirley, R. (2020). Active proportional electromyogram controlled functional electrical stimulation system. *Scientific Reports*, *10*(1). https://doi.org/10.1038/s41598-020-77664-0

Overduin, S. A., d'Avella, A., Roh, J., Carmena, J. M., & Bizzi, E. (2015). Representation of muscle synergies in the primate brain. *Journal of Neuroscience*, *35*(37), 12615–12624. https://doi.org/10.1523/JNEUROSCI.4302-14.2015

Pandarinath, C., Nuyujukian, P., Blabe, C. H., Sorice, B. L., Saab, J., Willett, F. R., Hochberg, L. R., Shenoy, K. V., & Henderson, J. M. (2017). High performance communication by people with paralysis using an intracortical brain-computer interface. *ELife*, *6*, 1–27. https://doi.org/10.7554/eLife.18554

Pandarinath, C., O'Shea, D. J., Collins, J., Jozefowicz, R., Stavisky, S. D., Kao, J. C., Trautmann, E. M., Kaufman, M. T., Ryu, S. I., Hochberg, L. R., Henderson, J. M., Shenoy, K. V., Abbott, L. F., & Sussillo, D. (2018). Inferring single-trial neural population dynamics using sequential auto-encoders. *Nature Methods*, *15*(10), 805–815. https://doi.org/10.1038/s41592-018-0109-9

Patel, P. R., Na, K., Zhang, H., Kozai, T. D. Y., Kotov, N. A., Yoon, E., & Chestek, C. A. (2015). Insertion of linear 8.4 μm diameter 16 channel carbon fiber electrode arrays for single unit recordings. *Journal of Neural Engineering*, *12*(4), 046009. https://doi.org/10.1088/1741-2560/12/4/046009

Peckham, P. H., Keith, M. W., Kilgore, K. L., Grill, J. H., Wuolle, K. S., Thrope, G. B., Gorman, P., Hobby, J., Mulcahey, M. J., Carroll, S., Hentz, V. R., & Wiegner, A. (2001). Efficacy of an implanted neuroprosthesis for restoring hand grasp in tetraplegia: A multicenter study. *Archives of Physical Medicine and Rehabilitation*, *82*(10), 1380–1388. https://doi.org/10.1053/apmr.2001.25910

Peckham, P. H., Kilgore, K. L., Keith, M. W., Bryden, A. M., Bhadra, N., & Montague, F. W. (2002). An advanced neuroprosthesis for restoration of hand and upper arm control using an implantable controller. *Journal of Hand Surgery*, *27*(2), 265–276. https://doi.org/10.1053/jhsu.2002.30919

Peckham, P. H., Marsolais, E. B., & Mortimer, J. T. (1980). Restoration of key grip and release in the C6 tetraplegic patient through functional electrical stimulation. *Journal of Hand Surgery*, *5*(5), 462–469. https://doi.org/10.1016/S0363-5023(80)80076-1

Peckham, P. H., Van Der Meulen, J. P., & Reswick, J. B. (1970). Electrical Activation of Skeletal Muscle by Sequential Stimulation. *The Nervous System and Electric Currents*, 45–49. https://doi.org/10.1007/978-1-4684-1836-1_8

Pistohl, T., Schmidt, T. S. B., Ball, T., Schulze-Bonhage, A., Aertsen, A., & Mehring, C. (2013). Grasp Detection from Human ECoG during Natural Reach-to-Grasp Movements. *PLoS ONE*, *8*(1). https://doi.org/10.1371/journal.pone.0054658

Pistohl, T., Schulze-Bonhage, A., Aertsen, A., Mehring, C., & Ball, T. (2012). Decoding natural grasp types from human ECoG. *NeuroImage*, *59*(1), 248–260.

https://doi.org/10.1016/j.neuroimage.2011.06.084

Polasek, K. H., Hoyen, H. A., Keith, M. W., Kirsch, R. F., & Tyler, D. J. (2009). Stimulation stability and selectivity of chronically implanted multicontact nerve cuff electrodes in the human upper extremity. *IEEE Transactions on Neural Systems and Rehabilitation Engineering*, *17*(5), 428–437. https://doi.org/10.1109/TNSRE.2009.2032603

Popović-Bijelić, A., Bijelić, G., Jorgovanović, N., Bojanić, D., Popović, M. B., & Popović, D. B. (2005). Multi-field surface electrode for selective electrical stimulation. *Artificial Organs*, *29*(6), 448–452. https://doi.org/10.1111/J.1525-1594.2005.29075.X

Popović-Maneski, L. P., Kostić, M., Bijelić, G., Keller, T., Mitrović, S., Konstantinović, L., & Popović, D. B. (2013). Multi-pad electrode for effective grasping: Design. *IEEE Transactions on Neural Systems and Rehabilitation Engineering*, *21*(4), 648–654. https://doi.org/10.1109/TNSRE.2013.2239662

Popović, D., Stojanović, A., Pjanović, A., Radosavljević, S., Popović, M., Jović, S., & Vulović, D. (1999). Clinical evaluation of the Bionic Glove. *Archives of Physical Medicine and Rehabilitation*, *80*(3), 299–304. https://doi.org/10.1016/S0003-9993(99)90141-7

Popovic, M. R., Kapadia, N., Zivanovic, V., Furlan, J. C., Craven, B. C., & McGillivray, C. (2011). Functional electrical stimulation therapy of voluntary grasping versus only conventional rehabilitation for patients with subacute incomplete tetraplegia: A randomized clinical trial. *Neurorehabilitation and Neural Repair*, *25*(5), 433–442. https://doi.org/10.1177/1545968310392924

Porter, R., & Lemon, R. (1995). *Corticospinal function and voluntary movement*. 428.

Powell, M. P., Verma, N., Sorensen, E., Carranza, E., Boos, A., Fields, D. P., Roy, S., Ensel, S., Barra, B., Balzer, J., Goldsmith, J., Friedlander, R. M., Wittenberg, G. F., Fisher, L. E., Krakauer, J. W., Gerszten, P. C., Pirondini, E., Weber, D. J., & Capogrosso, M. (2023). Epidural stimulation of the cervical spinal cord for post-stroke upper-limb paresis. *Nature Medicine*, *29*(3), 689–699. https://doi.org/10.1038/s41591-022-02202-6

Prochazka, A., Gauthier, M., Wieler, M., & Kenwell, Z. (1997). The bionic glove: An electrical stimulator garment that provides controlled grasp and hand opening in quadriplegia. *Archives of Physical Medicine and Rehabilitation*, *78*(6), 608–614. https://doi.org/10.1016/S0003-9993(97)90426-3

Ramos-Murguialday, A., Broetz, D., Rea, M., Läer, L., Yilmaz, Ö., Brasil, F. L., Liberati, G., Curado, M. R., Garcia-Cossio, E., Vyziotis, A., Cho, W., Agostini, M., Soares, E., Soekadar, S., Caria, A., Cohen, L. G., & Birbaumer, N. (2013). Brain-machine interface in chronic stroke rehabilitation: A controlled study. *Annals of Neurology*, *74*(1), 100–108. https://doi.org/10.1002/ana.23879

Randazzo, L., Iturrate, I., Chavarriaga, R., Leeb, R., & Millan, J. D. R. (2015). Detecting intention to grasp during reaching movements from EEG. *Proceedings of the Annual International Conference of the IEEE Engineering in Medicine and Biology Society, EMBS*, *2015-Novem*, 1115–1118. https://doi.org/10.1109/EMBC.2015.7318561

Rathelot, J. A., & Strick, P. L. (2006). Muscle representation in the macaque motor cortex: An anatomical perspective. *Proceedings of the National Academy of Sciences of the United States of America*, *103*(21), 8257–8262. https://doi.org/10.1073/pnas.0602933103

RaviChandran, N., Teo, M. Y., McDaid, A., & Aw, K. (2023). Conformable Electrode Arrays for Wearable Neuroprostheses. *Sensors*, *23*(6). https://doi.org/10.3390/s23062982

Reilly, K. T., Nordstrom, M. A., & Schieber, M. H. (2004). Short-Term Synchronization Between Motor Units in Different Functional Subdivisions of the Human Flexor Digitorum Profundus Muscle. *Journal of Neurophysiology*, *92*(2), 734–742. https://doi.org/10.1152/jn.00027.2004

Roux, F. E., Niare, M., Charni, S., Giussani, C., & Durand, J. B. (2020). Functional architecture of the motor homunculus detected by electrostimulation. *Journal of Physiology*, *598*(23), 5487–5504. https://doi.org/10.1113/JP280156

Rupp, R. (2020). Spinal cord lesions. In *Handbook of Clinical Neurology* (Vol. 168, pp. 51–65). https://doi.org/10.1016/B978-0-444-63934-9.00006-8

Russo, A. A., Bittner, S. R., Perkins, S. M., Seely, J. S., London, B. M., Lara, A. H., Miri, A., Marshall, N. J., Kohn, A., Jessell, T. M., Abbott, L. F., Cunningham, J. P., & Churchland, M. M. (2018). Motor Cortex Embeds Muscle-like Commands in an Untangled Population Response. *Neuron*, *97*(4), 953-966.e8. https://doi.org/10.1016/j.neuron.2018.01.004

Sadtler, P. T., Quick, K. M., Golub, M. D., Chase, S. M., Ryu, S. I., Tyler-Kabara, E. C., Yu, B. M., & Batista, A. P. (2014). Neural constraints on learning. *Nature*, *512*(7515), 423–426. https://doi.org/10.1038/nature13665

Safwat, M. D. E. D., & Abdel-Meguid, E. M. (2007). Distribution of terminal nerve entry points to the flexor and extensor groups of forearm muscles: An anatomical study. *Folia Morphologica*, *66*(2), 83–93.

Sanchez, J. C., Principe, J. C., Carmena, J. M., Lebedev, M. A., & Nicolelis, M. A. L. (2004). Simultaneous prediction of four kinematic variables for a brain-machine interface using a single recurrent neural network. *Annual International Conference of the IEEE Engineering in Medicine and Biology - Proceedings*, *26 VII*, 5321–5324. https://doi.org/10.1109/iembs.2004.1404486

Sanes, J. N., Donoghue, J. P., Thangaraj, V., Edelman, R. R., & Warach, S. (1995). Shared neural substrates controlling hand movements in human motor cortex. *Science*, *268*(5218), 1775–1777. https://doi.org/10.1126/science.7792606

Santello, M., Bianchi, M., Gabiccini, M., Ricciardi, E., Salvietti, G., Prattichizzo, D., Ernst, M., Moscatelli, A., Jörntell, H., Kappers, A. M. L., Kyriakopoulos, K., Albu-Schäffer, A., Castellini, C., & Bicchi, A. (2016). Hand synergies: Integration of robotics and neuroscience for understanding the control of biological and artificial hands. *Physics of Life Reviews*, *17*, 1–23. https://doi.org/10.1016/J.PLREV.2016.02.001

Santello, M., Flanders, M., & Soechting, J. F. (1998). Postural hand synergies for tool use. *Journal of Neuroscience*, *18*(23), 10105–10115. https://doi.org/10.1523/jneurosci.18-23-10105.1998

Santello, M., & Soechting, J. F. (2000). Force synergies for multifingered grasping. *Experimental Brain Research*, *133*(4), 457–467. https://doi.org/10.1007/s002210000420

Santurkar, S., Tsipras, D., Ilyas, A., & Madry, A. (2018). How does batch normalization help optimization? *Advances in Neural Information Processing Systems*, *2018-Decem*, 2483–2493.

Saxena, S., Russo, A. A., Cunningham, J. P., & Churchland, M. M. (2022). Motor cortex activity across movement speeds is predicted by network-level strategies for generating muscle activity. *ELife*, *11*, 1–31. https://doi.org/10.7554/eLife.67620

Sburlea, A. I., Wilding, M., & Müller-Putz, G. R. (2021). Disentangling human grasping type from the object's intrinsic properties using low-frequency EEG signals. *Neuroimage: Reports*, *1*(2). https://doi.org/10.1016/j.ynirp.2021.100012

Schalk, G., & Leuthardt, E. C. (2011). Brain-computer interfaces using electrocorticographic signals. *IEEE Reviews in Biomedical Engineering*, *4*, 140–154. https://doi.org/10.1109/RBME.2011.2172408

Schieber, M. H. (1991). Individuated finger movements of rhesus monkeys: A means of quantifying the independence of the digits. In *Journal of Neurophysiology* (Vol. 65, Issue 6). https://doi.org/10.1152/jn.1991.65.6.1381

Schieber, M. H. (1995). Muscular production of individuated finger movements: The roles of extrinsic finger muscles. *Journal of Neuroscience*, *15*(1 I), 284–297. https://doi.org/10.1523/jneurosci.15-01-00284.1995

Schieber, M. H., Gardinier, J., & Liu, J. (2001). Tension distribution to the five digits of the hand by neuromuscular compartments in the macaque flexor digitorum profundus. *Journal of Neuroscience*, *21*(6), 2150–2158. https://doi.org/10.1523/jneurosci.21-06-02150.2001

Schieber, M. H., & Hibbard, L. S. (1993, March 23). *How somatotopic is the motor cortex hand area?* Science; American Association for the Advancement of Science. https://doi.org/10.1126/science.8332915

Schieber, M. H., Lang, C. E., Reilly, K. T., McNulty, P., & Sirigu, A. (2009). Selective activation of human finger muscles after stroke or amputation. *Advances in Experimental Medicine and Biology*, *629*, 559–575. https://doi.org/10.1007/978-0-387-77064-2_30

Schirmer, C. M., Shils, J. L., Arle, J. E., Cosgrove, G. R., Dempsey, P. K., Tarlov, E., Kim, S., Martin, C. J., Feltz, C., Moul, M., & Magge, S. (2011). Heuristic map of myotomal innervation in humans using direct intraoperative nerve root stimulation: Clinical article. *Journal of Neurosurgery: Spine*, *15*(1), 64–70. https://doi.org/10.3171/2011.2.SPINE1068

Schroeder, K. E., Perkins, S. M., Wang, Q., & Churchland, M. M. (2022). Cortical Control of Virtual Self-Motion Using Task-Specific Subspaces. *Journal of Neuroscience*, *42*(2), 220–239. https://doi.org/10.1523/JNEUROSCI.2687-20.2021

Schwarz, A., Ofner, P., Pereira, J., Sburlea, A. I., & Müller-Putz, G. R. (2018). Decoding natural reach-and-grasp actions from human EEG. *Journal of Neural Engineering*, *15*(1).

https://doi.org/10.1088/1741-2552/aa8911

Schwemmer, M. A., Skomrock, N. D., Sederberg, P. B., Ting, J. E., Sharma, G., Bockbrader, M. A., & Friedenberg, D. A. (2018). Meeting brain–computer interface user performance expectations using a deep neural network decoding framework. *Nature Medicine*, *24*(11), 1669–1676. https://doi.org/10.1038/s41591-018-0171-y

Scott, S. H. (2008). Inconvenient Truths about neural processing in primary motor cortex. *Journal of Physiology*, *586*(5), 1217–1224. https://doi.org/10.1113/jphysiol.2007.146068

Seo, D., Neely, R. M., Shen, K., Singhal, U., Alon, E., Rabaey, J. M., Carmena, J. M., & Maharbiz, M. M. (2016). Wireless Recording in the Peripheral Nervous System with Ultrasonic Neural Dust. *Neuron*, *91*(3), 529–539. https://doi.org/10.1016/j.neuron.2016.06.034

Sergio, L. E., Hamel-Pâquet, C., & Kalaska, J. F. (2005). Motor cortex neural correlates of output kinematics and kinetics during isometric-force and arm-reaching tasks. *Journal of Neurophysiology*, *94*(4), 2353–2378. https://doi.org/10.1152/jn.00989.2004

Serruya, M. D., Hatsopoulos, N. G., Paninski, L., Fellows, M. R., & Donoghue, J. P. (2002). Instant neural control of a movement signal. *Nature*, *416*(6877), 141–142. https://doi.org/10.1038/416141a

Shah, K. G., DeLima, T., Felix, S., Sheth, H., Tolosa, V., Tooker, A., & Pannu, S. (2012). High-density, bio-compatible, and hermetic electrical feedthroughs using extruded metal vias. In *Technical Digest - Solid-State Sensors, Actuators, and Microsystems Workshop* (pp. 197–200). https://doi.org/10.31438/trf.hh2012.52

Shenoy, K. V., Sahani, M., & Churchland, M. M. (2013). Cortical control of arm movements: A dynamical systems perspective. *Annual Review of Neuroscience*, *36*(1), 337–359. https://doi.org/10.1146/annurev-neuro-062111-150509

Sherwood, A. M., Dimitrijevic, M. R., & Barry McKay, W. (1992). Evidence of subclinical brain influence in clinically complete spinal cord injury: discomplete SCI. *Journal of the Neurological Sciences*, *110*(1–2), 90–98. https://doi.org/10.1016/0022-510X(92)90014-C

Shokur, S., Mazzoni, A., Schiavone, G., Weber, D. J., & Micera, S. (2021). A modular strategy for next-generation upper-limb sensory-motor neuroprostheses. *Med*, *2*(8), 912–937. https://doi.org/10.1016/j.medj.2021.05.002

Simeral, J. D., Kim, S. P., Black, M. J., Donoghue, J. P., & Hochberg, L. R. (2011). Neural control of cursor trajectory and click by a human with tetraplegia 1000 days after implant of an intracortical microelectrode array. *Journal of Neural Engineering*, *8*(2), 24. https://doi.org/10.1088/1741-2560/8/2/025027

Singh, K., Richmond, F. J. R., & Loeb, G. E. (2000). Recruitment properties of intramuscular and nerve-trunk stimulating electrodes. In *IEEE Transactions on Rehabilitation Engineering* (Vol. 8, Issue 3). https://doi.org/10.1109/86.867869

Skomrock, N. D., Schwemmer, M. A., Ting, J. E., Trivedi, H. R., Sharma, G., Bockbrader, M. A., & Friedenberg, D. A. (2018). A Characterization of Brain-Computer Interface Performance

Trade-Offs Using Support Vector Machines and Deep Neural Networks to Decode Movement Intent. *Frontiers in Neuroscience*, *12*. https://doi.org/10.3389/fnins.2018.00763

Smith, B., Crish, T. J., Buckett, J. R., Kilgore, K. L., & Peckham, P. H. (2005). Development of an implantable networked neuroprosthesis. *2nd International IEEE EMBS Conference on Neural Engineering*, *2005*, 454–457. https://doi.org/10.1109/CNE.2005.1419657

Snoek, G. J., Ijzerman, M. J., In 't Groen, F. A. C. G., Stoffers, T. S., & Zilvold, G. (2000). Use of the NESS Handmaster to restore handfunction in tetraplegia: Clinical experiences in ten patients. *Spinal Cord*, *38*(4), 244–249. https://doi.org/10.1038/sj.sc.3100980

Sponheim, C., Papadourakis, V., Collinger, J. L., Downey, J., Weiss, J., Pentousi, L., Elliott, K., & Hatsopoulos, N. G. (2021). Longevity and reliability of chronic unit recordings using the Utah, intracortical multi-electrode arrays. *Journal of Neural Engineering*, *18*(6), 066044. https://doi.org/10.1088/1741-2552/ac3eaf

Srivastava, N., Hinton, G., Krizhevsky, A., Sutskever, I., & Salakhutdinov, R. (2014). Dropout: A simple way to prevent neural networks from overfitting. *Journal of Machine Learning Research*, *15*, 1929–1958.

Stephen H. Scott, Paul L. Gribble, Kirsten M. Graham, & D. William Cabel. (2001). Dissociation between hand motionand population vectors fromneural activity in motor cortex. *Nature*, *413*(September), 161–165.

Strick, P. L., Dum, R. P., & Rathelot, J. A. (2021). The Cortical Motor Areas and the Emergence of Motor Skills: A Neuroanatomical Perspective. *Annual Review of Neuroscience*, *44*, 425–447. https://doi.org/10.1146/annurev-neuro-070918-050216

Suresh, A. K., Goodman, J. M., Okorokova, E. V., Kaufman, M., Hatsopoulos, N. G., & Bensmaia, S. J. (2020). Neural population dynamics in motor cortex are different for reach and grasp. *ELife*, *9*, 1–16. https://doi.org/10.7554/eLife.58848

Sussillo, D., Nuyujukian, P., Fan, J. M., Kao, J. C., Stavisky, S. D., Ryu, S., & Shenoy, K. (2012). A recurrent neural network for closed-loop intracortical brain-machine interface decoders. *Journal of Neural Engineering*, *9*(2), 026027. https://doi.org/10.1088/1741-2560/9/2/026027

Szymanski, L. J., Kellis, S., Liu, C. Y., Jones, K. T., Andersen, R. A., Commins, D., Lee, B., McCreery, D. B., & Miller, C. A. (2021). Neuropathological effects of chronically implanted, intracortical microelectrodes in a tetraplegic patient. *Journal of Neural Engineering*, *18*(4). https://doi.org/10.1088/1741-2552/ac127e

Taylor, D. M., Tillery, S. I. H., & Schwartz, A. B. (2002). Direct cortical control of 3D neuroprosthetic devices. *Science*, *296*(5574), 1829–1832. https://doi.org/10.1126/science.1070291

Temmar, H., Willsey, M. S., Costello, J. T., Mender, M. J., Lam, J. L., Wallace, D. M., Kelberman, M. M., Patil, P. G., & Chestek, C. A. (2024). Artificial neural network for brain-machine interface consistently produces more naturalistic finger movements than linear methods. *BioRxiv*. https://doi.org/10.1101/2024.03.01.583000

Thakur, P. H., Bastian, A. J., & Hsiao, S. S. (2008). Multidigit movement synergies of the human hand in an unconstrained haptic exploration task. *Journal of Neuroscience*, *28*(6), 1271–1281. https://doi.org/10.1523/JNEUROSCI.4512-07.2008

Thomsen, M., & Veltink, P. H. (1997). Influence of synchronous and sequential stimulation on muscle fatigue. *Medical and Biological Engineering and Computing*, *35*(3), 186–192. https://doi.org/10.1007/BF02530036

Tigra, W., Dali, M., William, L., Fattal, C., Gélis, A., Divoux, J. L., Coulet, B., Teissier, J., Guiraud, D., & Azevedo Coste, C. (2020). Selective neural electrical stimulation restores hand and forearm movements in individuals with complete tetraplegia. *Journal of NeuroEngineering and Rehabilitation*, *17*(1). https://doi.org/10.1186/s12984-020-00676-4

Ting, J. E., Del Vecchio, A., Sarma, D., Verma, N., Colachis, S. C., Annetta, N. V., Collinger, J. L., Farina, D., & Weber, D. J. (2021). Sensing and decoding the neural drive to paralyzed muscles during attempted movements of a person with tetraplegia using a sleeve array. *Journal of Neurophysiology*, *127*(1), 2104–2118. https://doi.org/10.1152/jn.00220.2021

Todorov, E., & Ghahramani, Z. (2004). Analysis of the synergies underlying complex hand manipulation. *Annual International Conference of the IEEE Engineering in Medicine and Biology - Proceedings*, *26 VI*, 4637–4640. https://doi.org/10.1109/IEMBS.2004.1404285

Townsend, B. R., Paninski, L., & Lemon, R. N. (2006). Linear encoding of muscle activity in primary motor cortex and cerebellum. *Journal of Neurophysiology*, *96*(5), 2578–2592. https://doi.org/10.1152/jn.01086.2005

Tresch, M. C., & Bizzi, E. (1999). Responses to spinal microstimulation in the chronically spinalized rat and their relationship to spinal systems activated by low threshold cutaneous stimulation. *Experimental Brain Research*, *129*(3), 401–416. https://doi.org/10.1007/s002210050908

Tresch, M. C., & Jarc, A. (2009). The case for and against muscle synergies. *Current Opinion in Neurobiology*, *19*(6), 601–607. https://doi.org/10.1016/j.conb.2009.09.002

Tresch, M. C., Saltiel, P., & Bizzi, E. (1999). The construction of movement by the spinal cord. *Nature Neuroscience*, *2*(2), 162–167. https://doi.org/10.1038/5721

Vaskov, A. K., Irwin, Z. T., Nason, S. R., Vu, P. P., Nu, C. S., Bullard, A. J., Hill, M., North, N., Patil, P. G., & Chestek, C. A. (2018). Cortical decoding of individual finger group motions using ReFIT Kalman filter. *Frontiers in Neuroscience*, *12*(NOV), 751. https://doi.org/10.3389/fnins.2018.00751

Velliste, M., Perel, S., Spalding, M. C., Whitford, A. S., & Schwartz, A. B. (2008). Cortical control of a prosthetic arm for self-feeding. *Nature*, *453*(7198), 1098–1101. https://doi.org/10.1038/nature06996

Veltink, P. H., van Alsté, J. A., & Boom, H. B. K. (1989). Multielectrode intrafascicular and extraneural stimulation. *Medical & Biological Engineering & Computing*, *27*(1), 19–24. https://doi.org/10.1007/BF02442165

Vergara, M., Sancho-Bru, J. L., Gracia-Ibáñez, V., & Pérez-González, A. (2014). An introductory study of common grasps used by adults during performance of activities of daily living. *Journal of Hand Therapy*, *27*(3), 225–234. https://doi.org/10.1016/j.jht.2014.04.002

Vromans, M., & Faghri, P. D. (2018). Functional electrical stimulation-induced muscular fatigue: Effect of fiber composition and stimulation frequency on rate of fatigue development. *Journal of Electromyography and Kinesiology*, *38*, 67–72. https://doi.org/10.1016/j.jelekin.2017.11.006

Wagner, F. B., Mignardot, J. B., Le Goff-Mignardot, C. G., Demesmaeker, R., Komi, S., Capogrosso, M., Rowald, A., Seáñez, I., Caban, M., Pirondini, E., Vat, M., McCracken, L. A., Heimgartner, R., Fodor, I., Watrin, A., Seguin, P., Paoles, E., Van Den Keybus, K., Eberle, G., … Courtine, G. (2018). Targeted neurotechnology restores walking in humans with spinal cord injury. *Nature*, *563*(7729), 65–93. https://doi.org/10.1038/s41586-018-0649-2

Weiss, E. J., & Flanders, M. (2004). Muscular and postural synergies of the human hand. *Journal of Neurophysiology*, *92*(1), 523–535. https://doi.org/10.1152/jn.01265.2003

Welle, C. G., Gao, Y.-R., Ye, M., Lozzi, A., Boretsky, A., Abliz, E., & Hammer, D. X. (2020). Longitudinal neural and vascular structural dynamics produced by chronic microelectrode implantation. *Biomaterials*, *238*, 119831. https://doi.org/10.1016/j.biomaterials.2020.119831

Welle, E. J., Woods, J. E., Jiman, A. A., Richie, J. M., Bottorff, E. C., Ouyang, Z., Seymour, J. P., Patel, P. R., Bruns, T. M., & Chestek, C. A. (2021). Sharpened and Mechanically Durable Carbon Fiber Electrode Arrays for Neural Recording. *IEEE Transactions on Neural Systems and Rehabilitation Engineering*, *29*, 993–1003. https://doi.org/10.1109/TNSRE.2021.3082056

Willett, F. R., Avansino, D. T., Hochberg, L. R., Henderson, J. M., & Shenoy, K. V. (2021). High-performance brain-to-text communication via handwriting. *Nature*, *593*(7858), 249–254. https://doi.org/10.1038/s41586-021-03506-2

Willett, F. R., Kunz, E. M., Fan, C., Avansino, D. T., Wilson, G. H., Choi, E. Y., Kamdar, F., Glasser, M. F., Hochberg, L. R., Druckmann, S., Shenoy, K. V., & Henderson, J. M. (2023). A high-performance speech neuroprosthesis. *Nature 2023 620:7976*, *620*(7976), 1031–1036. https://doi.org/10.1038/s41586-023-06377-x

Willsey, M. S., Nason-Tomaszewski, S. R., Ensel, S. R., Temmar, H., Mender, M. J., Costello, J. T., Patil, P. G., & Chestek, C. A. (2022). Real-time brain-machine interface in non-human primates achieves high-velocity prosthetic finger movements using a shallow feedforward neural network decoder. *Nature Communications*, *13*(1). https://doi.org/10.1038/s41467-022-34452-w

Willsey, M. S., Shah, N. P., Avansino, D. T., Hahn, N. V., Jamiolkowski, R. M., Kamdar, F. B., Hochberg, L. R., Willett, F. R., & Henderson, J. M. (2024). A real-time, high-performance brain-computer interface for finger decoding and quadcopter control. *BioRxiv*. https://doi.org/10.1101/2024.02.06.578107

Witham, C. L., Fisher, K. M., Edgley, S. A., & Baker, S. N. (2016). Corticospinal inputs to primate

motoneurons innervating the forelimb from two divisions of primary motor cortex and area 3a. *Journal of Neuroscience*, *36*(9), 2605–2616. https://doi.org/10.1523/JNEUROSCI.4055-15.2016

Wodlinger, B., Downey, J. E., Tyler-Kabara, E. C., Schwartz, A. B., Boninger, M. L., & Collinger, J. L. (2015). Ten-dimensional anthropomorphic arm control in a human brain-machine interface: Difficulties, solutions, and limitations. *Journal of Neural Engineering*, *12*(1), 016011. https://doi.org/10.1088/1741-2560/12/1/016011

Wu, W., Shaikhouni, A., Donoghue, J. P., & Black, M. J. (2004). Closed-loop neural control of cursor motion using a kalman filter. *Annual International Conference of the IEEE Engineering in Medicine and Biology - Proceedings*, *26 VI*, 4126–4129. https://doi.org/10.1109/iembs.2004.1404151

Xie, Z., Schwartz, O., & Prasad, A. (2018). Decoding of finger trajectory from ECoG using deep learning. *Journal of Neural Engineering*, *15*(3), 036009. https://doi.org/10.1088/1741-2552/aa9dbe

Yan, Y., Goodman, J. M., Moore, D. D., Solla, S. A., & Bensmaia, S. J. (2020). Unexpected complexity of everyday manual behaviors. *Nature Communications*, *11*(1). https://doi.org/10.1038/s41467-020-17404-0

Yanagisawa, T., Hirata, M., Saitoh, Y., Goto, T., Kishima, H., Fukuma, R., Yokoi, H., Kamitani, Y., & Yoshimine, T. (2011). Real-time control of a prosthetic hand using human electrocorticography signals: Technical note. *Journal of Neurosurgery*, *114*(6), 1715–1722. https://doi.org/10.3171/2011.1.JNS101421

Ye, J., & Pandarinath, C. (2021). Representation learning for neural population activity with Neural Data Transformers. *Neurons, Behavior, Data Analysis, and Theory*, *5*(3). https://doi.org/10.51628/001c.27358

Yoshida, K., Bertram, M. J., Hunter Cox, T. G., & Riso, R. R. (2017). Peripheral nerve recording electrodes and techniques. *Neuroprosthetics: Theory and Practice: Second Edition*, 377–466. https://doi.org/10.1142/9789813207158_0014

Yoshida, K., & Horch, K. (1993). Selective Stimulation of Peripheral Nerve Fibers using Dual Intrafascicular Electrodes. *IEEE Transactions on Biomedical Engineering*, *40*(5), 492–494. https://doi.org/10.1109/10.243412

Yoshida Kozai, T. D., Langhals, N. B., Patel, P. R., Deng, X., Zhang, H., Smith, K. L., Lahann, J., Kotov, N. A., & Kipke, D. R. (2012). Ultrasmall implantable composite microelectrodes with bioactive surfaces for chronic neural interfaces. *Nature Materials*, *11*(12), 1065–1073. https://doi.org/10.1038/nmat3468

Young, D., Willett, F., Memberg, W. D., Murphy, B., Rezaii, P., Walter, B., Sweet, J., Miller, J., Shenoy, K. V., Hochberg, L. R., Kirsch, R. F., & Ajiboye, A. B. (2019). Closed-loop cortical control of virtual reach and posture using Cartesian and joint velocity commands. *Journal of Neural Engineering*, *16*(2). https://doi.org/10.1088/1741-2552/aaf606

Zimmermann, J. B., Seki, K., & Jackson, A. (2011). Reanimating the arm and hand with intraspinal microstimulation. *Journal of Neural Engineering*, *8*(5). https://doi.org/10.1088/1741-2560/8/5/054001